Enhancing selection and biological applications of oligonucleotide affinity reagents

A DISSERTATION
SUBMITTED TO THE FACULTY OF
UNIVERSITY OF MINNESOTA
BY

Sean Kawika Dembowski

IN PARTIAL FULFILLMENT OF THE REQUIREMENTS
FOR THE DEGREE OF
DOCTOR OF PHILOSOPHY

Michael T. Bowser, Adviser

August 2021

Acknowledgements

I owe a huge thanks to my Ph.D. advisor, Dr. Michael Bowser. You have always encouraged me to take risks and step outside my comfort zone, knowing that I could handle myself. I am so grateful that you provided guidance when needed without depriving me the opportunity to forge my own path as an independent researcher. So much of the scientist I am is thanks to you.

I am also indebted to all of the research advisers I have had along the way: Dr. Alex Sessions at Caltech, Dr. Christer Aakeröy at Kansas State University, Dr. Catherine Oertel at Oberlin College, Dr. Thomas Bruno at the National Institute of Standards and Technology, and particularly Dr. Rebecca Whelan as my honors research advisor at Oberlin College. Each of you were immensely kind, welcoming, and encouraging to a young researcher unsure of himself, and each of you played a huge role in shaping the path I find myself on today.

I have had too many amazing teachers and professors to count that have had a greater impact on me than they realize, but I would particularly like to highlight Gillian Bush and Dr. Robert Thompson. Ms. Bush, as my AP chemistry teacher, you helped me find and cultivate a love of science and a sense of awe at the natural world, both of which I still cherish. Professor Thompson, you brought an energy and excitement to your teaching of analytical chemistry that first got me excited about the field – only you could make instrumental analysis and error propagation so enjoyable. I am sure there would be a lot more chemists in the world if there were more teachers like the two of you.

I would not have survived my way through grad school without the friendship and support of all of my fellow Bowser group members, past and present: Thane Taylor, Amy Stading, Rachel Harstad, Matt Geiger, Sarah Anciaux, Megan Weisenberger, Kailey Soller, Alex Johnson, Jae-sung Kwon, Sarah Nelson, Matt LeMon, Nic Brinza, Ryan Hunt, Cecilia Douma, and Gretchen Burke. Whether going to baseball games, meeting for Dungeons & Dragons, commiserating about TA duties – or occasionally talking about actual research – I am grateful to have had all of you along for the ride. I would particularly like to thank Thane and Kailey for teaching an initially hesitant biologist how to culture cells, Rachel

for her knowledge and guidance with a finicky capillary electrophoresis instrument, and Nic for his IT expertise and his eager optimism in our shared work. Thank you all so much.

I cannot begin to thank my parents enough for all of their love and support through the years. You raised me to approach the world with curiosity and optimism, to try my hardest at everything I do, and to follow my heart, wherever it may lead. You instilled in me a love of learning and have never stopped devoting yourselves to my education, and it is only with your guidance and encouragement that I ever ended up where I am today.

And finally, there are no words to describe how thankful I am for my amazing wife Caitlin. You have been nothing but supportive through this entire endeavor and have helped me through all the emotional ups and downs that go along with it. When weeks' worth of experiments went belly up and made me want to cry, or when studying and grading lab reports kept me up late into the night, you were there with a spirited pep talk, a tasty baked treat, or just a hug and a smile that made it all a bit easier to deal with. You've listened to my elevator pitches, edited my resumes, and truly helped me to understand the importance of the work I'm doing. Your unconditional love and admiration have helped make everything, including this dissertation, a reality.

Dedicated to my loving parents and wonderful wife:
for always believing I could do it.

Abstract

Aptamers are unique sequences of single-stranded DNA or RNA that exhibit significant affinity toward a particular target of interest. They have a number of advantages over antibodies – ease of modification, cell-free synthesis, and spontaneous renaturation – yet the preference of most researchers for antibodies continues due to prevalence of commercial antibody sources, hesitance adjusting existing research protocols, and a subconscious association of binding behavior with proteins rather than nucleic acids. While aptamers have already shown their technical advantages in the literature, they will also need to demonstrate their practicality via a broader range of targets and useful applications in order for aptamers to become more widespread in bioanalytical research.

One challenge aptamers have faced is the inconsistency of SELEX, the combinatorial method by which new aptamers are identified, as well as a small pool of potential aptamer targets. This dissertation demonstrates the feasibility of aptamer selection against intact membrane proteins using a capillary electrophoresis-based SELEX technique, an achievement not yet demonstrated in the literature that opens SELEX to a much wider range of biologically significant potential targets. In addition to high affinity binding (K_d < 10 nM), these aptamers should undergo cellular internalization with their membrane receptor target, allowing hybrid aptamers to reach previously inaccessible intracellular targets as well.

Additionally, this dissertation serves to increase the body of work demonstrating the bioanalytical capabilities of aptamers and other oligonucleotide affinity reagents. First, progress is shown toward aptamers targeting mouse leptin for use in a real-time aptamer-based microfluidic assay to quantify leptin secretion in cultured adipocytes. This proposed device would allow measurement of leptin, an important metabolic protein related to obesity, on a sub-minute time scale in response to metabolic stimuli. Quantification involves on-line separation of aptamers and aptamer-leptin complexes by electrophoresis, a technique that lends itself well to oligonucleotide affinity reagents due to their highly negative charge.

Finally, a heart model based on cardiomyocyte differentiation from induced stem cells is demonstrated in preparation for measurement of physiological effects of aptamer-

like SPIDRs (small protein-interacting DNAs and RNAs) on cardiomyocyte beating. SPIDRs have been shown to bind to the calcium pump SERCA and its control protein phospholamban, increasing the calcium affinity of SERCA. The cardiomyocyte model will be used to evaluate the hypothesis that this increase in calcium affinity leads to measurable physiological changes in beating, namely the beat rate and fall time, demonstrating the therapeutic potential of SPIDRs. Herein, optimization of stem cell growth and differentiation to cardiomyocytes are shown, as well as preliminary quantitative data regarding the reproducibility of cell impedance measurements.

Table of Contents

List of Tables

List of Figures

List of Equations

List of Abbreviations

[#]WP	[#]-well plate
ABS	Acrylonitrile butadiene styrene
ACE	Affinity capillary electrophoresis
Ang2	angiopoietin-2
AU	Absorbance units
BME	Basement membrane extract
BMI	Body mass index
$C_{12}E_8$	Octaethylene glycol monododecyl ether
CE	Capillary electrophoresis
CE-SELEX	Capillary electrophoresis–systematic evolution of ligands by exponential enrichment
CM	Cardiomyocyte
CMACS	Continuous-flow magnetic activated chip separation device
CRP	C-reactive protein
D[#]	Day [#] (relative to start of differentiation, D0)
diH2O	Deionized (0.2 μm filtered) water
DMEM	Dulbecco's modified essential medium
DMSO	Dimethylsulfoxide
DNA	Deoxyribonucleic acid
dNTP	Deoxynucleoside triphosphate
DSLR	Digital single lens reflex
DTT	1,4-Dithiothreitol
E8	Essential 8 medium
EDL	Electrical double layer
EDTA	Ethylenediaminetetraacetic acid
EOF	Electroosmotic flow
ELISA	Enzyme-linked immunosorbent assay
FAM	6-Carboxyfluorescein
FDA	United States Food and Drug Administration

FP	Fluorescence polarization
GFP	Green fluorescent protein
GSK3	Glycogen synthase kinase-3
HE4	Human epididymis protein 4
HIV-RT	Human immunodeficiency virus reverse transcriptase
hVEGF165	Human vascular endothelial growth factor 165
IgE	Immunoglobulin E
iPSC	Induced pluripotent stem cell
ITC	Isothermal titration calorimetry
K_d	Dissociation constant
k_{off}	Rate constant for aptamer complex dissociation
LDL	Low-density lipoprotein
LDLR	Low-density lipoprotein receptor
M1	Differentiation media #1: RPMI 1640 + [B-27 supplement –insulin]
M2	Differentiation media #2: [RPMI 1640 –glucose] + B-27 supplement
M3	Differentiation media #3: RPMI 1640 + B-27 supplement
MMS	Micromagnetic separation chip
MOPS	3-(N-morpholino)propanesulfonic acid
NECEEM	Non-equilibrium capillary electrophoresis of equilibrium mixtures
NELF-E	Negative elongation factor E
nfH2O	Nuclease-free water
NGS	Next-generation sequencing
NMM	N-methyl mesoporphyrin
PCR	Polymerase chain reaction
PDMS	Polydimethylsiloxane
PLN	Phospholamban
PNA	Peptide nucleic acid
PSA	Prostate-specific antigen
PSMA	Prostate-specific membrane antigen
ptDNA	Phosphorothioate DNA

QPASS	Quantitative parallel aptamer selection system
RFU	Relative fluorescence units
R110	Rhodamine 110
RME	Receptor-mediated endocytosis
RNA	Ribonucleic acid
ROCK	Rho-associated protein kinase
RPMI 1640	Roswell Park Memorial Institute 1640 medium
RSD	Relative standard deviation
SCVI	Stanford University Cardiovascular Institute
SERCA	Sarco(endo)plasmic reticulum calcium ATPase
SELEX	Systematic evolution of ligands by exponential enrichment
siRNA	Small interfering ribonucleic acid
SPIDR	Small protein-interacting DNA and RNA
ssDNA	Single-stranded deoxyribonucleic acid
Taq	*Thermus aquaticus*
TBE	Tris-borate-EDTA buffer
Tfr1	Transferrin receptor 1
Tris	2-Amino-2-hydroxymethyl-propane-1,3-diol
UMII	University of Minnesota Informatics Institute
UMGC	University of Minnesota Genomics Center
UV	Ultraviolet
UV-Vis	Ultraviolet-visible absorption spectroscopy
µFFE	Micro-free flow electrophoresis
µFFE-SELEX	Micro-free flow electrophoresis–systematic evolution of ligands by exponential enrichment

Chapter 1: Introduction

1.1 Motivation

Affinity reagents, molecules designed to bind to a specific chemical or biological target, have become an integral part of our modern world. From monitoring metabolite levels in a patient's blood, to identifying toxins in packaged foods, to neutralizing environmental contaminants, to purifying and extracting a new laboratory synthesis product, affinity reagents are needed on their own or as a part of a larger assembly to detect, capture, or modify a limitless assortment of molecular targets. While affinity reagents can take many forms, the most well-known and widespread are antibodies, large glycoproteins generated by, and invaluable to, the immune systems of many animals. The large, rigid framework of an antibody equipped with variable "sticky" ends to find a matching antigen provides an excellent system to generate affinity for any target desired, and the advent of the antibody-secreting hybridoma in 1975[1] brought antibody production to a significantly more scalable platform. This paved the way for a new era of antibody discovery and research, and elevated the potential and feasibility of commercial affinity reagents. To be sure, antibodies are a valuable resource in research, medical, and commercial applications that facilitate many processes and procedures that might not otherwise be possible, and it could be argued that they are responsible for the revolution of affinity reagents that has taken place. However, their decades-long reign as the first of their kind has led antibodies to be viewed as the consummate affinity reagent rather than one example of many, with strengths and weaknesses just like any other.

The fact that scientists could take advantage of a host animal's immune response to generate large glycoproteins that were initially impossible to fully characterize, let alone synthesize on the benchtop, allowed antibody technology to proceed early and quickly. Now, however, it is this reliance on animals and cellular machinery that is the greatest weakness of antibodies. Because antibody production is carried out by the organism at the cellular level, there is little that researchers can do to control the process to reduce inherent batch-to-batch variation, and purification and characterization are much more complex and less efficient than for cell-free or recombinant synthesis. It is unsurprising, therefore, that antibody quality and variability is often cited as one of the chief causes of unreproducible, and therefore unreliable, biological research.[2] One study found that less than half of the

thousands of commercial antibodies tested had specific affinity to the advertised target,[3] and poor quality and variation in antibodies are believed to be largely to blame for a study that was unable to reproduce 47 of 53 landmark preclinical oncology studies.[4, 5]

One promising alternative is aptamers, short sequences of RNA or single stranded DNA with high affinity and selectivity for a particular target. Aptamers already exist for a wide range of targets, and unlike antibodies, aptamers are produced by *de novo* solid-phase synthesis, which requires no cells or animals and yields batches that are essentially identical. While numerous other advantages, such as enhanced stability and ease of modification, have also contributed to a recent surge in aptamer research, antibodies are still the default affinity reagent in most research and commercial applications despite their relative unreliability. While part of this is surely due to antibodies' legacy of ubiquity and researchers' disinclination to introduce new variables unnecessarily, part of the blame also lies with the process of selecting aptamers for a new target, which can be more complex and more limiting than at first glance. The principles of aptamer selection (SELEX) are simple enough, but the procedure can be difficult in practice, varying from lab to lab and from target to target, with some common issues and limitations that can scare away potential aptamer converts.

Significant improvements to the SELEX process are sorely need, particularly those to decrease the limitations of SELEX and increase its accessibility. Significant SELEX optimizations could lead to an increase in aptamer usage in novel applications and give researchers and consumers a choice of affinity reagent where antibodies have in the past been uncontested. Therefore, this dissertation centers on improving methods for selection of new aptamers which could be accessible to non-specialized research groups, and filling current gaps in the aptamer technology toolbox.

1.2 Aptamers

Though molecular biology's central dogma portrays nucleic acids as chemically static molecules designed for storage and transmission of genetic information,[6] the capacity of nucleic acids to carry out more varied processes in nature, such as catalysis, has been known since the 1970s.[7] Following the logical progression, scientists built on nature's

diverse usage of nucleic acids to develop sequences with new and useful functions. Aptamers, short sequences of single stranded DNA (ssDNA) or RNA with affinity for a particular target, were one such development that emerged from this work in the early 1990s, and they have grown in prevalence and capability ever since.[8-11] Aptamers have been selected for a huge range of targets including metal ions,[12-14] small molecules,[15-19] lipids,[20, 21] proteins and protein complexes,[22-26] viruses,[27-30] and even whole cells,[31-34] making them adaptable and appealing for a variety of uses.

1.2.1 Current applications of aptamers

Due to their flexibility and wide applicability, nucleic acid aptamers have found numerous applications across a variety of fields. In the realm of analytical assays, aptamers have been applied to affinity chromatography and other biomolecule purification,[35-37] including separating enantiomers,[38, 39] and many enzyme-linked immunosorbent assays (ELISAs) are switching from antibodies to aptamers as the affinity reagent.[40-42] Aptamers also feature in numerous commercial assays and applications such as detection of specific mycotoxins or bacteria in food,[43, 44] medical diagnosis based on blood biomarkers,[45, 46] cell sorting and protein pulldown,[47] and hot-start PCR.[48]

The medical field has been slower to embrace aptamers, but many aptamers are finding use as specific targeting agents for imaging contrast agents,[49, 50] small interfering RNA (siRNA),[51] and nanoparticles.[52] Unfortunately, while many in the field view pharmaceutical aptamers as the potential pinnacle of aptamer technology, only one aptamer-based drug, Macugen, has been FDA approved and made it to market. However, at least ten aptamer-based drugs have reached clinical trials so far (Table 1.1) for indications ranging from diabetes to cancer, and countless more are in preclinical stages.

1.2.2 Advantages of aptamers

Aptamers have a number of distinct advantages over other affinity reagents such as antibodies. Most notably, aptamers are generated by solid-phase synthesis, an inexpensive, scalable, and easily automated technique. In this way, aptamers can be generated (and adjusted) with nothing more than knowledge of the sequence. This stands in contrast to antibody production, which is primarily through expression in specific hybridoma cell lines

Clinical name (aptamer name)	Primary indication or usage	Status
Macugen (Pegaptanib)[53, 54]	Age-related macular degeneration	Approved
Zimura (ARC1905)[55, 56]	Age-related macular degeneration	II (C)
AGRO100 (AS1411)[57]	Myeloid leukemia	II (C)
Olaptesed pegol (NOX-A12)[58, 59]	Colorectal, pancreatic cancer	II (C)
Emapticap pegol (NOX-E36)[60, 61]	Type II diabetes, albuminuria	II (C)
Lexaptepid pegol (NOX-H94)[62, 63]	Anemia of chronic inflammation	II (C)
Egaptivon pegol (ARC1779)[64, 65]	Thrombosis, von Willebrand disease	II (C)
REG1 (rb006/rb007) [66-68]	Reversible anticoagulant	III (T)
Fovista (E10030)[69, 70]	Age-related macular degeneration	III (T)
ARC19499 (BAX499)[71, 72]	Hemophilia	I (T)
(NU172)[73]	Short-term anticoagulant	I (U)

Table 1.1: Therapeutic aptamers in clinical trial. In cases of aptamers in clinical trial for multiple indications, only the indication or usage (and corresponding trial status) for which the aptamer has completed the highest clinical trial phase is listed. Trial status lists the highest trial phase for the aptamer has reached along with whether this phase was completed ("C"), was terminated ("T"), or is unknown.

for each antibody. Thus, production not only inherits all of the batch-to-batch variation inherent in cell expression, but it requires access the specific hybridoma line itself, not to mention the associated time and expertise necessary for cell expression and maintenance. Additionally, aptamers are highly stable over a wide range of pH, temperature, and ionic strength, and they can refold spontaneously after denaturation.[74] This makes aptamers particularly well suited to platforms requiring repeated usage since they can be used to capture a target, selectively denatured by heat or pH to release the target, then renatured to allow tests to begin anew.[75] Finally, aptamers are easy to chemically link or modify during the synthesis process at virtually any position for customized applications. Aptamers' physical and synthetic flexibility gives them the added potential to function as both affinity probe and signaling entity with the addition of a fluorophore or fluorophore-quencher pair;[76] antibodies are far too large and rigid for this behavior to be accessible.[77]

1.3 SELEX

1.3.1 The SELEX method

First demonstrated independently by Ellington and Szostak[8] and by Tuerk and Gold[11] in 1990, the process of *in vitro* aptamer selection has come to be known as Systematic Evolution of Ligands by Exponential Enrichment (SELEX). The process starts with a randomized library of oligonucleotide sequences (oligos), either RNA or ssDNA.

Each sequence is composed of a static primer region of roughly 20 bases on each end sandwiching a random region – commonly 40 bases, but sometimes ranging from 20 to 60 bases. The ends serve as a primer region for PCR and may be labeled with a fluorophore, affinity tag, or other modification, particularly on the 5' end (Figure 1.1).

To begin, a small amount of the target of interest is incubated with the concentrated random oligo pool. The massive number of sequences (around 10^{13}) creates sufficient structural diversity for numerous sequences to compete for binding with the limited amount of target. The *in vitro* nature of this incubation allows parameters such as temperature and ionic strength to be adjusted for optimized binding under the specified conditions. Next, the unbound sequences are separated from target-oligo complexes and removed to waste. Selective partitioning is key, as either losing a large portion of complexes or collecting a large number of the unwanted unbound oligos can severely diminish the efficiency of the selection. This separation can be achieved by many different methods and will be addressed below and in Chapter 2. The complexed sequences are then amplified by PCR, which not only copies sequences with affinity but also provides an opportunity for sequence mutations, which may enhance binding. For RNA aptamers, transcription and reverse transcription steps are also required. Both DNA and RNA require that the double-stranded PCR product be separated and the complement strand removed in a purification step.[78] This purified product becomes the starting pool for the next round, and another cycle of incubation, separation, and amplification is performed. The generic process is outlined in Figure 1.2. The affinity of the pool for the target is measured periodically to estimate the

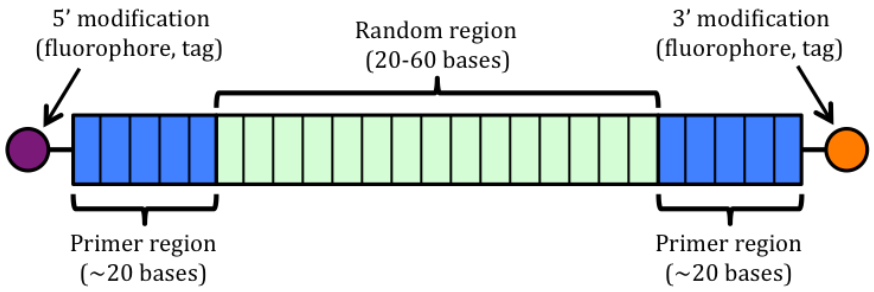

Figure 1.1: Schematic of the general oligonucleotide structure used in SELEX. Each oligonucleotide contains a random region, flanking primers, and possible modifications.

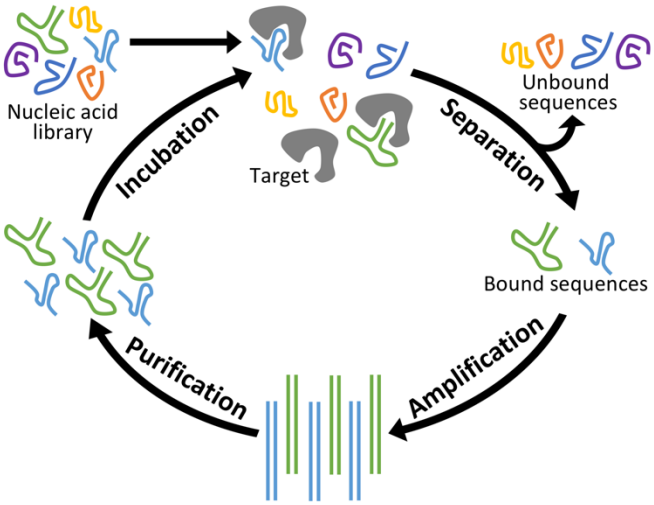

Figure 1.2: Outline of SELEX process for isolating aptamers. The oligonucleotide library undergoes incubation with the target of interest, separation to remove sequences not bound to the target, amplification of binding sequences, and purification to remove complementary nucleotide strands. RNA selections require additional transcription and reverse transcription steps (not shown).

progress of the selection, and the cycle is repeated until affinity reaches a plateau. The high-affinity pool is then sequenced to determine the specific aptamer sequences, of which a handful are chosen, randomly or systematically, for synthesis and characterization.

While there is typically some variation within the field concerning the specifics of the incubation, amplification, and purification steps, the source of by far the most variability between labs is the method of separation of bound complexes from non-binding or weakly binding sequences. SELEX was originally performed using a nitrocellulose membrane to filter the incubated sample, in theory allowing free oligos to pass through while catching any large proteins (and associated oligo sequences), but this step has evolved significantly since then to techniques with increased speed, efficiency, and flexibility. While a large number of alternate SELEX partitioning techniques are covered in depth in Chapter 2, with an emphasis on microfluidic techniques, all of the SELEX research presented herein used capillary electrophoresis as the separation mechanism.

1.3.2 Capillary electrophoresis

Capillary electrophoresis (CE) is a powerful technique that separates species in solution based on differences in their mobility in an applied electric field. CE typically uses a fused-silica capillary of 10-100 μm inner diameter and 10-60 cm in length. The capillary is filled with an electrolyte solution and a small plug of sample mixture is injected at the inlet. Then a high voltage is applied between the inlet and outlet, and species are separated based on their different rates of migration along the capillary. A small window is present

near the outlet for detection by laser-induced fluorescence (LIF) or ultraviolet-visible spectroscopy (UV-Vis), and the signal is plotted over time on an electropherogram.

Sample molecules or particles move through the capillary under the effect of multiple forces. The electrophoretic force stems from the electrostatic interaction between a molecule's net charge and the longitudinal electric field, and it is counteracted by the viscous force of the medium. A molecule's electrophoretic mobility (μ_{EP}), which is its electrophoretic velocity divided by the applied electric field, is

$$\mu_{\mathrm{EP}} = \frac{V_{\mathrm{EP}}}{E} = \frac{Q}{6\pi\eta R} \qquad \text{Equation 1.1}$$

where V_{EP} is the electrophoretic velocity, E is the applied electric field, Q is the net charge of the molecule, η is the viscosity of the medium, and R is the molecule's hydrodynamic radius. Viscosity is generally quite consistent among all analytes in a particular sample, so a molecule's electrophoretic mobility essentially varies with its charge-to-size ratio.

In addition to an electrophoretic force on charged species, the bulk solution experiences a net flow known as electroosmotic flow (EOF). For uncoated silica capillaries, the silanol groups on the interior surface ionize to negatively charged silanoates at neutral or basic pH, which causes cations in solution to collect against the surface wall to counteract the charge imbalance. The innermost layer of counterions is called the Stern layer and remains largely fixed to the capillary wall. The region just beyond marks the beginning of the diffuse layer, also called the mobile layer. The diffuse layer is still rich in cations due to incomplete shielding of the silanoates, but it is able to slide along the Stern layer. The Stern layer and diffuse layer together are referred to as electrical double layer, which is summarized in Figure 1.3.

When a voltage is applied along the capillary, the diffuse layer, which has a net positive charge due to excess solvated cations, moves toward the negatively charged cathode and pulls the bulk fluid with it. Because this force is generated primarily through the diffuse layer, the radial flow profile is flat except extremely close to the capillary wall, reducing band broadening compared to pressure-driven chromatographic separations. The strength of this bulk flow, the electroosmotic mobility (μ_{EOF}), is

$$\mu_{\mathrm{EOF}} = \frac{V_{\mathrm{EOF}}}{E} = \frac{\varepsilon\zeta}{4\pi\eta} \qquad \text{Equation 1.2}$$

where V_{EOF} is the electroosmotic velocity, ε is the solution dielectric constant near the capillary wall, and ζ is the zeta potential. The zeta potential is the radial electrical potential at the slip plane, the interface between the Stern and diffuse layers (Figure 1.3), and is affected by surface charge, ionic strength, and the presence of surfactants.

The apparent mobility (or net mobility) of an analyte is the vector sum of these two mobilities, μ_{EOF} and μ_{EP}. Apparent mobility (μ_{app}) can be determined experimentally and related to Equations 1.1 and 1.2 by

$$\mu_{app} = \mu_{EP} + \mu_{EOF} = \frac{L_d}{tE} \qquad \text{Equation 1.3}$$

where L_d is the length from the capillary inlet to the detector window, and t is the analyte peak time. Most analytes in this work have a net negative charge, meaning μ_{EOF} is toward the negative cathode and μ_{EP} is toward the positive anode. CE is typically run with the cathode at the outlet (referred to as normal polarity) so that EOF pushes all analytes toward the detector, though polarity may need to be reversed if the EOF is significantly reduced.

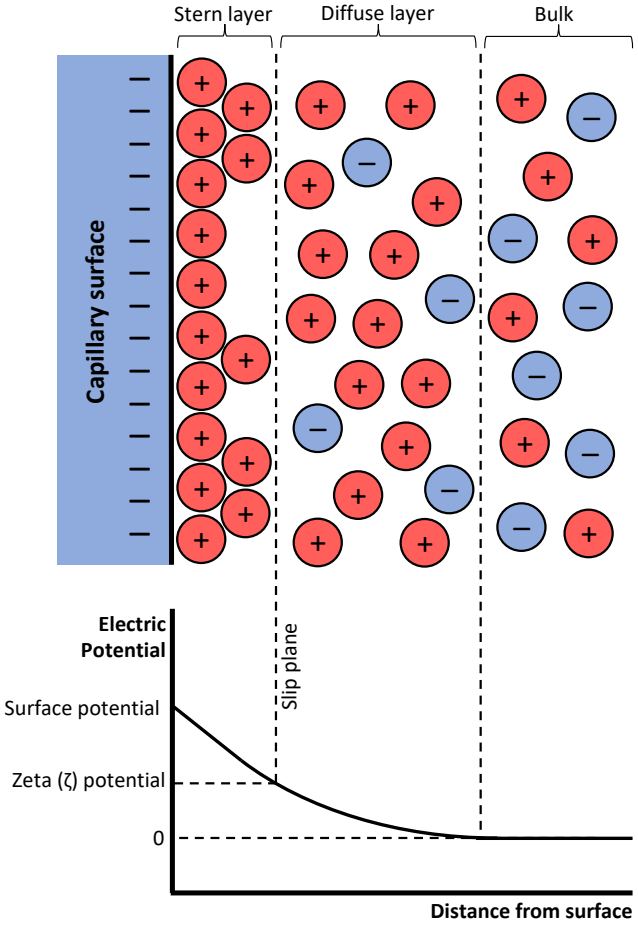

Figure 1.3: Cross-section of the electrical double layer at the capillary surface. **(Top)** The capillary wall is negatively charged at most pH, generating a double layer of solution cations. The Stern layer adheres strongly to the surface while the diffuse layer is net positive but largely mobile. **(Bottom)** The boundary between the layers (the slip plane) marks the effective edge of the solution, and the potential at this point (ζ) is proportional to EOF strength.

1.3.3 CE-SELEX separation

As with any SELEX method, capillary electrophoresis-SELEX (CE-SELEX) begins with incubation of random library DNA sequences with the target of interest to allow sequences with the best affinity to form a complex with a

target molecule. Once complexation occurs, a plug of the sample is injected and separated by CE. The separation in CE-SELEX is a specific case of affinity capillary electrophoresis (ACE), a CE separation based on noncovalent interactions between analytes and the resulting change in mobility. DNA is an excellent candidate for ACE because it has a charge-to-mass ratio of -3 kDa^{-1} (-1 charge per 330 Da), more negative than virtually any potential aptamer target. For reference, bovine serum albumin (BSA) at pH 7 has a charge-to-mass ratio less than one tenth of that.[79] As a result, any DNA-target complex experiences a significant reduction in magnitude of its electrophoretic mobility compared to free DNA.

In the majority of CE-SELEX cases, the separation is run with normal polarity. In this mode, EOF pulls all molecules to the outlet, but the electrophoretic mobility of negative analytes like DNA acts toward the inlet, so DNA elutes after most analytes. Because complexation causes a reduction in magnitude of the electrophoretic mobility, the complex with bound DNA emerges from the capillary before any free DNA (Figure 1.4A). The separation is run into a collection vial until just before free DNA begins to emerge from the outlet (calculated by capillary dimensions and the free DNA peak time), then the

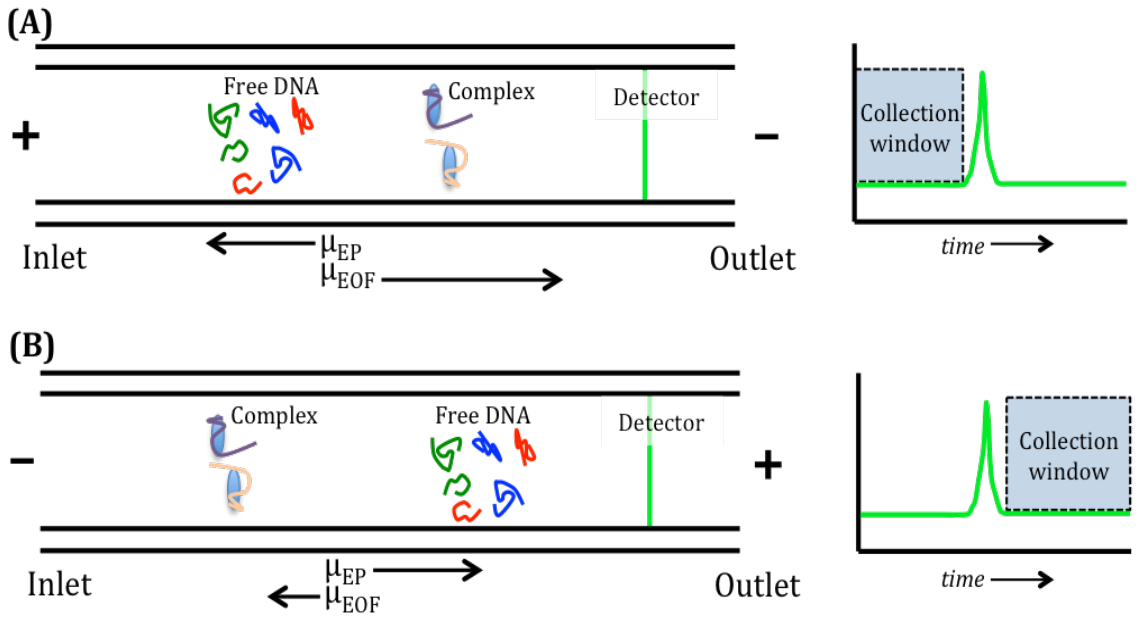

Figure 1.4: Schematic of CE-SELEX separation and electropherogram collection window. **(A)** In uncoated silica, net movement is dominated by μ_{EOF} toward the cathode, so CE is run in normal polarity and complexes are collected before free DNA. **(B)** When EOF is suppressed, net movement is dominated by μ_{EP} toward the anode, so CE is run in reverse polarity and complexes are collected after free DNA.

free DNA in the capillary is rinsed to waste. In order to increase the number of sequences collected, the CE run can be performed multiple times from the initial incubated sample.

Occasionally changes to conditions, such as high ionic strength or the presence some surfactants, can decrease the EOF significantly to the point where the magnitude of DNA's electrophoretic mobility exceeds that of the capillary's electroosmotic mobility. If this occurs, it is necessary to perform separations in reverse polarity, with the anode at the outlet, so that the electrophoretic force carries DNA toward the detector. In this case, free DNA elutes before any complex (Figure 1.4b). Therefore, the collection scheme is reversed: the separation is performed into a waste vial until the end of the free DNA peak has left the capillary, then the outlet is moved to a sample collection vial and the remaining complexes are eluted by voltage or pressure. To prevent free DNA that has already eluted from adhering to the outside of the capillary and transferring to the collection vial, the capillary outlet may be dipped into clean water or buffer before final elution.

1.4 Affinity measurement

An important part of the SELEX process is measuring the affinity of the aptamer pools for the target in question during selection, frequently in comparison to the baseline affinity for the randomized oligonucleotide library. This allows researchers to make qualitative and quantitative assessments of the selection progress and make changes to the selection if necessary. Additionally, specific sequences isolated from the completed SELEX process often undergo a battery of characterizations, such as structural modeling or kinetic studies, but assessment of affinity for the target is always the first step because of the amount of fundamental information it provides in relation to how simple the assay tends to be.

Numerous assays exist to quantify aptamer affinity for a target, each with its own advantages and disadvantages. For this research, emphasis was placed on techniques that do not require large samples, that were quick or easily automatable, and that could be performed under the relevant selection conditions. To the last point, many affinity techniques require immobilization of the target on a microbead or solid surface in order to facilitate physical separation of bound species. This makes a great deal of sense if the target

has already been immobilized during the selection process, as the conditions are representative and the method of immobilization has been optimized. However, a key advantage of CE-SELEX is that it requires no immobilization or labeling of the target, which might limit target choice or select aptamers for side targets (discussed in more detail in Chapters 2 and 3). Therefore, affinity assays were chosen which also required no target immobilization or labeling in order to maintain those advantages of CE-SELEX. CE and fluorescence polarization (FP) were chosen and are discussed after a general explanation of affinity calculation below.

1.4.1 Calculating the dissociation constant

For binding interactions between one aptamer (*A*) and one target (*T*) to form the aptamer-target complex (*C*),* all binding equations employed proceed from the generalized equilibrium

$$A + T \rightleftharpoons C \qquad \text{Equation 1.4}$$

and the corresponding equilibrium constant equation for the reverse (dissociation) reaction

$$\mathrm{K_d} = \frac{[A][T]}{[C]} \qquad \text{Equation 1.5}$$

where K_d is referred to as the dissociation constant, the most frequently used quantity to express ligand affinity. The dissociation constant is the concentration of target at which 50% of the ligand is bound and is generally in the low micromolar to high picomolar range for aptamers, with lower values representing a higher affinity.

The dissociation constant is not measured directly but is related to the fraction of aptamer bound, f_a, which for a 1:1 stoichiometry is defined as

$$f_a \equiv \frac{[C]}{[A]_t} = \frac{[C]}{[A]+[C]} \qquad \text{Equation 1.6}$$

where $[A]_t$ is the total amount of aptamer in a free or complexed state. By combining Equations 1.4 and 1.5, the equation

* Aptamer binding interactions typically have a 1:1 stoichiometry with the target except in rare cases. A different stoichiometry is often (but not always) visible via deviation in the data from Equations 1.6 or 1.7. This can be verified with the generalized Hill equation (with accurate enough data). Alternatively, analytical assays that provide kinetic data (such as surface plasmon resonance) or fundamental thermodynamic data (such as isothermal titration calorimetry) can more reliably verify the stoichiometry.

$$f_a = \frac{B_{max}[T]}{K_d + [T]} \quad \text{Equation 1.7}$$

is obtained, relating K_d and the fraction bound. B_{max} is a scaling parameter that corresponds to the calculated values for fully bound aptamer (more details below and in Chapters 3 and 4). The fraction bound can be determined experimentally by multiple techniques and is typically measured for 6-10 values of $[T]$. Equation 1.7 takes the form of a rectangular hyperbola in the first quadrant, so a hyperbolic fit of the graph f_a vs $[T]$ yields the values of K_d and B_{max}.

While the value of $[T]_t$, the total concentration of free and complexed target, is known from sample preparation, the free target concentration $[T]$ cannot be calculated without the K_d, technically leaving Equation 1.7 with too many unknowns. However, in cases where K_d is high and the total aptamer concentration $[A]_t$ is low, very little target becomes bound and $[T] \approx [T]_t$. Therefore, Equation 1.7 can be plotted versus $[T]_t$ to find a preliminary value of K_d. This value has little relative error in cases where $K_d >> [A]_{tot}$. However, this estimation breaks down when $K_d \leq [A]_{tot}$ and leads to significant error. In anticipation of low K_d aptamers, a more complete equation[80, 81] is used throughout which properly accounts for the change in $[T]$ due to complexation,

$$f_a = B_{max}\left(1 + \frac{K_d}{([T]_t - 0.5([A]_t + [T]_t + K_d - (([A]_t + [T]_t + K_d)^2 - 4[A]_t[T]_t)^{0.5})}\right)^{-1} \quad \text{Equation 1.8}$$

where the denominator represents $[T]$. Equation 1.8 provides an accurate K_d determination regardless of the relationship between K_d and $[A]_t$.

1.4.2 Fluorescence polarization

When plane polarized light illuminates a sample of organic fluorophores, only fluorophores with their transition dipole aligned parallel to the electric field of the incoming radiation are excited. Additionally, fluoresced photons are consistently emitted with that same orientation of polarization relative to the fluorophore structure. As a result, any deviation in polarization angle between the excitation and emission radiation ("depolarization") must be due to rotation of the fluorophore during the fluorescence lifetime, with a faster rotation giving rise to greater average depolarization in the emitted photons. The sample polarization (P) can be quantified with the equation

$$P = \frac{F_{||} - F_{\perp}}{F_{||} + F_{\perp}}$$ Equation 1.9

where $F_{||}$ and $F_{\perp}$ are the fluorescence intensity parallel to and perpendicular to the incident light, respectively. Thus, $P = 1$ represents no deviation from the incident plane ($F_{\perp} = 0$) while a $P = 0$ represents full depolarization of the light ($F_{||} = F_{\perp}$). Because a molecule's rate of rotation is proportional to its size, a fluorescent molecule will rotate much more slowly, and therefore yield emission with higher polarization, when bound to a large molecule than when free in solution (Figure 1.5).

Fluorescence polarization (FP), or fluorescence anisotropy, is an analytical technique which takes advantage of this phenomenon and provides information about the bound fraction of fluorescent molecules based on the polarization of emitted light. Specifically,

$$f_a = \frac{P - P_0}{P_B - P_0}$$ Equation 1.10

where P is the sample polarization, P_0 is the average polarization of free fluorophore, and P_B is the polarization value for fully bound aptamer. Unfortunately, P_B is not calculable *a priori* and can't always be found experimentally depending on the system. However, the value of P_B does not impact K_d, so the maximum change in polarization ($P_B - P_0$) is set to 100, approximately the highest polarization change seen in our aptamer FP experiments. If the target is sufficiently large to affect the rate of rotation of the fluorescent aptamer, incubating a fixed concentration of fluorescent aptamer with increasing amounts of target allows the fraction bound to be plotted against target concentration in order to extract K_d by applying Equation 1.8.

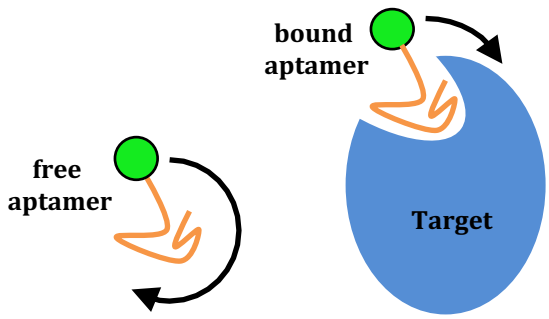

Figure 1.5: Fluorescence polarization scheme. Upon binding, the fluorescent aptamer rotates more slowly due to increased effective hydrodynamic radius, and therefore retains greater emission polarization.

Beyond the theory, FP is particularly useful because it is simple and quick to set up, and it uses small volumes of sample. Using a microplate reader, 80-100 µL of sample can generate an entire binding isotherm, and all measurements can be done in parallel in less than a minute. And because polarization is defined ratiometrically based

on parallel and perpendicular fluorescence intensities, FP is essentially insensitive to small changes in the total fluorophore concentration, which removes a substantial portion of the error inherent in sample preparation.

In practice, a number of factors can disrupt accurate FP measurement. Any change in viscosity can affect the rotational speed of species in solution, so temperature and surfactant concentration are tightly regulated during the assay. Control of the temperature and buffer composition also help to reduce fluctuation in fluorescence lifetime, which has a dramatic effect on measured polarization. One factor that can't be tightly controlled is the choice of probe molecule. FP experiments are typically designed to result in the largest possible change in polarization between the free and bound state, meaning that probes should be as small as possible while still exhibiting affinity, typically 1-2 kDa or less. However, because the intent of the assay is to measure aptamer affinity for the target, the probe used is the oligo strand itself, roughly 25 kDa for an 80mer. With such a large probe molecule, the observed depolarization is due less to rotation of the oligo in space and more to rotation of the dye moiety around single bonds and other local motion, referred to as propeller motion. This has benefits and disadvantages. Because the propeller motion is relatively fast, binding that constricts the motion mimics the large change in polarization seen from much smaller probes. Unfortunately, binding that does not cover the fluorophore, or oligos in which the fluorophore is internal but still mobile, are unlikely to give rise to significant changes in polarization. For this reason, positive binding results are typically quite accurate in aptamer FP assays (especially with large target molecules), but results showing no affinity should be considered carefully and verified by another method.

1.4.3 Capillary electrophoresis

Much has already been said about the ability of CE to efficiently separate free DNA from bound complexes, which also makes CE an excellent technique to calculate the bound aptamer fraction. CE shares with FP the ability to perform measurements on unlabeled targets in solution, which makes sample prep faster and more reproducible than for many other techniques. Though CE samples cannot be measured in parallel (except on specific multiplex instruments), commercial systems are equipped with an auto-sampler which can generally run the full assay without supervision. Unfortunately, CE affinity measurements

rely on comparison between baseline free DNA runs and sample runs that may occur hours later with many samples in between, so preventing sample degradation and instrumental drift during the assay is very important. As with FP, multiple samples are prepared and analyzed which contain a consistent amount of DNA and increasing amounts of the target. The method of affinity calculation varies depending on the stability and visibility of the complex band.

Subtractive K_d calculation (no dissociation, no complex peak). As soon as the sample is injected and begins to be separated, the complex is no longer in equilibrium with free DNA and target. This tends not to be an issue in many cases as the complex typically has a low rate of dissociation and remains bound long enough to fully separate from the free DNA band. There is frequently no visible peak containing the DNA-target complex due to low abundance, structural heterogeneity, or early dissociation. However, the free DNA peak is easily visible, and its size is proportional to the amount of unbound DNA in the sample. The increase in the bound fraction can be monitored by a corresponding decrease in the free DNA peak size using the equation

$$f_a = \frac{I_0 - I}{I_0} \qquad \text{Equation 1.11}$$

where I is the sample peak intensity (height or area) and I_0 is the average peak intensity in the absence of target. Note that the free DNA peak intensity of the fully bound aptamer is theoretically zero, hence its absence from the equation. Again, fitting based on Equation 1.8 allows extraction of the K_d. Frequently, peak area is preferred to height if the peak time varies more than 5-10%, whereas peak height may be preferred when a broad peak or noisy baseline makes determination of the area more difficult. In cases where height and area are both suitable, they can be analyzed independently. This analysis relies on an absolute fluorescence comparison rather than a ratiometric one, so sample preparation, injection, and detector sensitivity become more significant sources of error. These are generally still small compared to error in the data fitting, but an internal standard can be implemented to lessen these errors if necessary.

Ratiometric K_d calculation (complex peak or fast dissociation). In a small number of cases, the complex will be visible in the electropherogram, either as a fully

resolved peak or as a distinctive tail* of the free DNA peak. The latter occurs when the rate of dissociation is high and the DNA in the complex detaches from the target protein before it is fully resolved from the free DNA peak. (This population will continue to be referred to as "bound DNA" or "complex" even though it may not still be complexed at the time of detection.) In either case, the analysis uses the size of the free DNA signal (A_1) and the complex signal (A_2) to calculate the fraction of complex signal (C) by

$$C = \frac{A_2}{A_1 + A_2} \qquad \text{Equation 1.12}$$

for each sample. For a tailed peak, the peak is split consistently into the areas of the main peak (A_1) and the tail (A_2), as shown in Figure 1.6. Peak height cannot be used in these cases. From here, the increase in the fraction bound can be seen from the corresponding increase in the sample complex fraction according to

$$f_a = \frac{C - C_0}{1 - C_0} \qquad \text{Equation 1.13}$$

where C is the sample complex fraction and C_0 is the complex fraction in the absence of target. Fitting the fraction bound compared to target concentration by Equation 1.8 yields the K_d.

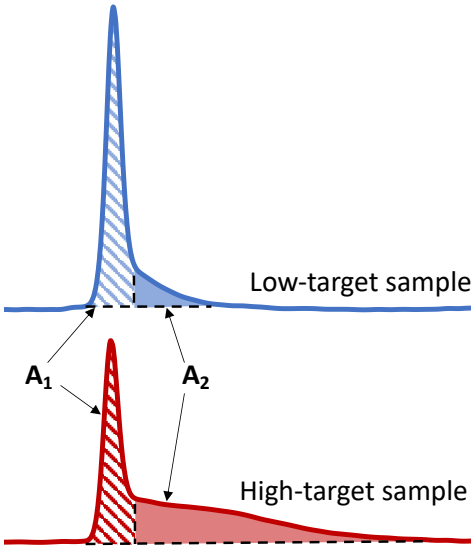

Figure 1.6: CE peak shape for aptamers that dissociate rapidly. **(Top)** A CE sample with low target concentration displays minimal tailing and has a larger free DNA peak (A_1, hashed) and a smaller complex signal (A_2, solid), resulting in a smaller complex fraction. **(Bottom)** With a high-affinity aptamer, a sample with higher target concentration displays significant tailing and has a smaller free DNA peak, larger complex signal, and higher complex fraction than in the lower target concentration case.

1.5 Scope of this dissertation

Aptamers and other functional oligonucleotides have enormous potential to influence the future landscape of analytical affinity reagents, clinical theranostics, and commercial tests and assays. To do so, however, they will have to demonstrate that they are superior to existing technologies, such as antibodies, in significant scientific and practical ways. Rather than focusing on a single train of scientific thought, this

* Note that the complex DNA presents as a tail in reverse polarity CE (as in Chapter 3) but as a front in normal polarity CE.

dissertation explores multiple threads of the aptamer story, working to improve tools for selection and characterization of functional oligonucleotides to add to their convincing case for more widespread adoption. Chapter 2 looks beyond CE-SELEX and provides an overview of recent advances in other microfluidic methods of aptamer selection and characterization, particularly with respect to efficiency and throughput. Chapter 3 describes the process of CE-SELEX against low-density lipoprotein receptor (LDLR), a membrane-bound protein which undergoes receptor mediated endocytosis, to provide proof of concept for SELEX against intact membrane proteins as well as aptamer-mediated transmembrane transport. Chapter 4 explored the process of CE-SELEX targeting leptin, an important soluble protein and adipokine involved in weight regulation and obesity, for use in future online microfluidic experiments measuring leptin secretion in real time. Chapter 5 looks at aptamer-like functional oligonucleotides which interact with the cardiac calcium cycling proteins SERCA and phospholamban, specifically exploring stem cell-derived cardiomyocytes as a system for characterizing the physiological effects of these oligos on cardiac contraction. Chapter 6 will serve as a summary of this body of work, with an eye specifically to future experimental directions to expand on the research and its applications.

Chapter 2: Microfluidic methods for aptamer selection and characterization

2.1 Summary

Nucleic acid aptamers have enormous potential as molecular recognition elements in biomedical targeting, analytical arrays, self-signaling sensors, and more. Given the tremendous applicability and the advantages of aptamers, it is not surprising that the number of aptamer-related papers has increased dramatically – indeed, 2019 and 2020 alone account for nearly a quarter of all aptamer publications to date.[82] However, the selection of aptamers for novel targets is less well represented in the literature, no doubt because of the time, resources, and expertise required to combine the disparate steps in aptamer development. In addition, successful selection of useful and applicable aptamers is never a guarantee, even in the most careful and well-intentioned cases. These practical limitations and inefficiencies in the SELEX process have hampered more widespread adoption of aptamer technologies. One innovation that has dramatically lessened the time- and labor-intensiveness of aptamer technologies is the incorporation of novel microfluidic strategies; no single advancement has led to as much improvement in speed, throughput, and automation in aptamer selection and characterization. (Microfluidics has also led to notable advances in aptamer-based sensing (aptasensors), especially involving electrochemical detection[83-86] and low-cost printed or paper-based devices;[87-89] however, this chapter will focus only on microfluidic selection and characterization techniques.) This chapter provides a detailed overview of the different types of microfluidic aptamer selection schemes, highlighting key examples of these families and the major contributions of the work. Current work in aptamer microarrays for selection and characterization is also covered.

2.2 Traditional SELEX techniques

New aptamers are selected by SELEX, an iterative combinatorial process described in Chapter 1. To recap briefly, a library of randomized RNA or ssDNA oligos is incubated with a small amount of the target of interest, where specific sequences in the library have affinity for, and bind to, the target. Next, unbound oligos are separated by one of a variety of partitioning techniques and discarded while those sequences complexed with the target are amplified by PCR. (In the case of RNA aptamers, sequences are reverse transcribed

prior to PCR and transcribed back to RNA afterward.) Finally, the PCR products are purified and complementary strands are removed. This results in a new single-stranded pool which has been enriched with sequences that display affinity for the target. At the end of each cycle, the average affinity of the pool for the target of interest is measured, and the cycle is repeated until optimal binding affinity is reached. Finally, the nucleotide pool is sequenced and analyzed, and a subset of those sequences is synthesized and characterized in terms of their affinity, selectivity, and physical properties.

Nitrocellulose filtration was the first major partitioning technique employed because of its ability to allow through nucleic acid strands while stopping larger proteins.[11] While the technique is simple in that it requires no immobilization of the target and little adjustment from protein to protein, filtration is relatively inefficient and time-consuming, requiring a dozen rounds of SELEX or more and weeks to months to achieve suitable affinity. Filtration is also only effective for large proteins, making it unsuitable for many proposed targets. Affinity chromatography-based techniques, which rely on immobilizing the target of interest on a solid support, were introduced to fill the gaps in nitrocellulose SELEX and are now the technique of choice for many. The most frequently used supports are microbeads,[90-92] which are easily retained by a microcolumn filter during selection, but other surfaces such as microplates are also used.[93, 94] In both cases, the target can be attached covalently with linker chemistry,[95] adsorbed non-specifically,[93] or linked with biotin to a streptavidin-coated surface.[96] While this technique enhances flexibility and the number of allowable targets, macroscale affinity chromatography on the whole does not significantly increase the efficiency of the selection and often uses relatively large amounts of material. Additionally, the solid supports, and any linker or capping molecules used, present potential surfaces with which aptamers may develop unwanted affinity, requiring extra negative selections to obtain target-specific aptamers.

2.3 Microfluidic SELEX techniques

While different SELEX techniques offer certain pros and cons, there are a number of advantages that hold true of most or all microfluidic SELEX methods. First, because most separation techniques typically only operate at a surface interface, shrinking the

system to yield a larger surface-to-volume ratio increases separation efficiency while reducing material consumption. In the case of affinity chromatography, this decrease in size also reduces the potential for non-specific and off-target binding, in many cases allowing negative selections to be removed altogether. Second, it has been shown that reducing the amount of target (thereby increasing the stringency of the selection) results in faster convergence of the aptamer pool to a small number of sequences.[97] Microfluidic methods excel at handling small amounts of reagents, both increasing stringency and cutting material costs. Finally, a major drawback to SELEX in general is that each phase of the cycle can be labor-intensive, time-consuming, and require special expertise. Microfluidic techniques have a much higher potential for automation and multiplexing of this process, which will reduce the time and energy invested into each new aptamer and streamline the SELEX process. This has led to the development of many microfluidic SELEX separation techniques, including those based on electrophoresis, microfluidic bead-based separations, and sol-gel encapsulation.

2.3.1 Electrophoresis-based SELEX

The first microfluidic technique introduced to enhance SELEX partitioning was capillary electrophoresis, introduced in Chapter 1. CE separates components of a mixture based on their electrophoretic mobility. Unbound DNA or RNA migrates together while oligo-target complexes, because of their altered size and charge, separate from the unbound sequences and are collected (Figure 2.1). Because DNA and RNA have a higher negative charge density than virtually any target molecule of interest, complexation results in a significant and predictable decrease in electrophoretic mobility. This, together with the

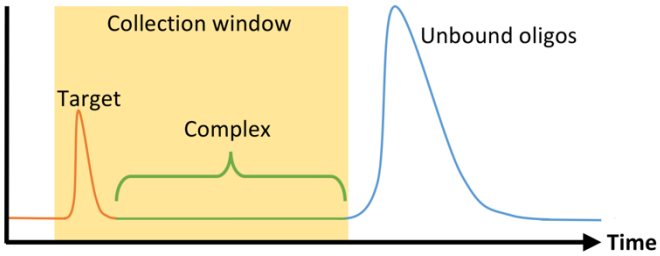

Figure 2.1: Example electropherogram of a CE-SELEX separation using normal polarity. Target and unbound oligos have very different electrophoretic mobilities and separate during CE. Target-oligo complexes migrate between the two component peaks. Target and complexes are collected for amplification while unbound oligos are not.

dramatic increase in the performance and prevalence of CE technology during the 1990s in response to the Human Genome Project, made CE the natural choice for SELEX's stringent nucleic acid separation requirements.

CE-SELEX was first implemented by Mendonsa and Bowser seeking a DNA aptamer for human immunoglobulin E (IgE).[98] Because of the high partitioning efficiency of CE, only four rounds of SELEX were required to obtain multiple aptamer sequences with K_ds below 30 nM, drastically shortening the overall selection time. Additionally, the entire incubation and separation process can be performed in free solution, which allows the process to be done without tagging or immobilizing either molecule. Similar CE-SELEX techniques have been used to select aptamers for a variety of proteins, including human immunodeficiency virus-reverse transcriptase (HIV-RT),[99] human vascular endothelial growth factor 165 (hVEGF165),[100] α-fetoprotein,[101] and human epididymis protein 4 (HE4).[102] Although the separation between bound and unbound sequences is more substantial with larger targets, CE-SELEX has also been used successfully on smaller targets including the 4.3-kDa neuropeptide-Y[103] and the 580-Da N-methyl mesoporphyrin (NMM),[15] demonstrating the flexibility and robust nature of the technique.

An additional advantage of CE-SELEX is that CE provides an excellent technique for determining the binding affinity of both the mixed selection pool and individual aptamer sequences. However, this is typically done in an additional post-selection step. The Krylov group developed a variant of CE-SELEX, deemed Non-Equilibrium Capillary Electrophoresis of Equilibrium Mixtures (NECEEM), which applied a novel analysis to extract kinetic and thermodynamic parameters of the nucleic acid pool without additional affinity measurements.[104] By supplying target-free buffer at the capillary inlet, the migrating complexes slowly unbound depending on the aptamer dissociation equilibrium and rate constants (K_d and k_{off}, respectively), which were analyzed in the separation electropherogram. Krylov further reduced the required time by removing the intermediate amplification and purification steps altogether. This "non-SELEX" method facilitated three successive NECEEM separation steps in one hour and improved the affinity of the DNA pool for the HRas protein by over four orders of magnitude.[105] While the selection stringency of this technique may be limited by the need to collect sufficient DNA for

subsequent partitioning steps, the utility of non-SELEX has been further demonstrated in identifying aptamers for three signal transduction proteins, each with at least three orders of magnitude improvement in affinity.[106]

One major concern over CE-SELEX is the small sample volume that CE can handle. Injections are often less than 10 nL,[100] so even when very high DNA concentrations are used, only about 10^{12}-10^{13} oligos are sampled per run. One way around this has been utilizing bulk separation techniques like nitrocellulose filtration prior to CE to remove a large portion of non-binding sequences before CE-SELEX.[107] This effectively samples more relevant sequences by removing a large fraction of non-binders before the CE step, although it does so at the cost of additional time and complexity.

Another approach to increase the number of sequences assessed is to move from discrete separations to continuous partitioning techniques. One example of this is micro-free flow electrophoresis (μFFE). In this technique, buffer and sample are pressure-driven through a planar channel while an electric field is applied across the channel, perpendicular to the direction of flow (Figure 2.2). Because species are deflected laterally based on their mobility, sample can be streamed continuously through the device rather than injected in discrete plugs. Binding sequences are collected through a separate exit port than non-binders. This continuous approach eliminates the complicated manual timing required in CE to obtain reproducible sample collections. A μFFE-SELEX technique was demonstrated that sampled nearly $2x10^{14}$ DNA sequences in a 30-minute separation, a 300-fold improvement over CE-SELEX.[108] Aptamers for human IgE with a Kd of 20-30 nM were selected in only two rounds, indicating no loss in performance versus CE-based techniques.

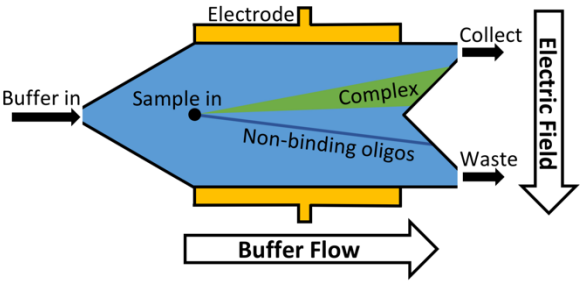

Figure 2.2: Schematic of μFFE-SELEX device. Buffer pressure at the inlet drives sample along the channel at a constant rate. A voltage is applied to the electrodes to create an electric field across the channel, deflecting non-binding sequences to waste while oligo-target complexes are collected from a separate outlet.

2.3.2 Bead–based microfluidic SELEX

Magnetic methods. Implementing microbeads as a solid support allows even small volume systems to benefit from a large surface area, increasing the physical

selection space. SELEX on microparticles was first implemented using magnetic beads almost 20 years ago and is still widely used today.[109, 110] Briefly, the target molecule is covalently attached to the surface of a magnetic (usually superparamagnetic) microparticle or nanoparticle and incubated with the nucleic acid library. Binding oligos complex with the target and become bound to the magnetic particles as well. A strong external magnet or magnetic field is then applied, which either isolates the particles from the suspension or holds them immobile while they are rinsed. While the theory is simple, the efficiency and practicality of bulk magnetic separation are limited compared to other techniques. However, combining a microfluidic approach with traditional microbead separation enhances the effectiveness of the technique drastically.

The Soh group was the first to implement magnetic microparticle SELEX on the microfluidic scale. Their first device, a continuous-flow magnetic activated chip separation device (CMACS), used a multi-stream laminar flow architecture to keep the bulk sample at the edges of the channel and a fresh buffer stream along the center (Figure 2.3). This layout had less lateral diffusion across the interface than in a single-stream flow, which enhanced separation efficiency.[111] Tiny ferromagnetic structures created strong, precise magnetic fields to guide the beads into the central buffer stream for collection. This microfluidic addition enhanced recovery of beads to over 99.5% under optimal conditions and achieved a bulk K_d of 33 nM in just one round.[112] Despite the excellent results, CMACS suffered from a number of difficulties in practice. Ideal flow conditions were only reached

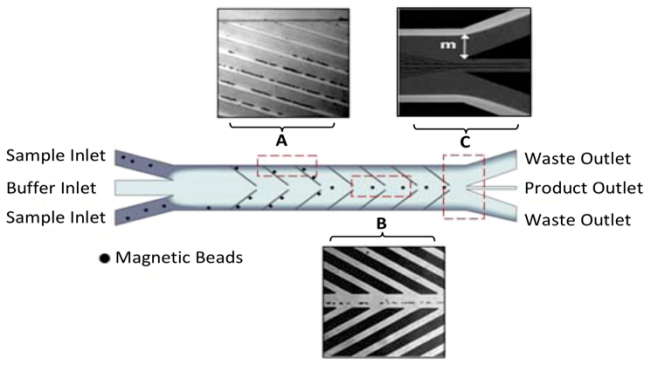

Figure 2.3: Schematic of CMACS device. Laminar flow architecture keeps the sample stream near the channel walls and flows to waste. Angled magnetized Ni strips guide the magnetic beads containing bound oligos into the central buffer stream which is collected through a separate outlet. Optical micrographs show the device during operation at **(A)** the channel wall, **(B)** the buffer stream, and **(C)** the outlet. The large distance m prevents diffusion of unwanted sequences into the central stream. Adapted from Lou *et al.*[111]

with careful adjustment under microscopic monitoring, undermining the robustness of the technique. Microbubbles and blockages also occurred frequently, which disrupted the flow streams and had a detrimental impact on aptamer separation.

To combat these issues, a new design was developed: the micromagnetic separation chip (MMS). The MMS relied on grids of patterned titanium and nickel, which were magnetized externally, to catch target-coated magnetic beads as they flowed through the channel. Once enough sample had passed through the chip, the channel was rinsed thoroughly to remove non-specifically adhered oligos. The external magnets were then removed, releasing the microbeads and target-binding sequences into solution for collection (Figure 2.4).[112] The MMS chip demonstrated recovery and partition efficiency as good as or better than those of CMACS (roughly 99.5% and 106, respectively) while offering significantly more robust and reproducible operation. MMS was first demonstrated using the protein streptavidin as the target, and later applied to platelet-derived growth factor-BB to obtain three aptamers with Kd's below 3 nM.[113] The process has also been incorporated into special selections, such as obtaining orthogonal aptamer pairs for sandwich assays,[114] aptamers with a long binding lifetime,[115] and self-reporting aptamer biosensors.[116]

Magnetic microbead SELEX continues to be perhaps the most popular microfluidic SELEX mechanism, with constant tweaking and adjustment pushing the boundaries of the technique. Recently, a device by Hong *et al.*[117] incorporated both a positive and negative selection chamber into the chip separated by a microvalve, reducing the time and hassle of negative selection. This work also performed quantitative fluorescence binding analysis on a separate microfluidic chip using magnetic target immobilization, demonstrating a trend towards miniaturization of other steps of aptamer selection as well.

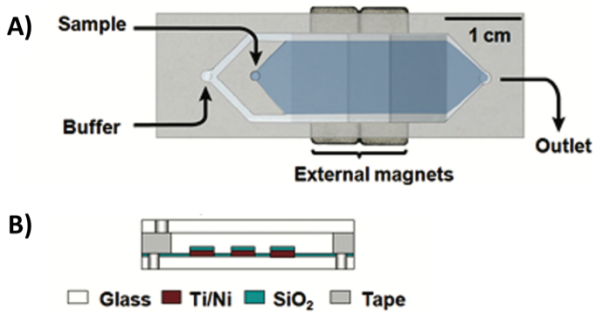

Figure 2.4: Schematic of MMS device. A **(A)** top view and **(B)** side view of the device are shown. Sequential buffer and sample inlets flow sample towards the outlet. The patterned Ti/Ni grids become magnetized by external rare-earth magnets and traps magnetic beads containing bound oligos. Adapted from Qian *et al.*[112]

Non-magnetic methods. Non-magnetic beads have also transitioned from bulk affinity chromatography-based separations to microfluidic SELEX. These beads, generally made of silica derivatives or organic polymers like agarose and acrylate, supply the same increased surface area with lower cost and without the challenges associated with magnetic separation. Recently, the Zhao group demonstrated a simple custom chip that used two sequential pinches to trap acrylate beads in the channel, the first beads containing multiple non-target proteins (negative selection) and the second beads functionalized with myoglobin (positive selection).[118] The chip is shown schematically in Figure 2.5. DNA was introduced continually at the top of the channel and flowed first through the negative selection zone to remove unwanted non-specific binders and then through the positive selection zone to retain sequences with affinity for myoglobin. The second pinch was then rinsed to remove weak binders before aptamers were eluted with DTT. This technique exemplifies the ease of performing simultaneous positive and negative selection that microfluidic SELEX offers. A peak K_d of 5 nM was obtained with exquisite specificity.

Since these beads do not move throughout the separation, similar strategies have been employed that forego the microbeads altogether, instead immobilizing the target directly on the device surface with similar effect. Liu *et al.* constructed a circuitous microfluidic path over a protein microarray so that oligos passed over four different negative selection proteins before reaching the region displaying the target, lactoferrin.[119] Then only those sequences bound to lactoferrin were eluted, achieving multiple sequences with K_ds below 10 nM.

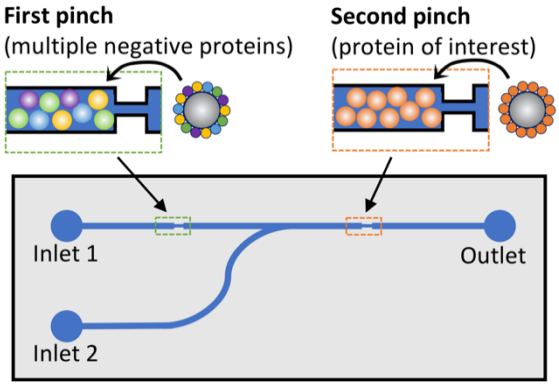

Figure 2.5: Schematic of dual positive-negative selection chip. Beads in the first pinch are coated with multiple non-target proteins for negative selection, while beads in the second pinch are coated with the target of interest. The oligos are flowed through inlet 1, and only sequences with affinity for the target but not for any of the negative proteins will bind in the second pinch. These oligos are then eluted by the addition of DDT to inlet 2. Adapted from Wang *et al.*[118]

In some cases though, the microbeads don't just provide a static surface but are actually a dynamic part of the device as with

many magnetic systems. Recently, a completely continuous separation device was developed using migration by acoustic waves (acoustophoresis) for aptamer selection.[120] Similarly to the CMACS device, the incubated sample of target-coated beads and DNA was introduced at the edges of the channel with a central buffer stream holding the sample stream against the channel walls. As sample passed down the channel, an acoustic standing wave field focused the beads to the node in the central buffer stream for collection while leaving smaller species such as unbound DNA in the waste-bound edge streams. An aptamer was obtained with sub-nanomolar affinity for prostate-specific antigen (PSA) after eight rounds of SELEX. As with other techniques not requiring a separate elution step (μFFE, CMACS), this device can overcome a common weakness of microfluidic SELEX, the small number of sequences sampled, by simply extending the time of continuous operation.

2.3.3 Sol-gel–based microfluidic SELEX

While SELEX techniques that rely on immobilizing the target have undoubtedly been successful in many cases, there has always been some concern over whether immobilization affects target conformation, occludes possible binding sites, or has other unintended consequences on the selection. One approach to circumvent covalent immobilization has been the use of sol-gel nanocomposites to trap proteins or other biomolecules.[121, 122] Briefly, monomers or nanoparticles of the gel precursor (often one or more silica derivatives) are dissolved to create an aqueous sol. Chemical additives, along with the target, are then mixed into the sol, causing the silica to coalesce and solidify into a porous framework, trapping the target in the growing gel. Gels with pores of two different sizes are favored; the smaller pores trap the macromolecule in place while the larger pores allow easy diffusion of aptamers or other ligands throughout the network. It has been shown that enzymes in the gel not only maintain their function but can be more stable against chemical and thermal denaturation than in free solution.[123, 124]

Sol-gel encapsulation was first demonstrated as a SELEX technique by Park *et al.*[125] The microfluidic device consisted of a narrow channel connecting five identical chambers, each constructed over an aluminum microheater. A droplet of the protein-containing sol-gel was spotted into each chamber and allowed to gel overnight, then a

polydimethylsiloxane (PDMS) cover sealed the chip. Incubated oligos were observed to bind with high efficiency to the trapped target but not significantly to the gel matrix. Applying current through the heater electrodes yielded enough heat to denature and elute the oligo sequences. A strength of the technique is high target density, with each 300-µm droplet holding about 0.6 ng of protein. The device isolated RNA aptamers with affinity for a yeast transcription factor[125] and TATA binding protein[126] with high affinity and in fewer rounds than with conventional SELEX. The high target density and heat-triggered release lend themselves well to a multiplexed selection, but the first attempts at simultaneous selection were fraught with issues of contamination. However, the design was improved by independent sample and elution lines as well as pneumatic valves between the reaction chambers (Figure 2.6). The new device performed selections against five targets simultaneously in less time than the previous system without contamination.[127] The capabilities and applicability of sol-gel–based SELEX have continued to expand, as the technique has selected aptamers

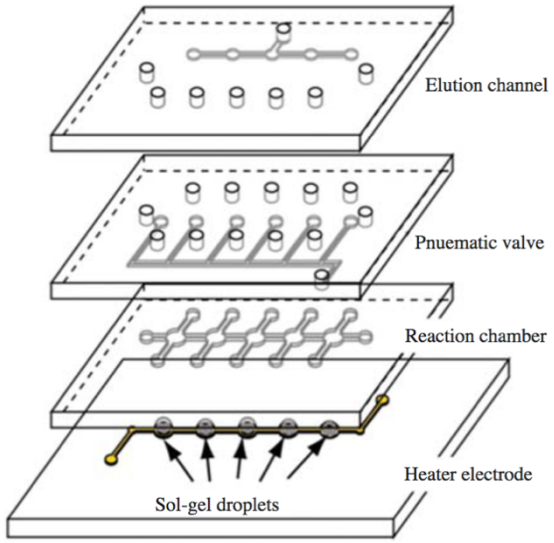

(a) Components of the platform

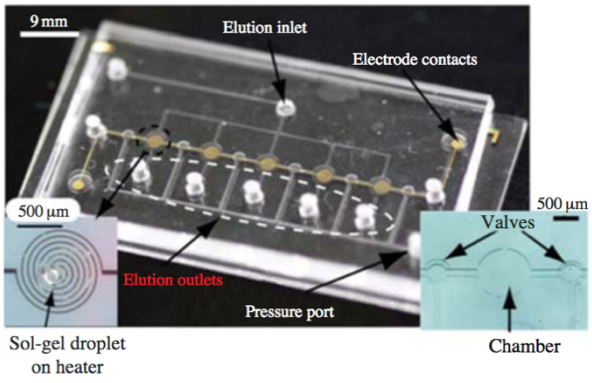

(b) Picture of the assembled platform

Figure 2.6: Schematic of multiplex sol-gel–based SELEX chip. **(a)** A schematic of the individual layers and **(b)** a picture of the assembled chip are shown. Electrode heaters (b, left inset) are patterned onto the bottom glass layer and spotted with the sol-gel. The pneumatic layer controls the valves between reaction chambers to prevent cross-contamination during elution, while the remaining layers contain the main fluidic network. With valves open, sample is flowed through the reaction chambers to incubate with each sol-gel droplet, followed by washing to remove non-specific binders. Valves are closed and aptamers are eluted by running current through the electrode heaters and collecting at each elution outlet. Reproduced from Lee *et al.*[127]

against the small molecule xanthine, even when traditional SELEX could not,[128] and against Bisphenol-A, which is too insoluble for other SELEX methods.[129]

2.3.4 Integrated microfluidic SELEX systems

As discussed previously, the SELEX cycle consists of four main steps: incubation of oligos with the target to compete for binding; partitioning of free oligos from those bound to the target; amplification of the oligo pool by PCR; and purification, whereby the complementary strand is removed to achieve a single-stranded pool again. (Additional transcription and reverse transcription steps are necessary when RNA aptamers are sought.) The techniques discussed thus far have focused on incorporating the partitioning and sometimes the incubation steps into to microfluidic environment. However, one of the main draws of a microfluidic SELEX technique, the enhanced potential for automation, is significantly limited until all parts of this cycle can be linked in a single integrated system. For this reason, many groups have pursued not only the microfluidic partitioning methods described above but also miniaturization of the amplification, purification, and intermediate steps as well.

The first major step to this end was a prototype by Hybarger *et al*. that incorporated transcription, incubation, selection, reverse transcription, and amplification into a system of microlines, all controlled by valves actuated in LabView.[130] The main achievement of the prototype was not just a seamless transition between the steps but also the use of pressurized reagent manifolds to fill, rinse, and clear sections of the system accordingly with no manual intervention. The full prototype still had a large footprint and its own share of practical difficulties, but it nonetheless set a high bar for future integrated SELEX systems.

The first integrated microfluidic SELEX chip, developed in the lab of Gwo-Bin Lee, was a three-layer, four-chamber PDMS and glass chip.[131] The processes of incubation, separation, and amplification were performed in a central sample chamber connected to reagent and waste chambers by pneumatic microvalves (Figure 2.7). The system used typical magnetic bead SELEX, first demonstrated with C-reactive protein (CRP) as the target conjugated to superparamagnetic polystyrene beads. Efficient mixing of the sample chamber was achieved within three seconds by deflection of the PDMS membrane layer

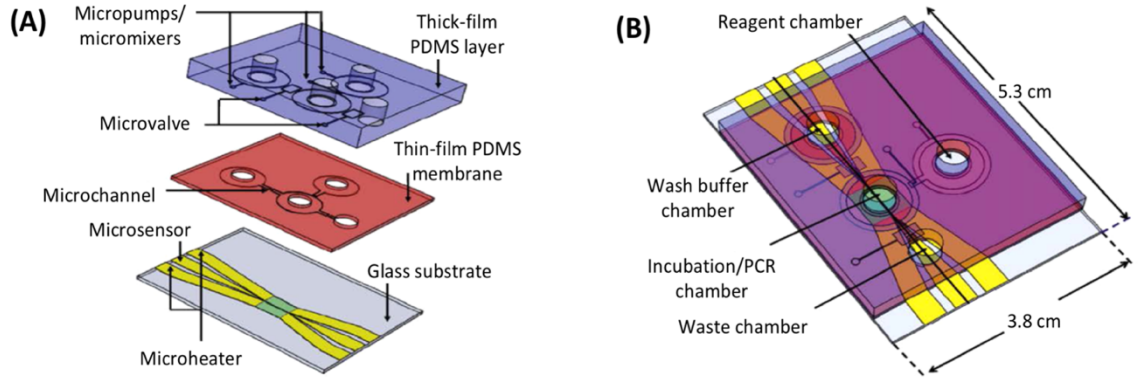

Figure 2.7: Schematic of integrated SELEX chip by Huang *et al*. **(A)** The bottom glass layer is patterned with microheaters and sensors (platinum) with associated electrodes (gold) for temperature control during PCR. The thin-film PDMS membrane and thick PDMS block facilitate all liquid handling, including pumping and mixing by pneumatic membrane deflection. **(B)** The assembled device contains a main incubation/PCR chamber connected to chambers for wash buffer, PCR reagents, and waste by low-volume microchannels to prevent dead space and bubble formation. Adapted from Huang *et al*.[131]

with pressurized air. After incubation, the microbeads and any bound aptamers were held by an external magnetic field and rinsed thoroughly from the wash buffer chamber. PCR reagents were then introduced and the temperature was cycled in the sample chamber using microheaters and microsensors patterned on the glass substrate. The inherent automation coupled with the faster temperature cycling allowed by on-chip PCR achieved a round of incubation, selection and amplification in under 60 minutes.

The system was further enhanced to improve mixing and transport, and a competitive assay chip was designed to accompany the SELEX chip and further improve automation and speed of the overall process.[132] Though the competitive assay chip was not a direct in-line addition and required intermediate manual processing, the increased efficiency of a chip-based assay provides a glimpse into the possible future of combined SELEX-aptamer characterization chips. The system has been continuously adapted and expanded to improve function and robustness. Example improvements include additional reagent and sample chambers, vacuum-driven pumps to accommodate live cells without lysis, and temperature-controlled regions of the device to speed cycling while avoiding reagent degradation.[133-135]

Purification of the PCR products to remove reagents and complementary nucleic acid strands has proven the most difficult piece to incorporate into microfluidic systems, either performed off-chip (reducing speed and automation) or absent altogether (reducing

efficiency) in the previous devices. A new design by the Lin group utilized a bead-based PCR system to isolate the active aptamer from its complement generated during PCR.[136] The device consisted of two chambers, one for incubation and selection, the other for amplification and purification (Figure 2.8). The chambers were connected by a gel-filled channel to facilitate electrophoretic transfer of the DNA from one chamber to the other and back. Each chamber was surrounded by a weir to keep the beads in the appropriate chamber while allowing reagents and buffers to come and go freely. The key to purification was the use of reverse PCR primers immobilized onto microbeads in the amplification chamber. By performing PCR with immobilized reverse primers, only aptamer strands were transferred back to the selection chamber while the complementary strands remained bound to the PCR beads. The device performed three complete rounds of selection in under 10 hours with no off-chip activity, obtaining aptamers for both protein (IgE) and small molecule (bisboronic acid) targets. While this strategy provided an elegant solution to the purification problem, the electrophoretic transfer was not without practical issues, which led to a new design that incorporated both electrophoresis and pressure-driven flow into the system.[137]

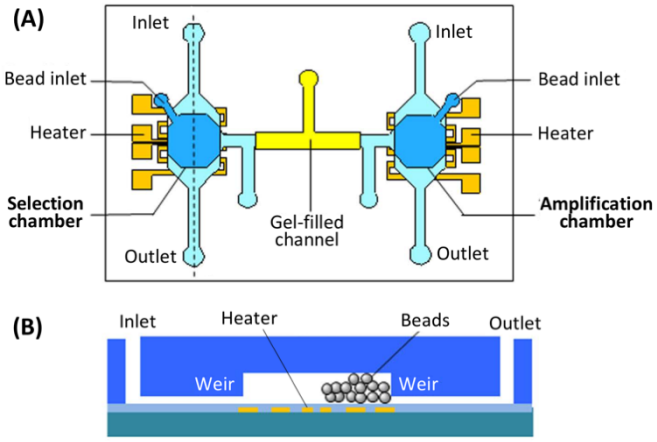

Figure 2.8: Schematic of integrated SELEX chip by Kim *et al*. **(A)** A top view of the device, showing the selection and amplification chambers connected by a gel-filled channel. **(B)** A side view of each chamber, showing weirs to prevent bead movement and patterned microheater for elution or PCR. Adapted from Kim *et al*.[136]

2.4 Microfluidic aptamer characterization

2.4.1 Sequencing

The majority of microfluidic influence in SELEX has focused on optimizing the separation and partitioning methods used in the selection itself, with the goal of obtaining sequence pools with the highest average affinity and the most high-affinity binders in the least amount of time. However, even given highly efficient selection and enrichment, the

ability to identify the best aptamers from the pool depends heavily on the nucleotide sequencing and binding characterization methods used.

Traditionally, aptamer pools were cloned into bacterial vectors and sequenced by the Sanger method, which demanded labor-intensive handling of individual bacterial colonies and usually returned a few dozen to a hundred sequences at most, a tiny percent of the selected pool. A small number of those sequences were then synthesized and had their affinity tested individually. Though this technique is still commonplace in the field, finding the best aptamers by this method is largely governed by blind luck in picking the colonies. The introduction of high-throughput next-generation sequencing (NGS) techniques has allowed researchers to view a much larger fraction of the pool and to rationally choose sequences for further characterization.[113, 138] While sequence-based criteria (usually the read count or enrichment-fold of a motif) are not always the best indicator of affinity,[100, 113] this strategy of rational sequence selection by NGS is arguably more effective than picking colonies randomly. As commercial NGS services become quicker and cheaper, choosing aptamer candidates via NGS analysis is rapidly becoming the method of choice.

2.4.2 Affinity measurement

Once individual sequences are chosen, some number of them, usually up to a few dozen, are synthesized in high purity, and the affinity of the individual sequence is determined for the target of interest as well as possibly for similar targets to determine selectivity. While NGS sequence analysis may hint at the best aptamers, it is no substitute for experimentally determining the affinity of a large number of sequences, as the true trends in affinity always deviate from those predicted by the informatics data. Even when using the microfluidic selection techniques above, affinity characterization has almost universally been done sequentially on large instrumentation. Microplate fluorescence assays, affinity capillary electrophoresis, and surface plasmon resonance are among the most common techniques for finding target affinity, in each case determining the amount of aptamer bound at many different concentrations of target to construct a binding curve and determine the aptamer dissociation constant. Because instrumental characterization techniques are robust and highly automated, it is unlikely that microfluidic characterization

methods outside microarrays will see widespread adoption until they display significant advances in performance, automation, or multiplexing.

Custom chip-based methods. DNA microarrays have largely cornered the market on microfluidic affinity assays, but custom characterization chips do still appear in the literature from time to time. For example, the magnetic microbead SELEX by Hong *et al*.[117] was presented with a custom chip that measured the fluorescence intensity of each magnetically bound sample post-partitioning, performing a microfluidic version of the normal microplate fluorescence binding assay. There is the potential for future integration of this type of technique directly into the selection, particularly when the partitioning already makes use of magnetic beads as well. Rather than toward integration, the Afi-Chip developed by Song *et al*.[139] has gone toward a universal, low-cost design for potential commercialization. The quantitative gas generation in a catalase-linked assay moves a dye bar for each sample, meaning little expertise and no expensive equipment is required to interpret the length-based results. These types of chip-based characterization platforms provide an interesting glimpse into the possible future of the microfluidic SELEX workflow; however, they don't yet represent an improvement in speed or performance compared to instrumental techniques, which is the main reason most researchers still rely on workhorse analytical techniques or DNA microarrays for characterization.

DNA microarrays. DNA microarrays are the only method of microfluidic characterization that has been widely adopted. A DNA microarray consists of thousands or millions of "spots" on a flat surface, with each spot containing many copies of a known DNA sequence. DNA can either be synthesized *in situ* or generated first and deposited onto the surface. A sample containing the fluorescently labelled target(s) of interest is then flowed over the array, and fluorescence intensity (and color, in the case of multiple targets) is scanned across the array to indicate binding. The basics of DNA microarrays and their usage in microfluidics have been reviewed elsewhere.[140, 141]

For characterization of aptamers, arrays were first used to examine and improve existing sequences. For example, aptamers against IgE have been of particular interest because a long consensus region is highly conserved through many known aptamers. Microarrays with thousands of sequences systematically mutated from a few IgE aptamers

have been used to interrogate the roles of specific bases.[142, 143] Mutations of certain bases or motifs completely eliminated binding behavior while other changes had no effect, allowing the original sequence to be truncated further.[142] Similar work has been done using microarrays with over 10,000 mutants to analyze and improve existing aptamer sequences binding to green fluorescent protein (GFP) and *Drosophila* negative elongation factor E (NELF-E).[144] Ever improving technology has continued to increase both the number of sequences that can be tested and the amount of sample space that can be interrogated by more complex rational algorithms to control mutation. Work by Kinghorn *et al*.[145] tested nearly 200,000 mutants of previously selected aptamers against a malarial antigen. The mutants were determined using the public tool Resample, which not only recognized and generated preliminary mutants around motif families but also filtered out candidates based on predicted disadvantageous pairing and structural motifs. The process produced a truncated version of an existing sequences, as well as three novel sequences, all with K_ds below 10 nM, substantially better than the starting aptamers.

Arrays are most commonly applied after SELEX in this manner, but their use as a part of the SELEX process is an interesting shortcut to condense the workflow and reduce backtracking. This was demonstrated by Cho *et al*. by combining the MMS device, NGS, and commercial microarrays into the quantitative parallel aptamer selection system (QPASS).[146] Briefly, four rounds of SELEX were performed on the MMS against the protein angiopoietin-2 (Ang2). A small aliquot from each pool underwent NGS and returned ~107 sequences, and the sequences were ranked by read count. Eight identical arrays were then generated, each containing the 235 most common sequences from each pool, including different types of linkers and control sequences, with each spot in triplicate per array. By incubating each array with a different concentration of fluorescent target, an 8-point binding isotherm (and the associated K_d) was determined simultaneously for each of the over 200 sequences. Characterizing that many sequences sequentially by standard methods would be totally unthinkable, demonstrating the power of array-based SELEX.

The researchers have since used this technique for rapid discovery of aptamer pairs that bind to different epitopes of the same target.[147] Such pairs are necessary for some highly selective analytical assays or for development of bidentate aptamer binding

schemes, but isolation of these aptamer pairs was difficult and relied largely on luck before this technique. By first generating an array of the Ang2 aptamers found previously, then incubating the target protein with the array, Ang2 was now presented for potential binding but with the binding epitope of the first aptamer occluded. A new library was then flowed over this protein-bound array to identify new sequences that bound to an independent epitope. Screening of this huge number of sequences allowed identification of multiple pairs with the strongest original aptamer sequence. By connecting these two aptamer sequences with a poly-T linker, the resulting aptamer exhibited an astounding 62 pM K_d, 300-fold stronger affinity than either sequence individually. There is still tremendous room for growth, as these examples can be scaled up to current commercially-available arrays of 1-2 million features with almost no change in time or labor. As the scale, complexity, and economics of microfluidic DNA arrays continue to improve, it seems inevitable that microarrays will become inextricably linked with the SELEX process itself.

2.5 Conclusions

Despite many advantages of aptamers over other affinity reagents such as antibodies, conventional SELEX methods for isolating new aptamers are labor-intensive and fickle at best, which has bottlenecked progress in the field. However, incorporating new microfluidic SELEX techniques, either by scaling down existing procedures or by inventing novel strategies only feasible at the microscale, has produced tremendous growth in all parts of the selection and characterization process. While it is likely that no single SELEX technique will emerge as the optimal method in all cases (given the variety of targets, selection requirements, and intended aptamer uses), these abundant new microfluidic SELEX methods all have improved efficiency and speed over the older bulk techniques they have begun to replace.

Based on the current state of the field, the author predicts two significant future directions. First, extensive work has already been done on specific selection techniques, and the author anticipates a continued shift toward integrated microfluidic methods combining selection with purification, characterization, negative selection, and/or multiplexing to take full advantage of the superb automation that microfluidics provides.

Second, the trend has thus far been towards increased complexity in prototype design to maximize speed and elegance, creating a divide between method-focused groups designing new selection techniques and those groups selecting aptamers for use in their research. The author anticipates a future movement toward simpler designs that are more cost-effective and accessible to these application-focused groups with less microfluidics expertise, such as 3D printed devices or commercially available disposable devices. In both cases, we eagerly await exciting future microfluidic developments to meet the growing aptamer screening needs in bioanalytical and medical fields.

Chapter 3: CE-SELEX against intact low-density lipoprotein receptor for aptamer-mediated endocytosis

3.1 Motivation

The advantages of DNA aptamers as affinity reagents – their stability, flexibility, and reproducible *in vitro* synthesis, to name a few – have already been expounded on in this dissertation. Unfortunately, one major drawback of aptamers has been the limited number of biomedically relevant molecules that can be targeted, which has two main factors. First, most current SELEX methods are incompatible with intact membrane proteins, which make up the majority of pharmacological targets of interest. Second, aptamers are unable to cross the plasma membrane to reach intracellular targets due to their size and charge. Because CE-SELEX separates targets without the need for immobilization and is amenable to the use of lipids to mimic the cell membrane, it is the perfect technique to develop a robust and generalizable method for aptamer selection against membrane proteins. In addition, aptamers selected for endocytosing receptors would provide a method for delivery of drugs, nanoparticles, or even other aptamers in a cell-specific manner. The work here focuses on optimization of the CE-SELEX method to target an intact membrane protein (as-yet unseen in the literature) and on development of DNA aptamers targeting low-density lipoprotein receptor for future use in aptamer-mediated endocytosis.

3.2 Background

3.2.1 Limitations of current techniques

Many of the issues with SELEX separations have largely been solved through creative negative selections, new separation techniques, methods of reducing contaminants and non-selective binding, and fine-tuned rinsing and collection that increases bound sequence retention. But one of the most pressing issues yet to be addressed is finding ways to reliably select membrane protein-targeting aptamers. Membrane proteins generally have significant non-polar regions to facilitate insertion into the plasma membrane, which can cause issues with structure and solubility when attempting to work with them in isolation. They constitute nearly a quarter of the human proteome and more than half of current drug targets,[148, 149] making them far too prevalent and important for the aptamer community to continue to simply write them off as "untargetable." A small number of aptamers have been selected for certain specific membrane proteins by cleaving the transmembrane region or

by using only a small, soluble portion of the protein.[24, 150, 151] The most significant example of this is aptamers targeting prostate specific membrane antigen (PSMA), which are known to undergo efficient receptor-mediated endocytosis (RME) and have been used as prostate cancer drug targeting agents with immense success.[152]

Despite individual successes, extracellular domain cleavage is not a reliable strategy for SELEX against membrane proteins for two reasons. First, many important membrane targets cannot be easily truncated to yield a significant, representative soluble portion. Perhaps the most exciting drug target research today involves G-protein coupled receptors (GPCRs), which are the targets of more than one third of small molecule drugs.[153] Each GPCR relies heavily on its seven non-polar transmembrane helices to anchor the tertiary structure of its selective binding site.[154] Cleavage of the transmembrane regions completely disrupts the loop interactions and any semblance of the previous structure. This is just one example superclass, but many important proteins fall into this category. The second problem is that, even for a protein with a large extracellular domain, truncating the domain may create a structure which is unrepresentative of the membrane-bound version. This may be because it exposes a region which is normally sterically inaccessible, because the end of a cleaved chain interacts with another domain, or because the transmembrane region (or the membrane itself) is necessary to maintain proper structure of the extracellular domains. For these reasons, it is unsurprising that many subsequent selections against truncated proteins have not produced aptamer sequences that perform well with intact, bound targets.

Other methods besides truncation have their merit. Cell-SELEX, in which the entire cell is targeted, or selections against vesicles prepared from cell membranes, are both techniques seen in the literature.[155] However, the target molecule cannot be chosen with these methods, and it often cannot even be identified following the selection.[156, 157] These methods represent an interesting strategy for certain types of selections but are not appropriate for obtaining aptamers for a specific membrane protein.

3.2.2 CE-SELEX with membrane-bound proteins

Besides truncation, another strategy for preventing aggregation and conformational changes in membrane proteins is the use of a surfactant membrane model. This allows the

protein to adopt a physiological conformation by solubilizing any intra- or transmembrane region in the non-polar center of the membrane model. While many common SELEX techniques, such as filtration and affinity chromatography, are incompatible with such surfactant structures, CE is known to be amenable to a wide variety of surfactants. In fact an entire class of CE separations, micellar electrokinetic chromatography (MEKC), uses charged surfactant micelles to enhance separation of uncharged analytes. Therefore, CE is an ideal choice of analytical technique to separate membrane proteins which have been solubilized in a surfactant membrane model. It is believed that this method should be far more generalizable and more likely to produce applicable aptamers than truncation.

Several types of surfactant membrane models exist, the most common of which is the micelle. A micelle is a spherical assembly of a single type of amphiphilic molecule with no internal aqueous space. The polar or charged head group faces out to interact with the aqueous environment while the tails point inward to create a wholly non-polar interior. Depending on the specific protein's structure and normal interaction with the membrane, the membrane-bound region can fully span the micelle or simply be inserted into it. While micelles have a high degree of curvature compared to the cell membrane, they were chosen for this work due to their implementation being simple and consistent. A nonionic micelle presented the best opportunity for separation between the solubilized protein and the highly negatively charged DNA, as well being the most forgiving on separation performance in the event of poor micelle size homogeneity. Octaethylene glycol monododecyl ether ($C_{12}E_8$) was used for this work, a micelle-forming nonionic surfactant frequently seen in both biological and analytical research.[158, 159]

3.2.3 Low-density lipoprotein receptor

Low-density lipoprotein receptor (LDLR) is a transport protein found on the surface of virtually all human cells. It is responsible for importing low-density lipoprotein (LDL) particles, a source of lipids for mechanical and metabolic purposes, into the cell by RME (Figure 3.1). LDLR was chosen as a SELEX target for this work for a number of reasons. First, the ultimate goal of this project was to select one or more aptamers that could not only bind to the target but also be endocytosed by the receptor. LDLRs are known to undergo RME on a short time scale (every 12-15 minutes) and in the absence of ligand,[160]

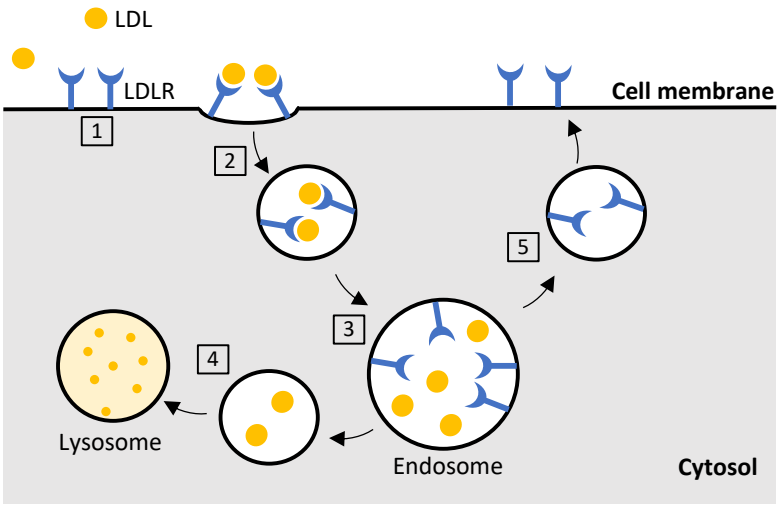

Figure 3.1: LDLR endocytic cycle. **1)** The LDLR is embedded in the cell membrane facing the extracellular space. LDL particles are trapped by the receptor and remain bound. **2)** The surrounding membrane buds inward to form a vesicle containing the LDLR, along with any bound LDL. **3)** Once the vesicle joins with the endosome, bound LDL is released into the endosomal lumen. **4)** Free LDL is sorted and exits the endosome in a vesicle bound for the lysosome, where it will be degraded. **5)** LDLR exits the endosome in a vesicle to return to the cell membrane to begin another cycle.

increasing the likelihood that internalization would take place and be observable. Second, LDLR has a large and chemically heterogeneous extracellular portion – 3 domains incorporating 767 amino acids – and only a small 50-residue cytosolic portion. Because successful SELEX depends on aptamers binding in higher numbers to the extracellular side than the cytosolic side (since the cytosolic side may be exposed when the protein is solubilized in the micelle), such a difference in size and chemistry of the two ends makes it overwhelmingly more likely that any selected aptamers are binding to one of the extracellular domains. Finally, LDLR is expressed ubiquitously in human cells, making it very easy to find sample cell lines for future testing which express (or overexpress) LDLR and exhibit spontaneous RME.

3.2.4 Optimizing selection and buffer conditions for future applications

Aptamers use a variety of different types of interactions to maintain their structure and to bind to their target, including hydrogen bonding, ring stacking, and backbone interactions.[161] For this reason, aptamer structure and binding can be sensitive to a variety of gross factors – such as temperature, pH, or ionic strength – as well as to specific ions like potassium for G quadruplex formation.[162-166] Therefore, while aptamers are "stable" over a large range of conditions in that they are not easily permanently altered, changes in these interactions due to the environmental conditions mean that aptamers may not perform equally well in all conditions. This makes it advantageous to consider the intended

applications of the aptamers during the selection process and the corresponding conditions for these applications if at all possible. This is equally as important for the target molecule, as crucial co-factors or other environmental factors may be necessary to obtain a representative target molecule structure during selection. In this particular case, aptamers targeting intact membrane-bound proteins will clearly be of most utility in physiological settings, whether with cultured cells *in vitro* or used for *in vivo* applications. The specifics of "physiological" can vary from case to case, but a number of factors are generally consistent, such as an aqueous environment with neutral pH (7-8), elevated temperature (37˚C), and high ionic strength.

On the flip side, there can be no aptamers without a successful selection, so conditions that adversely affect the selection process need to be considered carefully. For example, the CE current increases significantly with ionic strength of the running buffer, which can lead to poor temperature control, unwanted changes in viscosity, and even potential issues with instrument electronics. Therefore, prior to commencing CE-SELEX with the micelle system, multiple CE and buffer conditions were optimized to determine what level of pseudo-physiological conditions the CE instrumentation could tolerate without significant breakdown in selection or affinity assay performance.

3.3 Methods

3.3.1 Reagents

Nuclease-free water (nfH_2O) was obtained from Ambion (Austin, TX). A set of four deoxynucleoside triphosphates (dNTP, 100 mM) was obtained from Denville Scientific (Metuchen, NJ). Agarose powder and glacial acetic acid were obtained from Fisher Scientific (Waltham, MA). Molecular biology grade 3-(N-morpholino)propanesulfonic acid (MOPS) was obtained from Fluka (St. Lous, MO). All DNA libraries and sequences were obtained from Integrated DNA Technologies (Coralville, IA). Sequences of the library and labeled primers used were: 5'-6FAM-AGC AGC ACA GAG GTC AGA TG-N_{40}-CCT ATG CGT GCT ACC GTG AA-3' (FAM-labeled library), 5'-6FAM-AGC AGC ACA GAG GTC AGA TG-3' (FAM-labeled sense primer), and 5'-Biotin-TTC ACG GTA GCA CGC ATA GG-3' (biotin-labeled antisense

primer). NaOH powder was obtained from Macron Chemicals (Radnor, PA). Hyperladder DNA ladder (25-base) was obtained from Bioline Reagents (Cincinnati, OH). Boric acid powder, $CaCl_2$, KCl, and $MgCl_2$ were obtained from Mallinckrodt Pharmaceuticals (St. Louis, MO). Taq polymerase and accompanying ThermoPol buffer were obtained from New England Biolabs (Ipswitch, MA). Recombinant human low-density lipoprotein receptor (LDLR, TP300006) was obtained from OriGene (Rockville, MD). Tris(hydroxymethyl)aminomethane (Tris) was obtained from Roche Applied Science (Penzberg, Germany). Octaethylene glycol monododecyl ether ($C_{12}E_8$) powder, NaCl, glycerol (99.5%), ethidium bromide, disodium ethylenediaminetetraacetic acid (EDTA), and disodium fluorescein were obtained from Sigma-Aldrich (St. Louis, MO). $MgCl_2$ solution (25 mM) and streptavidin-coated agarose resin were obtained from Thermo Scientific (Waltham, MA).

3.3.2 Buffers and solutions

(1) CE running buffer contained 20 mM MOPS, 0.1% w/v $C_{12}E_8$, 5 mM KCl, 20 mM NaCl unless otherwise noted, and was adjusted to pH 7.5 with NaOH. (2) Sample buffer was prepared in nfH_2O and contained 20 mM MOPS, 0.1% w/v $C_{12}E_8$, 5 mM KCl, 1 mM $CaCl_2$, 16 mM NaCl unless otherwise noted, and was adjusted to pH 7.5 with NaOH. (3) PCR master mix was prepared fresh for each use in nfH_2O and contained 540 nM FAM-labeled sense primer, 540 nM biotin-labeled antisense primer, 216 nM each dNTP, 8.1 mM $MgCl_2$, and 1.08x ThermoPol buffer. (4) TBE buffer for gel electrophoresis contained 45 mM tris, 45 mM boric acid, 50 mM EDTA. (5) Purification buffer was prepared in nfH_2O and contained 10 mM tris, 50 mM NaCl, 1 mM EDTA.

3.3.3 CE equipment and protocols

All CE work was performed on a P/ACE MDQ (Beckman-Coulter) or P/ACE MDQ-Plus (SCIEX) automated CE instrument using 32 Karat data collection software. Uncoated fused silica capillary of 50-µm inner diameter and 360-µm outer diameter was used throughout, cut to 39.7 cm total length with a detection window (2-5 mm wide) burned 29.5 cm from the inlet. Unless otherwise specified, CE sample storage was set to 37˚C while capillary temperature was set to 25˚C. Rinses used 20 psi forward pressure and sample injections were made with 10 s of 0.5 psi forward pressure. Before first use, new

capillaries were rinsed with 0.15 M NaOH for 3 min, rinsed with nfH_2O for 3 min, rinsed with running buffer for at least 30 minutes, and allowed to equilibrate with running buffer for 48 hours. The capillary was rinsed with running buffer for 5 min between runs and for 15 minutes at the start and end of each day. LIF detection (488 nm excitation/520±10 nm emission) was used throughout, unless otherwise specified.

3.3.4 SELEX separation

DNA was heated at 72˚C for 5 minutes and cooled before use. For each round of SELEX, a 20-μL sample containing DNA and 10 nM LDLR in sample buffer was incubated at 37˚C for 20 minutes before selection. The first round used 100 μM random library DNA while each subsequent round used purified DNA from the previous round to make the sample as concentrated as possible, generally 1-5 μM. The sample was separated by CE at -30 kV until the end of the free DNA had migrated off the capillary (calculated from the electropherogram and capillary dimensions). The separation was then stopped manually and the outlet was dipped into a clean vial of nfH_2O and placed in a collection vial containing 50 μL of running buffer. The capillary was rinsed for 2 minutes to push bound DNA into the collection vial. The whole injection, separation, and collection process were repeated two to three additional times into the same collection vial.

3.3.5 PCR and gel electrophoresis

PCR samples were prepared with 92.5 μL master mix, 7.0 μL of DNA sample, and 0.5 μL (2.5 units) Taq polymerase, with Taq polymerase being added once the sample reached 94˚C. Each PCR experiment was run with at least one positive control (DNA sample = 50 pM random DNA library) and at least one negative control (DNA sample = nfH_2O). The thermocycler performed 25 rounds of 94˚C (30 s), 53˚C (30 s), and 72˚C (20 s) sequentially, followed by a final 10 minutes at 72˚C and storage at 4˚C.

Gel electrophoresis was performed on all non-identical PCR samples (including PCR controls) to verify amplification and check for contamination. A 1.5% or 2% w/v agarose gel made with TBE and 100 μg of ethidium bromide was run in TBE buffer at 200 V for 40 min. Gels were imaged on an ultraviolet transluminator with a Canon 1300d DLSR.

3.3.6 DNA purification

In a 10-mL affinity chromatography column, 300 μL of streptavidin-coated agarose resin and 500 μL of purification buffer were vortexed and then flushed. PCR-amplified sample DNA and 100 μL of purification buffer were introduced to the column and incubated at room temperature, vortexing periodically. After flushing with 5 mL of purification buffer, the column was then incubated at 37˚C with 200 μL of 0.15 M NaOH, vortexing periodically, and eluted into equimolar acetic acid. This NaOH incubation and elution was repeated into the same collection. The collected sample was spun in a 10-kDa centrifugal filter, rinsed with nfH_2O, spun again, and collected in two clean microcentrifuge tubes, which were vacuum centrifuged to dryness at 50˚C then stored frozen.

3.3.7 Affinity measurement

DNA was heated at 72˚C for 5 minutes and cooled before use. Samples were prepared containing 20 nM random library or aptamer pool, or 10 nM aptamer sequence, along with 0-250 nM LDLR in sample buffer, unless otherwise specified. All samples were incubated at 37˚C for 20-30 minutes before measurement.

For CE measurement, samples were separated at -30 kV and the free DNA peak height and area(s) were recorded. Samples were measured in triplicate from lowest to highest protein concentration. The uncorrected fraction bound for each concentration was calculated by the subtractive method (Equation 1.11). If the tailing of the free DNA peak increased at higher protein concentration and poor fitting was achieved with Equation 1.11, then the ratiometric calculation (Equations 1.12 and 1.13) was employed. The capillary was changed after each affinity assay.

FP measurements were performed on a BioTek Synergy 2 (Agilent) plate reader using 20-μL samples in an opaque 384-well plate. Measurements were made at 37˚C using a tungsten lamp (485±10 nm excitation/528±10 nm emission). Polarization values were measured in triplicate for all samples simultaneously with a 5-second mix between each. The uncorrected fraction bound for each concentration was calculated by Equation 1.10.

The K_d for each aptamer or pool was calculated in Origin 9.6 by fitting the triplicate uncorrected fraction bound data to a custom fit equation (Equation 1.8) with the constraints $K_d > 0$ and $B_{max} > 0$.

3.3.8 DNA sequencing and preliminary sequence analysis

Prior to sequencing, the ssDNA pool underwent PCR as above except that unlabeled primers were substituted for the FAM- and biotin-labeled primers. PCR product was then concentrated by centrifugal filtration and submitted to the University of Minnesota Genomics Center (UMGC) for Illumina sequencing library preparation (TruSeq Nano) and high-throughput sequencing (MiSeq Nano 2x150 PE).

Sequence data files were compiled using PEAR. The sense primer sequence and reverse complement sequence of the antisense primer were trimmed using Cutadapt, along with any bases outside of those sequences, to remove extraneous bases from sequencing library creation. Untrimmed reads (due to incomplete or incorrect primer sequences) were discarded. The read count of each sequence was determined using the collapser function of Fastx Toolkit and ranked for each sequence length between 35 and 45 bases. Sequences were manually removed which contained the complete sense primer or antisense primer reverse complement sequence, or which differed from one of these by one point mutation. The original primer sequences were added back to all remaining reads.

3.4 Results and Discussion

3.4.1 CE optimization

A base running buffer of 20 mM MOPS, 5 mM KCl, and 0.1% w/v $C_{12}E_8$ was initially used. MOPS was selected because of its near-physiological pK_a (7.2) and because its zwitterionic nature would add to the effective ionic strength without contributing to capillary current. MOPS concentration was limited to 20 mM as recommended for work with mammalian cells[167] in case the buffer was necessary in future cell work. Potassium is required for proper formation of the G-quadruplex, a common stabilizing DNA secondary structure.[168] First attempts also used 1 mM $CaCl_2$ in the base running buffer, as Ca^{2+} is required as a cofactor for proper LDLR folding.[169] Unfortunately, divalent cations such as Ca^{2+} can cause significant inconsistencies in the EOF, even in small quantities.[170] Initial use of calcium ion in the running buffer as well as the sample buffer gave rise to substantially less consistent peak times and shapes than in the absence of calcium, so 1 mM

$CaCl_2$ was used in the sample buffer but not in the running buffer in preparation for SELEX against LDLR.

CE buffer salt concentrations. CE separations were performed on FAM-labeled library DNA with increasing amounts of NaCl added to the base running buffer to increase the ionic strength and determine the maximum tolerable salt concentrations that could be used for selections. For this experiment, the sample buffer contained $CaCl_2$ but no NaCl. As seen in Figure 3.2A, the peak shape of library DNA changed minimally between 0 mM and 20 mM, but a substantial splitting and broadening was observed at 24 mM NaCl. The experiment was repeated and yielded similar results, indicating that concentrations of NaCl above 20 mM in the running buffer give rise to poor and unreproducible peak shape. Although performing a selection with such a peak might still be manageable, any future quantitative experiments such as affinity measurements would suffer greatly from this degraded peak shape, so 20 mM was determined to be the optimal NaCl concentration in the running buffer.

Because the addition of calcium ion increased the ionic strength of the sample buffer as compared to the running buffer, it was unknown whether the sample buffer NaCl concentration should be decreased to compensate. While high ionic strength would be preferable from an applications perspective, care must be taken when considering the

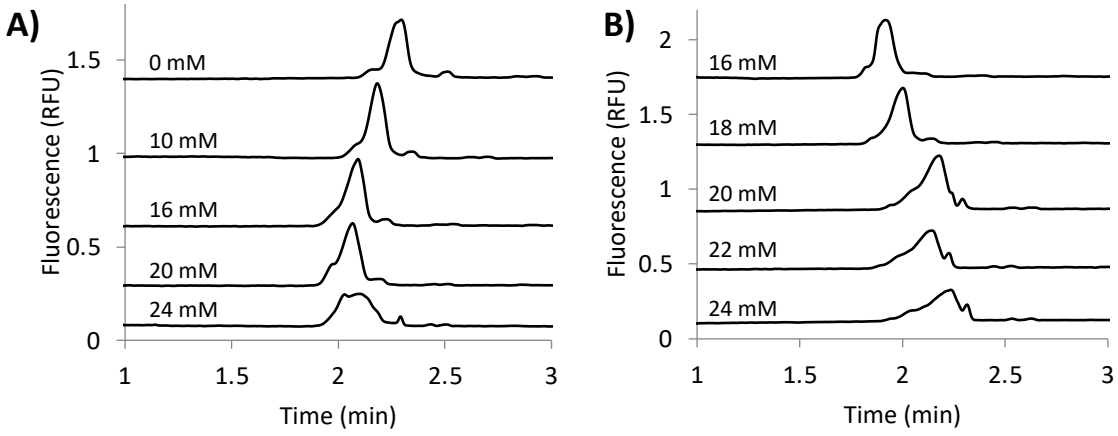

Figure 3.2: Effects of NaCl concentration on CE peak shape. **(A)** Increasing [NaCl] in the base CE running buffer had little effect on the DNA peak shape at or below 20 mM NaCl, but significant broadening and splitting was observed above 20 mM. A concentration of 20 mM NaCl in the running buffer was determined to be optimal. **(B)** Using running buffer with 20 mM NaCl, [NaCl] in the sample buffer was adjusted to observe its effect on peak shape and time. The changes observed were gradual, but the most significant change was seen between 18 mM and 20 mM NaCl. Therefore, 18 mM NaCl in the sample buffer was determined to be ideal.

relative ionic strengths of the separation and injection buffers. In typical CE, the injection plug often has a lower ionic strength than the running buffer, which generates a greater electrophoretic velocity in the injection plug when the voltage is first applied. This causes a local increase in concentration and decrease in band width when the sample reaches the boundary between the injection plug and the running buffer and slows down, a long known phenomenon called stacking.[171, 172] The reverse phenomenon occurs when the sample plug has a higher ionic strength than the running buffer: sample bands can be broadened and even split, depending on the difference in ionic concentrations.

While maintaining a constant NaCl concentration of 20 mM in the running buffer, sample incubation buffers containing 1 mM $CaCl_2$ and differing amounts NaCl were tested, and the effects on peak shape were monitored. As seen in Figure 3.2B, the free DNA peak became somewhat later and much broader as the NaCl concentration was increased steadily from 16 mM to 24 mM. Although the change in peak shape was more gradual than for the running buffer NaCl concentration, making determining the optimum concentration more difficult, the change in peak time and width seemed to be most distinct between 18 mM and 20 mM. Therefore, 18 mM was selected as the optimal sample buffer NaCl concentration.

Capillary temperature. Sample incubation at physiologically-relevant temperatures (around 37˚C) poses no performance issue for CE, but it was unclear whether separation at 37˚ would be tolerated by the assay. Increased temperature in the capillary reduces solution viscosity, which leads to increased current and can result in broader peaks. While obtaining sharp peaks and high resolution are not normally necessary in CE-SELEX because there is generally a wide window between the free DNA peak and the target complex, sharper DNA peaks allow for more efficient separation (requiring fewer selection rounds to maximize affinity) as well as more reproducible CE-based K_d measurements. Therefore, current and peak shape were monitored as the temperature was increased to determine whether a 37˚C separation was feasible.

In previous work, it was noted that a capillary current above 90-100 μA introduced substantial current fluctuation and seemed to decrease peak time reproducibility. Therefore, 10-minute separations were performed on library DNA at capillary temperatures

varying between 25˚C and 37˚C while the maximum current was monitored. The maximum current observed, 80.5 µA at 37˚C, was well below the cutoff of 90-100 µA (Figure 3.3A). In addition, no non-linear relationship between current and temperature was observed, which would have indicated Joule heating that could not be compensated by the capillary coolant system. The resulting traces in Figure 3.3B demonstrate that the DNA peak shape did not deteriorate at increased temperatures. In fact, the peak became somewhat earlier and sharper at 37˚C, which were both desirable changes.

Glycerol. Glycerol is commonly added to commercially available membrane proteins, as it was to the LDLR in this work, in high concentrations in order to circumvent issues with protein aggregation. The presence of glycerol in these experiments raised several possible CE performance issues including affecting $C_{12}E_8$ micelles, affecting EOF through surface adhesion, and affecting electrophoresis through changes in viscosity. CE runs were performed with DNA library in sample buffer that also contained increasing amounts of glycerol in order to determine if the presence of glycerol would be deleterious. The glycerol concentration was taken up to 2.5% by volume, which would be the highest concentration anticipated during affinity measurements. The effects of glycerol were surprisingly significant, as seen in Figure 3.4. Even at low concentrations, the peak became substantially deformed, with the peak height decreasing more than 5-fold at 2.5%. Additionally, multiple runs at the same glycerol concentration saw the peak become later

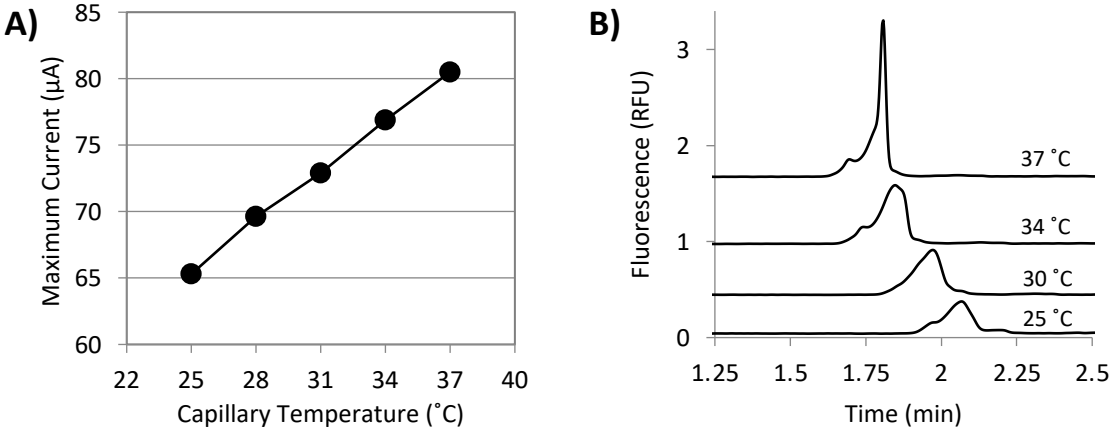

Figure 3.3: Impact of capillary temperature on CE current and peak shape. **(A)** The maximum current observed was plotted against the capillary set temperature. Even at 37˚C, the current was below the planned cutoff of 90-100 µA. Additionally, the linear relationship indicates no excessive Joule heating which would impact performance. **(B)** CE peaks of random DNA are earlier and sharper at increased temperature.

and shorter, so there are also undoubtedly effects of cumulative runs beyond the glycerol concentration of the current sample. Although a similar experiment to determine the effect of glycerol on FP performance had initially been planned, the effect of glycerol on CE performance alone was substantial enough to necessitate a complete buffer swap of the LDLR to remove all glycerol before any CE was performed.

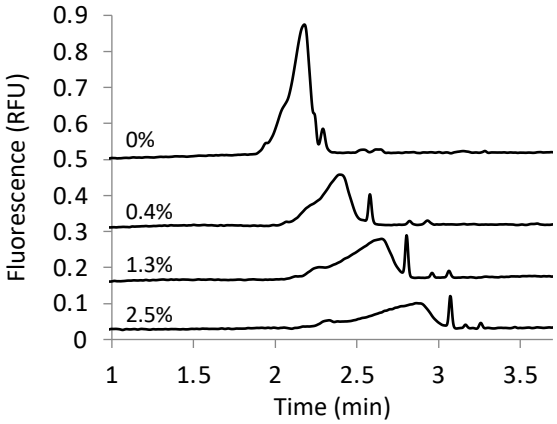

Figure 3.4: Effects of glycerol in sample buffer on CE peak shape. The DNA peak shifts later and becomes substantially smaller and broader in the presence of glycerol. The effect is concentration dependent and noticeable even at low levels of glycerol.

3.4.2 CE-SELEX against LDLR and pool sequencing

Concurrent with optimization experiments, multiple preliminary CE-SELEX experiments were performed including any optimized conditions known at the time. The purpose of these selections was to confirm proper operation of the other components of the SELEX method – collection, amplification, affinity measurements, and the like – with the LDLR target and micelle-containing buffer. Unfortunately, technical instrumentation issues precluded subsequent selections after optimized conditions were finalized, so all further data presented extends from the final preliminary selection. The selection differed from the optimized conditions above only minimally, as outlined in Table 3.1.

Four complete rounds of CE-SELEX were carried out, consisting of incubation, CE separation, PCR amplification, and purification. During CE, the end of the free DNA peak was judged to be the point at which the fluorescence intensity crossed below 1% of the peak height above the baseline. This point is shown for rounds 1 and 2 in Figure 3.5. (A peak height of 100 RFU, the detector maximum, was used for round 1 even though the peak surely extends significantly above this.) Separation was stopped manually when this point reached the end of the capillary, calculated by multiplying the electropherogram time by the ratio of the full capillary length to the inlet-to-detector length (1.357). The complex DNA remaining in the capillary was then collected separately with a pressure rinse into a

small collection vial. Because the amount of DNA collected was unknown, preliminary PCR assays and agarose gel electrophoresis were performed on dilutions of the collection ranging from 1× to 0.001× to determine the ideal dilution for amplification. The remaining collected DNA was diluted appropriately and amplified, usually yielding 10-14 sample tubes of PCR. Gel electrophoresis was performed on each amplified sample and any tubes with poor amplification or incorrectly sized sequences were excluded. This generated enough DNA to prepare a new incubation pool of 1-5 μM while saving enough for affinity measurements and sequencing.

	Actual	Optimized
MOPS (RB/SB)	20 mM	20 mM
KCl (RB/SB)	5 mM	5 mM
$C_{12}E_8$ (RB/SB)	0.1%	0.1%
NaCl (RB)	20 mM	20 mM
NaCl (SB)	**16 mM**	**18 mM**
$CaCl_2$ (SB)	1 mM	1 mM
Glycerol (SB)	Removed	Removed
pH (RB/SB)	**7.5**	**7.4**
Sample temperature	37˚C	37˚C
Capillary temperature	**25˚C**	**37˚C**

Table 3.1: LDLR CE-SELEX actual and optimized conditions. Elements of the CE running buffer (RB), sample buffer (SB), or CE conditions are shown, comparing the actual conditions used for the selection with the ideal conditions based on optimization experiments. The three deviations between actual and optimized conditions are shown in bold.

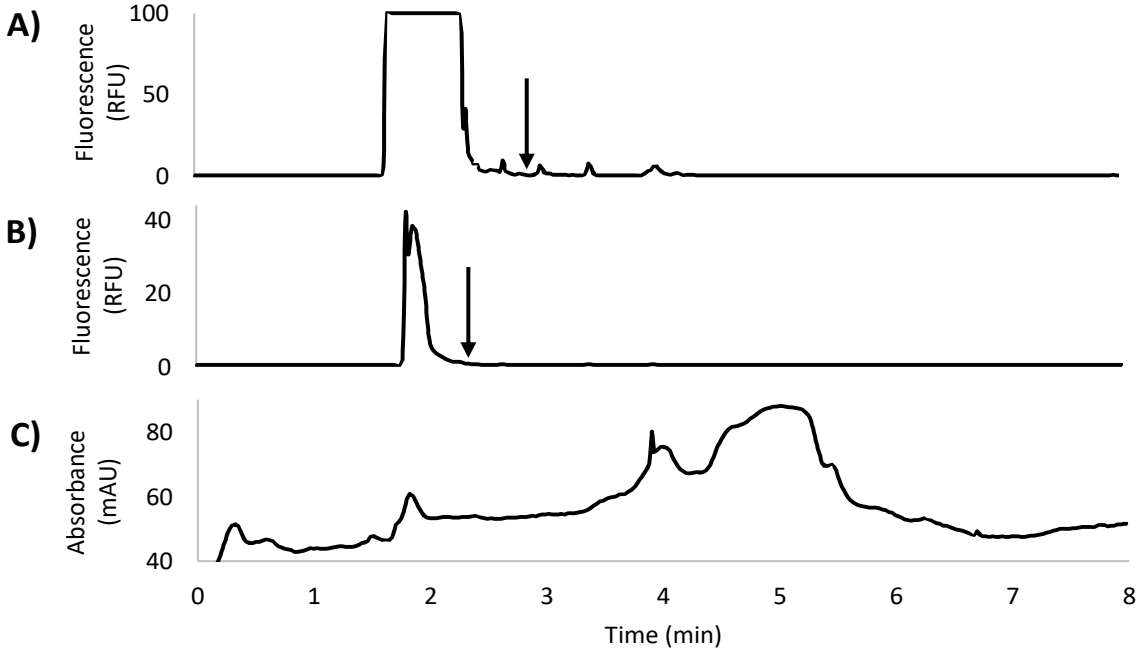

Figure 3.5: CE-SELEX sample traces for LDLR selection. **(A)** The LIF trace for round 1 of selection is shown, with the arrow indicating the start of the collection window. Note that the 100-μM DNA sample maxed the detector here. **(B)** The LIF trace for round 2 of selection shows a free DNA peak at a similar time but smaller than in round 1 (to be expected), so the collection window began earlier. Subsequent rounds of selection were visually similar to round 2. **C)** A UV trace (200 nm) of LDLR alone confirms that the main LDLR band passes the detector after the DNA, around 4-5 minutes.

The affinity of the starting library for LDLR was measured to be 303±64 nM by FP (Figure 3.6), and the affinity of each purified pool for LDLR was measured in turn to evaluate the trend in affinity over the course of the selection. As seen in figure 3.6B, the decrease in K_d to rounds 3 and 4 marks a 5-fold improvement over the starting library, indicating an apparently successful selection.

The round 4 aptamer pool was sequenced and reads were processed to yield a list of approximately 380,000 sequences. The most common sequences are shown in the Appendix (Table A.1)**.** The highest read count among all sequences was 740, making up less than 1% of the sequencing pool, and only six sequences had a read count above 100. Though the lack of convergence is surprising, previous CE-SELEX research in our group has suggested that the technique leads to more heterogeneous aptamer pools than do other SELEX methods.[100] About 97% of sequences with the proper primer structure had between 79 and 81 bases, initially suggesting good performance of amplification phases. However, around 1000 sequences had sections of the random region identical to within one point mutation of the sense primer or the antisense primer reverse complement. It is statistically unlikely this would have happened once by chance let alone multiple times, so it is clear that primers were improperly inserted during PCR on multiple occasions. One possible

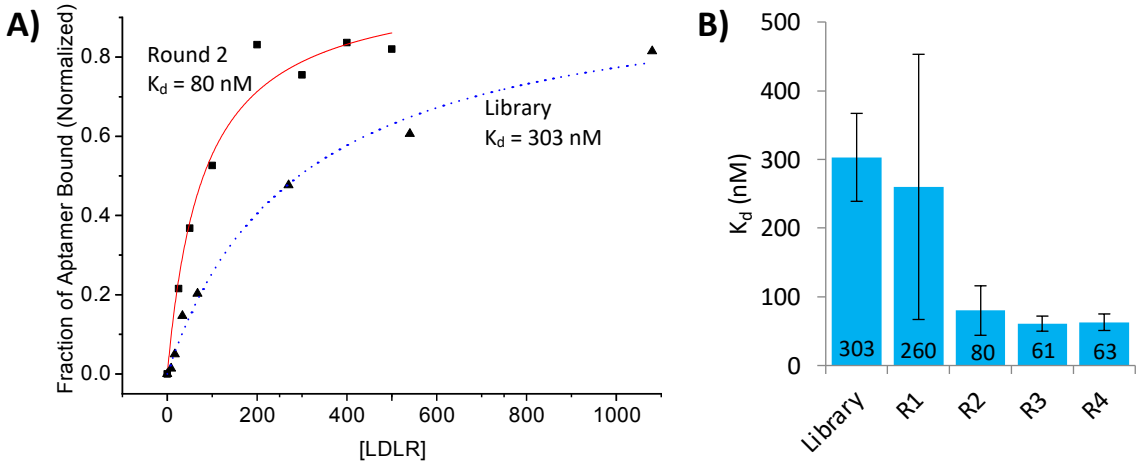

Figure 3.6: LDLR aptamer pool affinity trend measured by FP. **(A)** Binding plots are shown for the starting library (triangle, dashed line) and round 2 aptamer pool (square, solid line), illustrating the increase in affinity during SELEX. Error bars are omitted for clarity. The hyperbolic fit line (Equation 1.8) for each pool is shown, from which the K_d was calculated. **(B)** The K_d shows a significant downward trend from one round to the next, indicating an apparently successful selection. Error bars indicate the standard error of the K_d based on the fit. Note that the value shown for "Library" indicates data for one affinity assay trial performed prior to sequencing, not an average of all library affinity data.

culprit for this unusual behavior is the use of an intentionally mutation-prone PCR method during selection to encourage substitutions during amplification to enlarge the sequence space sampled. Regardless of the cause, these sequences were clearly present in the pool due to biases in amplification rather than affinity selection, so they were removed before any further analysis.

Current high throughput methods of aptamer characterization like DNA microarrays are not amenable to the $C_{12}E_8$ system, so only a handful of sequences could be selected for further analysis (Table 3.2). First, all sequences with a read count greater than one (approximately 4200 sequences) were grouped into clusters with high base position similarity using AptaCluster. An example cluster is shown in the Appendix (Table A.2). AptaCluster identified 42 clusters, nine of which contained 10 or more sequences. These nine clusters were ranked by the sum of the read counts of all sequences in the cluster, and the most abundant sequence in each of the top three clusters was chosen for analysis. This was done in an attempt to select sequences that were representative of the pool while not being similar to each other. By this method, A1, A3, and A4 were selected. While these turned out to be the three highest abundance sequences in the pool, the more complex analysis of clustering and read counting illustrated that there were also a large number of

A1
AGCAGCACAGAGGTCAGATG**CTCATACGTTTAACTTGATTCTGCTAATTTAAGACTCTGG**TTCACGGTAGCACGCATAGG
A3
AGCAGCACAGAGGTCAGATG**TTGCATGGATTGAGTTTCATTACGTTATACATGGTCATTG**TTCACGGTAGCACGCATAGG
A4
AGCAGCACAGAGGTCAGATG**ACATCATGGGTTATATGCACACAGGTTTAACATCGTGTAC**TTCACGGTAGCACGCATAGG
A10
AGCAGCACAGAGGTCAGATG**AGGAGTACACAAGCATAAGTTAATCAGGGTTTCTGTCTCA**TTCACGGTAGCACGCATAGG
A3492
AGCAGCACAGAGGTCAGATG**ATCGGGGTCAAGAAAAAGCGACGAGTTCCTGCCACATCAG**TTCACGGTAGCACGCATAGG
A178749
AGCAGCACAGAGGTCAGATG**CGCACGTGTAAGACATCGGAGTCTGTCCGTATCCAGCTGG**TTCACGGTAGCACGCATAGG
A0 (Poly-T control)
AGCAGCACAGAGGTCAGATG**TTTTTTTTTTTTTTTTTTTTTTTTTTTTTTTTTTTTTTTTTTTT**TTCACGGTAGCACGCATAGG

Table 3.2: LDLR aptamer sequences selected for further characterization. Sequences are shown with the random region in bold. A1, A3, and A4 were selected fully rationally. A178749 was selected completely randomly. A10 and A3492 were partly rational and partly random. A0 is a poly-T control sequence.

other very similar abundant sequences in the pool, adding confidence to the decision to select these.

While choosing sequences from the list rationally, such as by read count, would seem to improve the odds of finding high-affinity sequences, some sources indicate that using read count or other statistical metrics does not lead to better results than choosing sequences randomly from the sequence pool.[100, 113] Therefore, increasing amounts of randomness were introduced while selecting the final three sequences. First, from the remaining clusters containing 10 or more sequences, one cluster was chosen randomly and the highest abundance sequence was selected for characterization (A10). Additionally, one sequence was chosen randomly from among the approximately 4,200 sequences with a read count of two or higher (A3492). Finally, one sequence was chosen randomly among all sequences in the aptamer pool of roughly 380,000 (A178749). An additional control sequence was synthesized with a poly-T random region (A0) intended to display little secondary structure or binding.

3.4.3 Affinity of selected aptamers

The affinity of each of the selected aptamers, along with A0 and the initial random library, was evaluated by FP and CE (Table 3.3). For FP assays, the uncorrected fraction bound was calculated with Equation 1.10 using $(P_B - P_0) = 100$, since the theoretical polarization value of the fully bound condition was unknown. Hopes were high that FP would provide reliable data given the strength of the fit for the selection rounds. However,

Aptamer (K_d, nM)	FP	CE (subtractive)	CE (ratiometric)
A1	15.7 ± 8.8	>250	5.5 ± 1.8
A3	>250	132 ± 19	--
A4	>250	16.4 ± 1.9	--
A10	2.4 ± 8.7**	107 ± 39	--
A3492	160 ± 600**	>250	>250
A178749	>250	>250	--
A0	>250	>250	--
Library	266 ± 67 (n = 3)	108 ± 18	--

Table 3.3: Measured affinity of selected aptamers for LDLR by FP and CE. For each sequence, the K_d reported is calculated from a single assay (unless specified with "n=") with samples measured in triplicate. The error reported is the standard error in K_d calculated from the fit, or the root mean square of each standard error for n>1. (**) indicates that the fit converged but was questionable due to poor fit (R^2<0.5). ">250" indicates that the fit did not converge, or that the CE fit was rejected due to low absolute signal change (B_{max}<0.3). (--) indicates that the ratiometric calculation was not performed.

the FP data for some of the aptamers showed no visual trend nor convergence of the fit (Figure 3.7A). Because 250 nM was the highest concentration of LDLR tested for many of the FP assays, the K_d for all of these cases is listed as ">250 nM." Additionally, some of the cases that converged did so with a poor fit (low R^2) that accounts for little of the observed variation. For sequences with $R^2<0.5$, the K_d is listed in Table 3.3 but marked as questionable. While it is important to remember that FP commonly yields false negative binding data for aptamer systems due to propeller motion (section 1.4.2), there is no way to tell from FP data alone when this is the case. Only aptamers A1 and A10 showed possible high affinity by FP, though A10 binding is questionable due to low R^2. A1 showed the highest B_{max} of the aptamer sequences tested and displayed a K_d of 15.7±8.8 nM, nearly a 17-fold improvement over the starting library. FP binding curves and fit parameters are shown in the Appendix (Figures A.1 and A.2).

For CE assays, the uncorrected fraction bound was calculated by Equation 1.11 using the free DNA peak height. Evaluation of Equation 1.11 using total peak area did not converge for any aptamer, which is unusual. Closer inspection of the data showed that the total peak area unexpectedly increased with increasing [LDLR], either initially or throughout, even in cases where peak height decreased. However, free DNA peak height data provided a much better fit than total area and was used to calculate the K_d in the

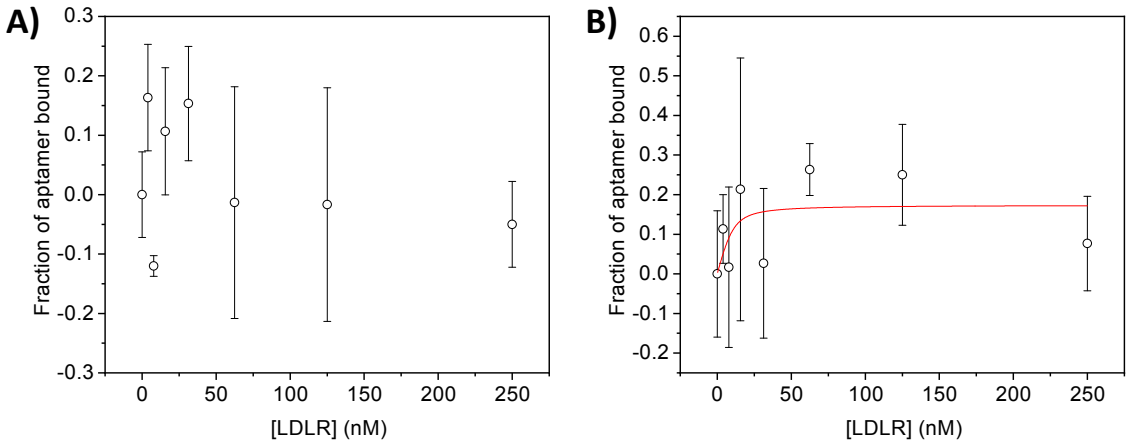

Figure 3.7: Example aptamer FP affinity assays with no convergence or questionable convergence. Error bars indicate standard deviation of at least three replicate measurements for each sample. **(A)** A3's signal seems largely random and actually trends downward at high [LDLR], leading to non-convergence. **(B)** While the red fit line is shown for the A10 data, its low R^2 (0.097) indicates a poor fit that accounts for little of the observed variation. Additionally, B_{max} is barely over 0.15 while most of the individual points have standard deviations above 0.15.

subtractive case. Compared to FP results, the relative standard error of replicate measurements of the CE data was significantly lower, leading to increased R^2 and much more visually credible fit data. There was also a solid fit for more aptamers, though it is unclear if this is due to superior reproducibility or to physical differences in the techniques. For A1 and A3492, where the CE traces showed obvious changes in peak shape (Figure 3.8), the data was also evaluated by the ratiometric calculation using Equations 1.12 and 1.13.

Unfortunately, issues with the instrument led to unreproducible current at high protein concentrations, limiting our ability to increase the maximum LDLR concentration to more appropriate levels. Possibly because of this, some aptamers displayed a very small overall decrease in peak height, which frequently coincided with large relative error bars. While it is rare to see the peak completely disappear at high protein concentration, we would expect to see the free peak intensity decrease by 30-50% or more (corresponding to a B_{max} of 0.3-0.5) in the event of binding. Therefore, CE fit data with B_{max}<0.3, such as for A178749 with B_{max} = 0.08, was deemed inconclusive and ignored. These aptamers were treated the same as data with no fit convergence and are listed as ">250 nM." All CE binding curves and fit parameters are shown in the Appendix (Figures A.3 and A.4)

Aptamer A1 showed the best affinity by CE, 5.5±1.8 nM by ratiometric area percent (Figure 3.9A). This is a 20-fold improvement over the library CE data, which is in strong agreement with the high affinity measured by FP. A4 was close behind at 16±2 nM by height (Figure 3.9B). Interestingly, the measured K_d of the library was much lower by CE (108 nM) than by FP (266 nM), though again it is unclear if this stems at all from the larger uncertainty in the FP measurements. A3 and A10

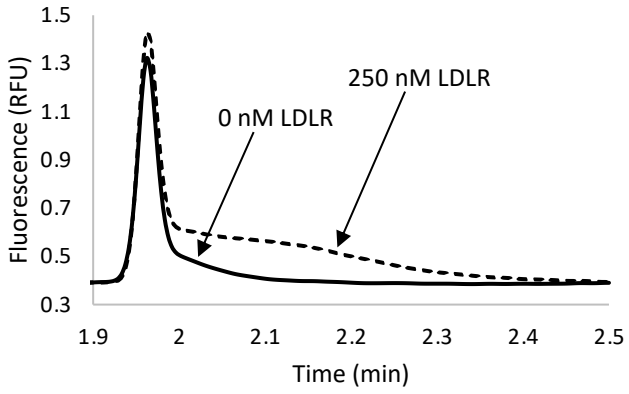

Figure 3.8: Example of CE peak shape change indicative of binding. CE traces are shown for A1 with no LDLR (solid) and 250 nM LDLR (dashed). The high-LDLR sample exhibits a distinct shoulder due to dissociated complex DNA not present in the LDLR-free sample, indicating that the ratiometric calculation should be used.

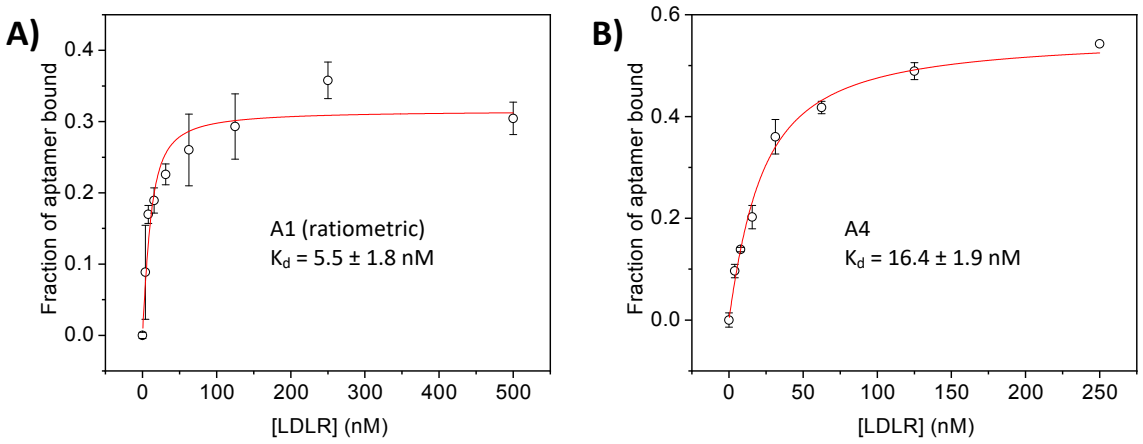

Figure 3.9: Plots of fraction bound by CE for **(A)** A1 and **(B)** A4. Error bars indicate standard deviation of at least three replicate measurements for each sample.

registered affinity by CE but had K_d values closer to that of the random library. Overall, some aptamers exhibited evidence of strong affinity, with A1 displaying around 15- to 20-fold improvement by both assays. However, additional affinity data, through repeated trials, higher LDLR concentrations, or new affinity techniques, will be required in order to draw more specific conclusions.

3.5 Conclusions

In summary, aptamers were selected by CE-SELEX against an untruncated membrane protein target in free solution, an accomplishment that has not been seen in the literature to our knowledge. The significance of this method lies in its ability to be generalized to any membrane protein target, even one that cannot be easily truncated or immobilized. Considerable time was devoted to optimization of the CE selection platform to create a representative LDLR target and to improve the likelihood of obtaining aptamers useful for a variety of applications. CE was found to be amenable to the uncharged $C_{12}E_8$ micelle system for LDLR stabilization, as well as to elevated temperatures and somewhat increased NaCl concentrations to mimic physiological conditions, but the glycerol often used to stabilize commercial membrane proteins was highly deleterious to the CE separation.

High-throughput sequencing demonstrated that the aptamer pool was extremely heterogeneous, which has been documented before for CE-SELEX. Three sequences were chosen for further characterization based on read count ranking and sequence clustering,

while three were chosen from the pool more randomly. The aptamers, along with a control sequence and the starting library, were assayed by CE and FP to determine their K_d for LDLR. Two aptamers, A1 and A4, were found to have K_ds below 20 nM, a significant improvement over the control and starting library. The data also suggest that, in this instance, the aptamers chosen rationally outperformed those chosen randomly. Unfortunately, a significant amount of the FP affinity data was difficult to interpret due to poor reproducibility of the instrument. On top of that, the many negative binding results by FP are inconclusive given that false negatives due to propeller motion are common with aptamers. More binding data, through further trials as well as new techniques like isothermal titration calorimetry (ITC), is needed to make more accurate and sweeping conclusions about the individual aptamers. In addition, cell studies are needed to evaluate transport of aptamers across the membrane.

3.6 Acknowledgements from this chapter

I would like to acknowledge the University of Minnesota Genomics Center (UMGC) for performing the DNA sequencing, Dr. Juan Abrahante and the University of Minnesota Informatics Institute (UMII) for customized DNA sequence processing scripts and technical assistance with sequence analysis, and Nicholas Brinza for performing all AptaCluster analysis.

Chapter 4: Toward DNA aptamers for real-time leptin quantification

4.1 Motivation

The prevalence of obesity worldwide continues to increase, even amid growing public health campaigns, expanded treatment options, and improved scientific understanding of the disease.[173] This is a problematic trend given that obese individuals are at increased risk for a variety of other serious medical conditions including cardiovascular disease and cancer.[174] One of the key molecular players in obesity is leptin, a protein generated by adipocytes (fat cells) that helps control hunger and balance energy expenditure in the body. While the long-term relationships between leptin and obesity have been explored, the main tools used to study leptin levels, such as ELISA assays, are not suited to deal with faster leptin variation in response to specific metabolic stimuli.

One way to measure these faster variations is a proposed microfluidic system able to quantify leptin secretion from cultured adipocytes in real time. The system combines a flow cell to perfuse adipocytes and collect cell secretions, online incubation with a fluorescent leptin-specific aptamer, and micro-free flow electrophoresis (μFFE) separation to partition and quantify free aptamer and leptin-bound aptamer, allowing for calculation of leptin concentration. Aptamers present the ideal affinity tag in this scenario due to their efficient separation by electrophoretic modes, though an aptamer with high and consistent affinity will allow more accurate quantification. The work herein describes evaluation of existing leptin-targeting aptamers and progress toward selection of new aptamer sequences for leptin for use in the proposed microfluidic system.

4.2 Introduction

4.2.1 Obesity and leptin

Obesity, taken simplistically, is caused by an imbalance between energy intake via food and energy expenditure via physical activity, leading to excess accumulation of adipose deposits (fat tissue) around the body. Far beyond the related cosmetic effects, obesity is a serious health condition associated with increased rates of type 2 diabetes, cardiovascular disease, stroke, severe symptoms of COVID-19, some types of cancer, depression, sexual health issues, digestive and pulmonary issues, and more.[173-179] For such a serious issue with a seemingly simple solution – eat less and exercise more – it stands to

reason that overweight and obesity should be decreasing as public awareness of the disease and its impacts grows. However, nothing could be further from the truth. Since 1980, the rate of obesity has doubled among American adults and tripled among children.[175] As of 2018, 13% of the world adult population is obese, with the age-adjusted prevalence exceeding 40% in the United States (Figure 4.1).[180-183] The disease's continued growth is a clear illustration of the many hidden complexities of obesity. Adding to the complication of studying and treating obesity is the sheer number of factors that play a role in obesity: genetic factors, socioeconomic status, race, age, gender, mental health status, and numerous environmental factors show significant differences in rates and outcomes of obesity on a group level, not to mention differences in personal behavior and habits based on everything from family and regional differences to cultural and religious identity.[173, 184-186] Untangling these many factors is quite difficult, which means that observational and correlational research studies are relatively limited in their conclusions and recommendations for specific interventional strategies. For this reason, methods for studying obesity from a molecular and mechanistic approach are of increasing importance.

One molecule of particular interest to the study of obesity is leptin, a protein secreted by adipocytes. The discovery of leptin in 1994 is largely responsible for the realization that adipose tissue plays an active role in endocrine signaling rather than just

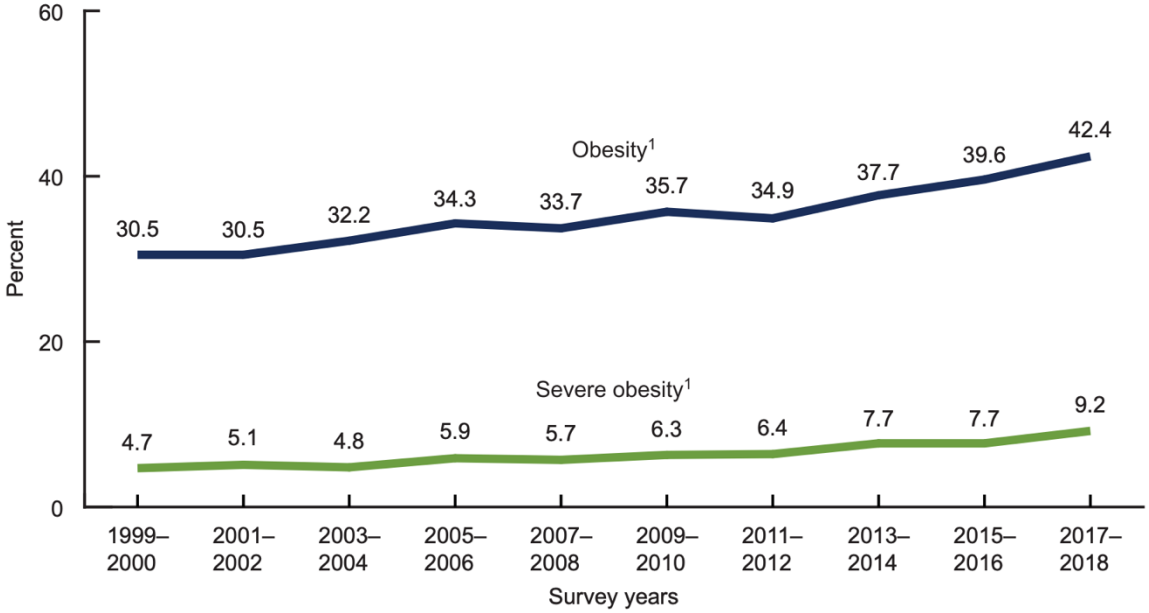

Figure 4.1: Trends in age-adjusted obesity and severe obesity prevalence among U.S. adults aged 20 and over: 1999 through 2018. Obesity is defined as individuals with a body mass index (BMI) of 30 or higher. Severe obesity is defined as individuals with a BMI of 40 or higher. Adapted from Hales *et al*.[183]

passive energy storage.[187] The most important role of leptin is to regulate energy balance by decreasing both food-seeking behaviors and feelings of hunger.[188] Serum levels of leptin increase exponentially with body fat, normally causing the individual to decrease food intake when the body has sufficient fat stores.[189, 190] However, most obese individuals continue to display normal eating habits despite exhibiting four-fold higher serum leptin levels than do those of healthy weight, suggesting a mechanism of leptin resistance that impairs normal leptin-based energy regulation.[191-193] While long-term trends in leptin relative to body weight and obesity have been well established, and intermediate trends such as those in response to sleep or fasting have been explored, little is known about the short-term trends and effects of leptin levels at a sub-30 minute time scale.[189, 191, 194-196] A more comprehensive temporal understanding of leptin secretion in response to specific metabolic stimuli, such as artificial sweetener consumption, is needed in order to provide a complete picture of leptin signaling and yield answers about leptin and obesity that have so far evaded elucidation.

4.2.2 Leptin measurement by perfusion and online micro-free flow electrophoresis

In research and some clinical settings, leptin concentrations are most frequently measured using ELISA kits,[197-204] radioimmunoassays,[205-208] or mass spectrometry.[209, 210] These techniques are highly reproducible, and some are well suited to parallel detection of multiple analytes, but they are all time-consuming and labor-intensive. Because of this, they are not well suited to make the type of repeated or continuous measurement necessary to scrutinize immediate responses and short-term trends in leptin secretion. One method ideally suited to quick measurement is micro-free flow electrophoresis (μFFE), a technique which continuously streams sample through a wide channel and uses an electric field to deflect analytes based on their electrophoretic mobility.[108, 211, 212] μFFE devices can be 3D printed for fast prototyping, and they are easily coupled to different sampling methods, detection schemes, and other online components to create a highly customized device for specific uses.[213-218]

In a device proposed by this research group, adipocyte-like cells are cultured in a small flow cell and perfused with buffer, which can be spiked with glucose, insulin, artificial sweeteners, or other metabolic stimuli. Analytes secreted by the cells (such as

leptin) are swept up in the continuous buffer flow and carried downstream where they are mixed with fluorescently labeled aptamer with a known affinity for leptin. A sufficiently long incubation tube or channel allows sample leptin and fluorescent aptamer to reach binding equilibrium before the sample flows into the µFFE separation channel. Free aptamer and the leptin-aptamer complex are pushed down the channel by the buffer flow and separated laterally in a continuous manner by electrodes on either side of the channel. The quantities of bound and free aptamer are measured by LIF, and the ratio is used to calculate the amount of leptin present using Equation 1.7 and the known aptamer affinity. The main parts of the proposed assay are shown in figure 4.2.

4.2.3 Leptin aptamer characterization and selection

Research regarding the construction and optimization of the flow cell and µFFE device proceeded independently at the hands of other researchers. Instead, the work here

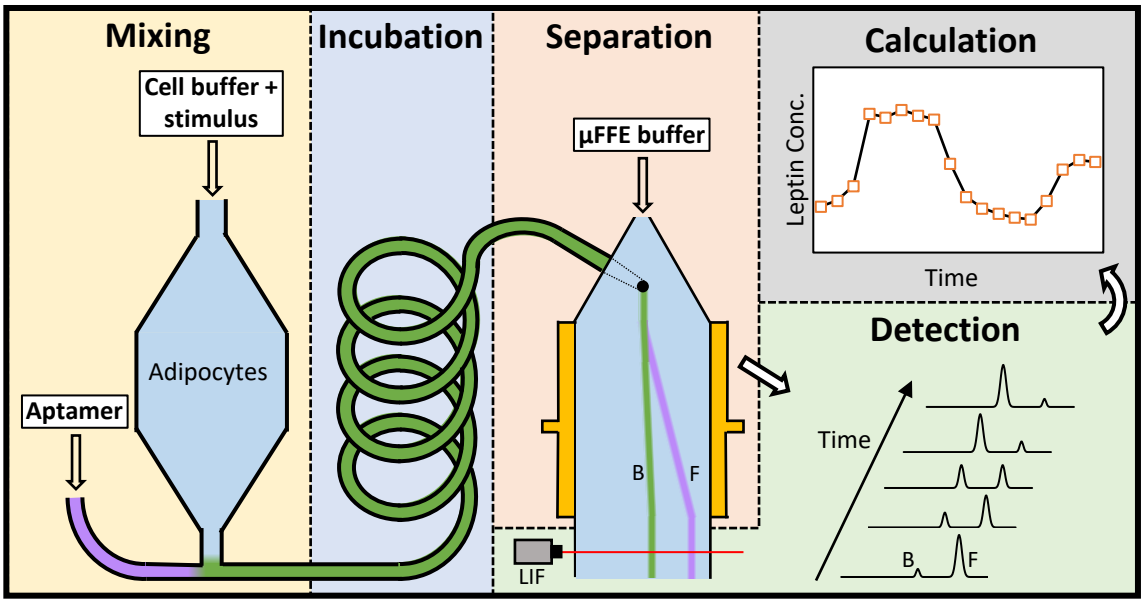

Figure 4.2: Outline of proposed aptamer-based real-time leptin quantification system. **Mixing:** A basic buffer, with or without a metabolic stimulus (such as glucose or insulin), is perfused over adipocyte-like cells, stimulating cells and collecting secreted leptin. The outflow is mixed with a known concentration of leptin-targeting aptamer. **Incubation:** The sample travels through a sufficiently long incubation tube or channel to reach binding equilibrium. This region could be temperature controlled if needed. **Separation:** Sample is streamed continuously onto a µFFE chip. Buffer flow pushes the sample down the channel while electrodes on either side separate bound (B) and free (F) aptamer laterally. **Detection:** Once separated, the bound (B) and free (B) aptamer peaks are each quantified by LIF. Due to the continuous separation, the rate of collection is limited only by the detector. **Calculation:** For each time point, the peak intensity of bound and free DNA are used to determine the proportion of aptamer complexed, from which the leptin concentration can be calculated and plotted over time.

focuses solely on progress toward a well-characterized, selective, high affinity aptamer for leptin required for successful functioning of the proposed microfluidic device.

Plans for the device center around the use of adipocyte-like cells differentiated from 3T3-L1 cells, with which our group has extensive experience. While these cells are a commonplace in the study of obesity as it pertains to humans, 3T3-L1 cells are mouse-derived cells rather than a human cell line. This made it clear, therefore, that preliminary work would require aptamers against mouse leptin rather than human leptin. Efforts were made to find aptamers in the literature that could fill our requirements, thereby saving the time and cost of independent aptamer selection. While aptamers against mouse leptin with a published sequence were absent from the literature, a publication by Ashley and Li[219] indicated the sequences of multiple aptamers against human leptin from their research. Aside from targeting human rather than mouse leptin, these aptamers seemed ideal for our uses: the aptamers were found by CE-SELEX, which reduced any fears of negative impact from the electric field in the μFFE chip; the selection used free rather than immobilized leptin, which matched the anticipated usage; and the sequences had already been selected with the appropriate 5' fluorescent tag for this work. Given that some antibodies display affinity for both human and mouse leptin,[220] coupled with a 93% sequence similarity between the two, it seemed worth further investigation of these literature aptamers despite their different initial target.

The work in this chapter begins with measurement of the affinity of two of the literature aptamers (Lep2 and Lep3) for mouse leptin in order to assess its feasibility in the proposed microfluidic assay. Next, progress is demonstrated toward a new CE-SELEX selection to obtain novel aptamer sequences with higher affinity for mouse leptin.

4.3 Methods

4.3.1 Reagents

Nuclease-free water (nfH_2O) was obtained from Ambion (Austin, TX). A set of four deoxynucleoside triphosphates (dNTP, 100 mM) was obtained from Denville Scientific (Metuchen, NJ). Agarose powder, glacial acetic acid, and $NaHCO_3$ were obtained from Fisher Scientific (Waltham, MA). Molecular biology grade 3-(N-

morpholino)propanesulfonic acid (MOPS) was obtained from Fluka (St. Lous, MO). D-glucose was obtained from Gibco (Waltham, MA). All DNA libraries and sequences were obtained from Integrated DNA Technologies (Coralville, IA). The DNA sequences were: 5'-6FAM-AGC AGC ACA GAG GTC AGA TG-N_{40}-CCT ATG CGT GCT ACC GTG AA-3' (library), 5'-6FAM-AGC AGC ACA GAG GTC AGA TG-3' (sense primer), 5'-Biotin-TTC ACG GTA GCA CGC ATA GG-3' (antisense primer), 5'-6FAM-CTT CTG CCC GCC TCC TTC CTG GGT GGC CTC CCG TTT ATT CGA GAT TTG GTT GAA TTT GTG GAG ACG AGA TAG GCG GAC ACT-3' (FAM-labeled Lep2), and 5'-6FAM-CTT CTG CCC GCC TCC TTC CGT TAA TGG GGG ATC TCG CGG CCG TTC TTG TTG CTT ATA CAG GAG ACG AGA TAG GCG GAC ACT-3' (FAM-labeled Lep3). KH_2PO_4 was obtained from J.T. Baker Inc. (Phillipsburg, NJ). NaOH powder was obtained from Macron Chemicals (Radnor, PA). Hyperladder DNA ladder (25-base) was obtained from Bioline Reagents (Cincinnati, OH). Boric acid powder, $CaCl_2$, KCl, and $MgCl_2$ were obtained from Mallinckrodt Pharmaceuticals (St. Louis, MO). Taq polymerase and accompanying ThermoPol buffer were obtained from New England Biolabs (Ipswitch, MA). Tris(hydroxymethyl)aminomethane (Tris) was obtained from Roche Applied Science (Penzberg, Germany). Recombinant mouse leptin (≥98%), NaCl, glycine, rhodamine 110 (R110), ethidium bromide, disodium ethylenediaminetetraacetic acid (EDTA), disodium fluorescein, and Tris·HCl were obtained from Sigma-Aldrich (St. Louis, MO). $MgCl_2$ solution (25 mM) and streptavidin-coated agarose resin were obtained from Thermo Scientific (Waltham, MA).

4.3.2 Buffers and solutions

(1) CE running buffer (pH 7.5) contained 3.6 mM Tris and 16.4 mM Tris·HCl (20 mM Tris total), 5 mM KCl, 10 mM NaCl unless otherwise specified, 5 mM glucose, and 1.8 mM $NaHCO_3$. (2) Sample buffer (pH 7.5) was prepared in nfH_2O and contained 3.6 mM Tris and 16.4 mM Tris·HCl (20 mM Tris total), 5 mM KCl, 30 mM NaCl unless otherwise specified, 1 mM $CaCl_2$, 5 mM glucose, and 1.8 mM $NaHCO_3$. (3) PCR master mix was prepared fresh for each use in nfH_2O and contained 540 nM FAM-labeled sense primer, 540 nM biotin-labeled antisense primer, 216 nM each dNTP, 8.1 mM $MgCl_2$, and 1.08× ThermoPol buffer. (4) TBE buffer for gel electrophoresis contained 45 mM tris, 45

mM boric acid, 50 mM EDTA. (5) Purification buffer was prepared in nfH_2O and contained 10 mM tris, 50 mM NaCl, 1 mM EDTA. (6) TGK (1×) for literature leptin aptamer experiments contained 25 mM Tris, 192 mM glycine, 5 mM KH_2PO_4, and was adjusted to pH 8.3 with HCl.

4.3.3 CE equipment and protocols

All CE work was performed on a P/ACE MDQ (Beckman-Coulter) or P/ACE MDQ-Plus (SCIEX) automated CE instrument using 32 Karat data collection software. Uncoated fused silica capillary of 50-µm inner diameter and 360-µm outer diameter was used throughout, cut to 39.7 cm total length with a detection window (2-5 mm wide) burned 29.5 cm from the inlet. CE sample storage and capillary temperature were set to 25˚C. Rinses used 20 psi forward pressure and sample injections were made with 10 s of 0.5 psi forward pressure. Before first use, unless otherwise specified, new capillaries were rinsed with 0.15 M NaOH for 3 min, rinsed with nfH_2O for 3 min, rinsed with running buffer for at least 15 minutes, and allowed to equilibrate with running buffer for at least one hour. The capillary was rinsed with running buffer for 5 min between runs and for 10 minutes at the start and end of each day. LIF detection (488 nm excitation/520±10 nm emission) was used unless otherwise specified.

4.3.4 SELEX separation

DNA was heated at 72˚C for 5 minutes and cooled before use. For each round of SELEX, a 20-µL sample containing 2 nM leptin and DNA in sample buffer was incubated at 25˚C for 20 minutes before selection. The first round used 100 µM random library DNA while each subsequent round used half of the purified DNA from the previous round to make the sample as concentrated as possible. The sample was separated by CE at 30 kV into a collection vial containing roughly 50 µL of sample buffer. Unless otherwise specified, the separation was manually stopped 10 seconds before the free DNA peak reached the end of the capillary (calculated from the electropherogram and the capillary dimensions). The separation was repeated 2-3 additional times into the same collection vial.

4.3.5 PCR and gel electrophoresis

PCR samples were prepared with 92.5 μL master mix, 7.0 μL of DNA sample, and 0.5 μL (2.5 units) Taq polymerase, with Taq polymerase being added once the sample reached 94˚C. Each PCR experiment was run with at least one positive control (DNA sample = 50 pM random DNA library) and at least one negative control (DNA sample = nfH_2O). The thermocycler performed 25 rounds of 94˚C (30 s), 53˚C (30 s), and 72˚C (20 s) sequentially, followed by a final 10 minutes at 72˚C and storage at 4˚C.

Gel electrophoresis was performed on all non-identical PCR samples (including PCR controls) to verify amplification and check for contamination. A 1.5% or 2% w/v agarose gel made with TBE and 100 μg of ethidium bromide was run in TBE buffer at 200 V for 40 min. Gels were imaged on an ultraviolet transluminator with a Canon 1300d DLSR.

4.3.6 DNA purification

In a 10-mL affinity chromatography column, 300 μL of streptavidin-coated agarose resin and 500 μL of purification buffer were vortexed and then flushed. PCR-amplified sample DNA and 100 μL of purification buffer were introduced to the column and incubated at room temperature, vortexing periodically. The column was then flushed with 5 mL of purification buffer. The column was then incubated at 37˚C with 200 μL of 0.15 M NaOH, vortexing periodically, and eluted into equimolar acetic acid. This NaOH incubation and elution was repeated into the same collection. The collected sample was spun in a 10-kDa centrifugal filter, rinsed with nfH_2O, spun again, and collected in two clean microcentrifuge tubes, which were vacuum centrifuged to dryness at 50˚C then stored frozen.

4.3.7 Affinity measurement

DNA was heated at 72˚C for 5 minutes and cooled before use. CE and FP samples were prepared containing 20 nM random library or approximately 20 nM aptamer pool with 0-16 μM leptin in sample buffer, or 10 nM literature aptamer sequence with 0-40 μM leptin in 1× TGK. Samples were incubated at 25˚C for at least 20 minutes before measurement.

For CE measurement, samples were separated using 30 kV and 0.3 psi of forward pressure, and the peak height and area the free DNA peak and complex peak (if present) were recorded. CE running buffer was used unless otherwise specified. The leptin-free sample was separated multiple times until the free DNA peak settled (see Figure 4.2) and three consecutive measurements with less than 5% RSD in height or area were obtained. Samples were measured in triplicate from lowest to highest protein concentration. The uncorrected fraction bound for each concentration was calculated subtractively (Equation 1.11) for all assays and ratiometrically (Equations 1.12 and 1.13) where appropriate.

FP measurements were performed on a BioTek Synergy 2 (Agilent) plate reader using 20-μL samples in an opaque 384-well plate. Measurements were made at 25˚C using a tungsten lamp (485±10 nm excitation/528±10 nm emission). Polarization values were measured in triplicate for all samples simultaneously with a 5-second mix between each. The uncorrected fraction bound for each concentration was calculated by Equation 1.10.

For CE and FP experiments, the K_d for each aptamer or pool was calculated in Origin 9.6 by fitting the triplicate uncorrected fraction bound data to a custom fit equation (Equation 1.8) with the constraints $K_d > 0$ and $B_{max} > 0$.

Isothermal titration calorimetry (ITC) measurements were performed on a TA Instruments Nano ITC. Solutions of 75 μM leptin aptamer and 10 μM mouse leptin, each in 1× TGK, were degassed under vacuum immediately prior to measurement. The leptin sample was stirred at 400 RPM and kept at 25˚C throughout, and 250 μL of aptamer solution was delivered over 16 injections, 30 seconds each and 5 minutes apart. A reference cell of degassed deionized water was used. Aptamer K_d was calculated automatically by the instrument software NanoAnalyze.

4.4 Results and Discussion

4.4.1 Affinity of literature leptin aptamers

At the time of writing, only a single paper by Ashley and Li[219] indicated any leptin aptamers with a published sequence. The aptamers seemed like a possible fit for the project but had been selected against human leptin, which has only 85% identity with and is a 93% positive match for mouse leptin. Two literature aptamers with the strongest reported

binding (Lep2 and Lep3) were synthesized in order to assay their affinity for mouse leptin. While the intention was to eventually tailor the selection buffer to more closely match the conditions seen in the proposed device, in this case affinity measurements were made using 1× TGK, the buffer used for selection of Lep2 and Lep3, in place of sample buffer and CE running buffer in order to maximize the chance of binding.

FP experiments were performed first due to ease and speed, but the fit data did not converge for either aptamer. As explained in section 1.4.2, false negative FP binding results can arise due to propeller motion of the fluorescent tag, which seems likely in this case due to leptin's small relative size. However, both CE and ITC data (Table 4.1) demonstrate a significant difference from the literature data for human leptin, with CE showing over ten-fold lower affinity. Additionally, non-equilibrium capillary electrophoresis of equilibrium mixtures (NECEEM) affinity analysis, though similar in some respects to ratiometric CE analysis, requires quantification of the complex peak. No complex peak was observed in our CE experiments, even at high leptin concentration, further corroborating the lower affinity we observed. Overall, Lep2 and Lep3 exhibited relatively poor affinity for mouse leptin, indicating they did not lend themselves well to the proposed assay. For this reason, we moved forward with the plan to perform CE-SELEX in house against mouse leptin under conditions optimized for the proposed assay.

4.4.2 Optimization

Optimization of SELEX conditions is always a compromise between conditions similar to future applications (for the sake of representative conformation and binding) and conditions that simplify the selection and affinity measurement process. Unlike in Chapter 3, the future application for these aptamers is known quite specifically, meaning that the balancing act could be weighed much more precisely. Preliminary work with the 3T3-L1s in the flow

Assay type	Lep2 K_d (µM)	Lep3 K_d (µM)
FP	>40	>40
CE (height)	33 ± 10	22 ± 8
ITC	5.3 ± 2.1	2.4 ± 1.2
*NECEEM**	*0.41 ± 0.13*	*0.32 ± 0.50*
*Fluorescence**	*1.18 ± 0.39*	*1.50 ± 0.25*

Table 4.1: Measured affinity of Lep2 and Lep3 aptamers for mouse leptin by multiple techniques. FP data did not converge, suggesting either very low affinity or a false negative due to propeller motion. Both CE and ITC results demonstrate a lower than ideal affinity for use in this research. Techniques with (*) were performed by Ashley and Li[219] using human leptin and are shown for comparison.

cell prototype indicated that they were tolerant of perfusion with a buffer based on Ringer's solution, so the SELEX optimization was performed assuming this media for future perfusion. Ringer's is designed to be isotonic for mammalian physiology, and our perfusion buffer contained the 120 mM NaCl, 5 mM KCl, and 1 mM $CaCl_2$ typical of Ringer's as well as 1.8 mM $NaHCO_3$ for pH control and 5 mM glucose to maintain basal metabolic activity. Conveniently, these KCl and $CaCl_2$ concentrations are similar to common SELEX buffers to facilitate G-quadruplex formation and backbone bridging, respectively (such as in Chapter 3). The bicarbonate and low glucose concentrations were not expected to negatively impact the sample buffer, though additional buffer capacity would be needed to maintain pH and avoid redox acidification. The main predicted issue was the 120 mM NaCl. As explained previously (section 3.4.1), ionic strength in the running buffer must be relatively low to avoid excessive instrument current, and the ionic strength of the sample buffer cannot significantly exceed that of the running buffer to avoid poor peak shape due to sample destacking.

Buffer compounds tris, HEPES, and MOPS (chosen for their pK_a near 7.5) were tested in the initial stages to see if one was preferable, and tris was chosen due to good DNA signal and frequent use in SELEX buffers. Further CE optimization was performed with 20 nM random DNA using the sample and running buffers specified in section 4.3.2 but both with 10 mM NaCl. Optimization proved more difficult than expected due to poor reproducibility of the free DNA peak, with peak time varying substantially from day to day, and peak height frequently changing both randomly and systematically over the course of several runs. An internal standard of 2 nM fluorescein or 4 nM R110 was added to the sample to see if this could correct for peak size (for better quantification during affinity measurements), but no significant changes were seen in the internal standard (Figure 4.3). Internal standards are typically used to correct for imprecision in sample preparation, injection volume, or detector sensitivity, but the impressive consistency of the fluorescein peak suggested that the primary cause of the DNA peak size inconsistency was none of these and in fact due to a DNA-specific (or at least small molecule-independent) effect. After a number of runs, the DNA peak height and time seemed to settle somewhat and the

large systematic changes lessened noticeably, although the uncertainty in DNA peak height was still significantly greater than those of fluorescein or R110. The number of runs required for the DNA peak to settle (determined by three consecutive peaks within 5% peak height or area) seemed to vary from a dozen or more for a new capillary to 2-5 for a well-worn one. Peculiarly, the peak did not always settle to a similar final value, and on occasion the peak height increased rather than decreased to settle on its final value. This effect seemed to depend on the number of injection runs and not on any time factor (though overall inconsistency made it difficult to determine for sure), so it was speculated that the systematic effect was somehow due to DNA or Ca^{2+} interaction with the capillary wall.

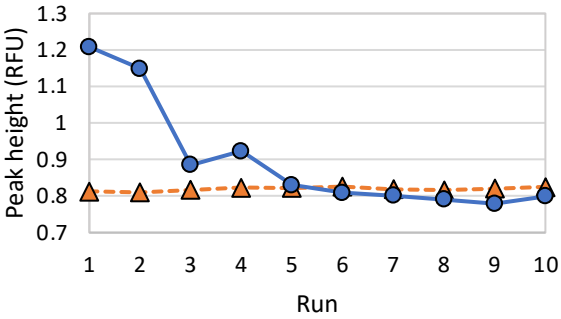

Figure 4.3: Shifting DNA peak height in CE over the course of multiple runs. Ten separations were performed from a sample containing random DNA (circle, solid) and an internal standard of fluorescein (triangle, dashed). The DNA signal changed significantly, particularly early on, while the fluorescein showed <1% RSD in peak height, suggesting a DNA-specific issue. The DNA peak does seem to settle into a relatively consistent height after multiple runs but still displays much greater uncertainty than the fluorescein peak, which was representative of DNA peak behavior.

Ten millimolar NaCl was not expected to be the optimized concentration for the running buffer, but this buffer already gave a current of 60 μA, similar to that seen Chapter 3. Because these runs were over twice as long as the LDLR runs (redox changes are a product of current and separation time) and they already displayed significant run-to-run variation, the running buffer was left at 10 mM to avoid increasing uncertainty or separation time. Increasing amounts of NaCl were added to the sample buffer while using the running buffer with 10 mM NaCl, and 30 mM NaCl was selected as the maximum usable concentration due to disruption of the DNA peak shape at higher levels.

While 30 mM NaCl is significantly lower than the 120 mM present in the perfusion buffer, it was decided that the aptamer solution could be mixed into the proposed device in a NaCl-free version of the buffer at a 1:1 or 2:1 ratio. This would lead to a final incubation solution in the device of 60 mM or 40 mM NaCl, respectively, which is much closer to the 30 mM NaCl to be used for selection. This also allowed the SELEX experiments to be performed at room temperature even in the event that 37˚C perfusate was used.

4.4.3 CE-SELEX against mouse leptin

For the first round of selection, concentrated library DNA and 2 nM leptin were incubated for 20 minutes and then separated by CE to examine the behavior of the peak (Figure 4.4A), and a number of small peaks were observed before the main free DNA peak. This is a common occurrence, as minimal purification is performed on the random DNA to avoid biasing the library before selection. Additionally these early peaks typically disappear after the first round of amplification, suggesting that the species that cause them don't contain the correct primers for amplification and can therefore be ignored. However,

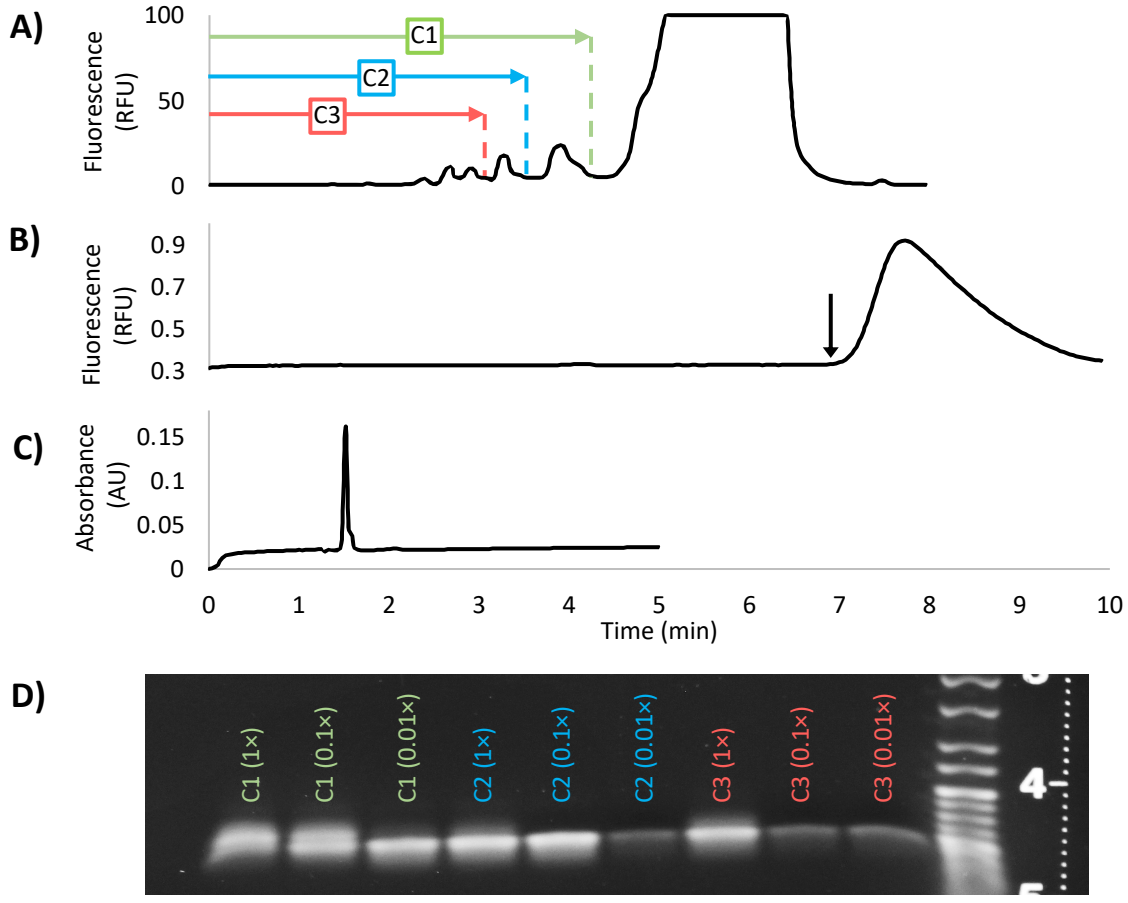

Figure 4.4: Peak times and collection windows for leptin CE-SELEX. **(A)** The LIF trace of the first round of selection displayed multiple early peaks, so different collection windows (C1-C3) were tried. Note that this sample has maxed the detector. **(B)** The round 2 selection trace did not display any early peaks, though the main peak was much later. The end of the collection window is shown (arrow). **(C)** A UV trace (200 nM) of leptin shows an early detector time (as expected) of 1.6 minutes. All traces (A-C) are plotted on the x-axis shown here. **(D)** Agarose gel electrophoresis was performed on test PCR conditions using multiple dilutions of each different collected sample. The gel shows that the DNA collected in C3 was sufficient for amplification (at full concentration) but substantially less than in C1 and C2.

the early peaks were somewhat larger and more spread out than usual, extending into the expected location of the complex peak (roughly 3-4 minutes). Because of this, additional flexibility was built into the first round by using three different time windows to collected during different runs and into different vials, each successively more stringent (Figure 4.4A). Each collection window was picked to correspond roughly to a different local minimum, and separation was stopped manually when the end of the collection window reached the end of the capillary, calculated by multiplying the electropherogram time by the ratio of the full capillary length to the inlet-to-window length (1.357). The different collected samples were amplified by PCR at multiple dilutions to check for the presence of appropriate DNA (Figure 4.4D). As expected, the longer window (C1) collected a larger amount of amplifiable DNA than the stringent C3 window. However, C3 still collected enough DNA for maximal amplification at its highest concentration (Figure 4.4D, "C3 (1×)"), and it was expected that more generous collection would only serve to increase the proportion of unwanted free DNA in the sample. Therefore, C3 was used for full amplification to generate the pool for the next round.

As expected, the early peaks were entirely absent from future rounds of selection, confirming that they were from species that were not efficiently amplified during PCR. Interestingly, the later rounds of SELEX seemed to have the free DNA peak somewhat later than in round 1 (Figure 4.4B), though there was still enough variation in peak time from day to day to make this determination less confident. In the second round of selection onward, the end of the collection window was 10 seconds before the beginning of the free DNA peak reached the detector. The start of the peak was defined as two consecutive time points more than 10% above the baseline intensity. Four rounds of selection were performed.

The K_d of each pool and the starting library were measured by FP, but as with Lep2 and Lep3, there was no fit convergence for any of the samples measured. Even looking at the FP plots (Appendix, Figure A.5), there was no qualitative difference between the pools. The first CE affinity assay with random library showed the emergence of an apparent complex peak (Figure 4.5, A_2), which was welcome since ratiometric quantitation with the free and complex peak would serve to reduce some of the error due to peak size uncertainty.

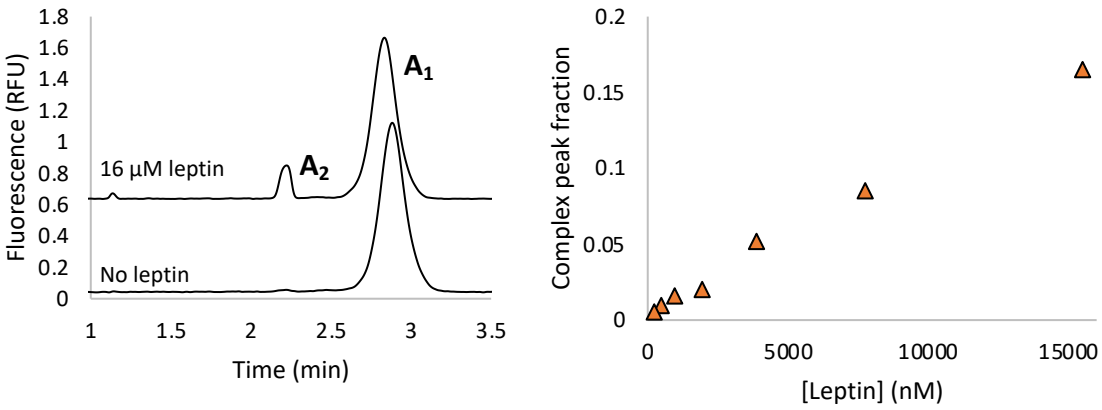

Figure 4.5: Emergence of the complex peak in leptin-library affinity measurements. **(Left)** The free DNA peak (A_1) remained relatively constant throughout, but a smaller peak (A_2), assumed to be the complex peak became more prominent at higher leptin concentrations. **(Right)** The complex fraction, calculated from equation 1.12 using peak height, is shown. While the increase is expected, the linear rather than hyperbolic shape indicates poor binding (K_d >> 16 µM).

The fraction of signal in the complex peak was calculated ratiometrically using Equations 1.12 and 1.13. While the complex peak grew in with increasing leptin concentration, the fraction bound increased quite linearly, which is indicative of a K_d higher than the largest ligand concentration used (16 µM). The affinity of the round 2 and round 4 pools were also evaluated by CE, but no complex peak greater than 1% was ever visible, and no trend was seen in the free DNA peak height or area (Appendix, Figure A.6).

4.4.4 Estimation of complex mobility

In trying to understand the cause(s) of this unsuccessful selection, one possibility identified was that the collected sample from the CE separation did not contain a higher proportion of leptin-DNA complexes as intended. Indeed, the disappearance of the complex peak might suggest that these binding sequences were partially or completely excluded from the collected sample, accidentally selecting for sequences *without* affinity for leptin. A simple approximation of the electrophoretic mobilities of leptin and DNA in our system was performed in order to better estimate the location of the complex during selection, since it was not visible on the electropherogram. This would allow us to determine more clearly whether the complexes had been included in or excluded from the collected sample. New measurements of leptin, random DNA, and the neutral dye rhodamine 110 (R110) were taken on the same day to reduce the impact of day-to-day drift (Figure 4.6).

Calculation of leptin and DNA mobilities. As described in section 1.3.2, each analyte in CE experiences an apparent mobility (μ_{app}, Equation 1.3) that is the vector sum of its electrophoretic mobility (μ_{EP}) and its electroosmotic mobility (μ_{EOF}). μ_{EOF} acts through a bulk buffer flow and affects all analytes in the run equally, though its magnitude can drift because of its sensitivity to small variations in capillary surface chemistry and buffer conditions (Equation 1.2). In CE, neutral compounds are unaffected by electrophoresis and migrate only under the effect of EOF, so R110 was used to measure the μ_{EOF} for these conditions. In the experiments shown in Figure 4.6, R110 took 67.5 s to reach the detector (295 mm from the inlet), yielding an electroosmotic velocity of 4.37 mm/s. All separations used 30 kV along a 397 mm capillary for an applied field (E) of 75.6 V/mm (Table 4.2). With the electroosmotic velocity and applied field known, the μ_{EOF} was calculated to be 5.78×10^{-8} m^2/V·s by Equation 1.2 for the Figure 4.6 experiments.

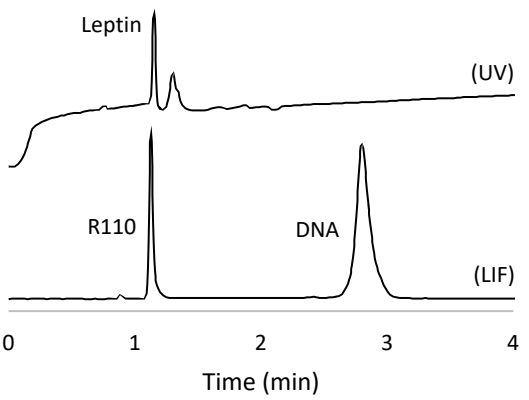

Figure 4.6: CE comparison of R110, leptin, and free DNA. Neutral R110 was detected at 1.125 min (LIF), leptin at 1.171 min (UV), and the DNA at 2.800 min (LIF). UV detection was performed at 200 nm.

In order the find the μ_{EP} for the free DNA, the net mobility was first calculated from Figure 4.6. DNA traversed the detector length of 295 mm in 168 s (2.80 min), corresponding to a net velocity 1.76 mm/s in the 75.6 6 V/mm electric field, or a net mobility of 2.32×10^{-8} m^2/V·s. Since net mobility is the sum of μ_{EP} and μ_{EOF} and the μ_{EOF} was found above, the μ_{EP} of the free DNA was calculated to be -3.46×10^{-8} m^2/V·s (Table 4.2). The same strategy was applied for leptin, with its 70.2 s peak time (Figure 4.6), to find the μ_{EP} of -2.22×10^{-9} m^2/V·s. Note that both species have a negative μ_{EP}, indicating an electrophoretic force toward the inlet and opposite the EOF direction.

Estimation of hydrodynamic radii and complex mobility. The μ_{EP} for free DNA was used to estimate its hydrodynamic radius in our system using Equation 1.1.* For this

* It should be noted that use of this equation makes a number of simplifying assumptions about the system. For example, Equation 1.1 is valid for a centralized point charge rather than a finite size particle with charge distribution. In addition, the equation considers only the nominal charge of the compound itself and

	μ_{EP} (m^2/V·s)	z	R (nm)
Free DNA	-3.46×10^{-8}	-82.0	22.6
Leptin	-2.22×10^{-9}	-4.5	19.3
Complex	-3.11×10^{-8}	-86.5	26.6

E (electric field) = 75.6 V/mm	Length = 295 mm	η (viscosity) = 8.90×10^{-4} Pa·s

Table 4.2: Summary of selected values for CE mobility calculations. Electrophoretic mobility (μ_{EP}), charge number (z), and calculated hydrodynamic radius (R) are shown for free DNA, leptin, and the theoretical DNA-leptin complex. The electric field strength (E), length of capillary to the detector, and solvent viscosity (η) used for calculation are also shown.

approximation, the charge number of -82 (-1 per base and -2 for the carboxyfluorescein dye) was multiplied by the electron charge to find Q (1.31×10^{-17} C), and the viscosity of pure water at 25˚C (8.90×10^{-4} Pa·s) was used for η since the solution was relatively dilute. This yielded an estimated hydrodynamic radius of 22.6 nm. The same strategy was employed for leptin using a charge number of -4.5. This value was calculated from the amino acid sequence[221] for mature mouse leptin, including the disulfide bond, using Prot pi's protein calculator at pH 7.5.[222] This yielded a hydrodynamic radius of 19.3 nm for leptin.

Without specific a priori knowledge of the likely binding interaction, several assumptions were made about the hypothetical leptin-DNA complex to facilitate simple calculation. First, it was assumed that the net charge of the complex would be the sum of the net charge of free DNA and leptin, or a charge number of -86.5 at pH 7.5. Second, it was assumed that ssDNA, leptin, and the complex were roughly spherical, allowing their hydrodynamic volume to be calculated by $^4/_3\pi R^3$. This calculation yielded hydrodynamic volumes for free DNA and leptin of 4.86×10^{-23} m^3 and 3.02×10^{-23} m^3, respectively. Finally, it was estimated that the hydrodynamic volume of the complex would be the sum of the

does not account for an excess of counterions within and surrounding the DNA structure. However, a number of factors justify the use of Equation 1.1. First, this analysis is performed in one direction (to predict species' hydrodynamic radii) and then in the other (to predict complex mobility from its radius), suggesting that many inaccuracies from these assumptions will largely be nullified in the overall analysis. Second, a number of other assumptions are made throughout the estimation, such as the sphericality of the species or the additivity of volume on complexation, that are unavoidable and seem more significant in magnitude. Finally, more complex analyses that take more of these factors into account, such as the Smoluchowski expression or Manning electrophoresis equation, have more variables that are not known precisely and would therefore require additional assumptions or approximations in their use as well. Using the simplified equation increases the transparency and accessibility of this analysis.

hydrodynamic volumes of free DNA and leptin.* This led to a volume of 7.88×10^{-23} m^3 for the complex, corresponding to a hydrodynamic radius for the complex of 26.6 nm. Using the same calculations for Q and η as above, the complex was calculated to have an μ_{EP} of -3.11×10^{-8} $m^2/V\cdot s$ by Equation 1.1.

Using the model to evaluate previous data. As mentioned previously, the drift in peak times is based almost entirely on variations in EOF resulting from slight changes in the capillary surface and/or buffer composition.[223-225] Therefore, the value of μ_{EOF} was adjusted, keeping μ_{EP} values constant, to examine previous data. First, the library DNA affinity data collected by CE (Figure 4.5) had a free DNA peak time of 2.875 minutes, corresponding to a net mobility of 2.26×10^{-8} $m^2/V\cdot s$. Keeping the free DNA μ_{EP} constant, the new μ_{EOF} was determined to be 5.72×10^{-8} $m^2/V\cdot s$. Therefore, the net mobility of the complex for this run was the sum of its μ_{EP} and the run μ_{EOF} of 5.72×10^{-8} $m^2/V\cdot s$, or 2.62×10^{-8} $m^2/V\cdot s$. This net mobility yielded a calculated peak time for the complex of 2.49 minutes. This is somewhat close to the A_2 peak (Figure 4.5) observed at 2.28 minutes which was believed to be the complex, but not as close as might be expected. There are two possibilities that could lead to this disparity. It could be that the A_2 peak belonged to the complex but differed from the time calculated by the model. The small time difference between the R110 and leptin peaks in the initial calculation means that errors in peak time would be amplified through the calculation. Additionally, a number of assumptions and simplifications were made in the calculations (particularly of the complex radius). These factors could definitely have led to the 8% time difference observed. Alternatively, it could be that the A_2 peak belonged to some fluorescent contaminant and not the complex. If the leptin sample was contaminated prior to sample preparation, the contaminant would be expected to increase linearly with leptin concentration, which matches with the trend observed (Figure 4.5). No fluorescent contaminant was observed previously or subsequently in the leptin stock, but this does not preclude a one-time contamination event leading to the results observed.

* On one hand, this assumption overestimates the thickness of the hydration shell of the complex, leading to a calculated volume and radius that are too large. On the other hand, assuming that two roughly spherical molecules combine to form a larger sphere (rather than a more oblong shape) would underestimate the radius of the new complex. Without any knowledge of their magnitude or simple methods to correct them, these errors were considered to offset each other.

Finally, the round 1 selection data (Figure 4.4) was examined to estimate the location of the complex band in order to determine whether the complexes were collected or not. Unfortunately, because the free DNA peak maxed the detector for this run, it is impossible to tell the exact peak time, but it was estimated visually to be in the range of 5.6-6.1 minutes. Using the early end of the range, 5.6 minutes was equivalent to a net mobility of 1.16×10^{-8} $m^2/V\cdot s$, necessitating a μ_{EOF} of 4.62×10^{-8} $m^2/V\cdot s$. This μ_{EOF} combined with the complex μ_{EP} (-3.11×10^{-8} $m^2/V\cdot s$) gave the complex a net mobility of 1.52×10^{-8} $m^2/V\cdot s$, corresponding to a peak time of 4.29 minutes. This is the earliest we would calculate the complex would reach the detector since using a higher estimate of the free DNA peak time (such as 6.1 minutes) would give rise to a lower μ_{EOF} and ultimately a later complex peak. The calculated 4.29 minutes is over one minute after the end of the collection window used in round 1 of selection (Figure 4.7), a significantly larger difference than observed in the library affinity data above. This essentially confirms that any DNA complexes were not collected in round 1. Even though the collection window was moved later in subsequent rounds, it is very likely that there were too few binding sequences at this point given their exclusion in round 1. This is consistent with the unsuccessful selection that occurred, as well as the possible complex peak observed in the affinity measurement of random library but not in subsequent SELEX rounds.

Fortunately, while the selection was unsuccessful, an incorrect collection window is a very easy problem to fix, highlighting the tunability of CE-SELEX. Additionally, the mobility model for this system developed above will allow more precise calculation of the

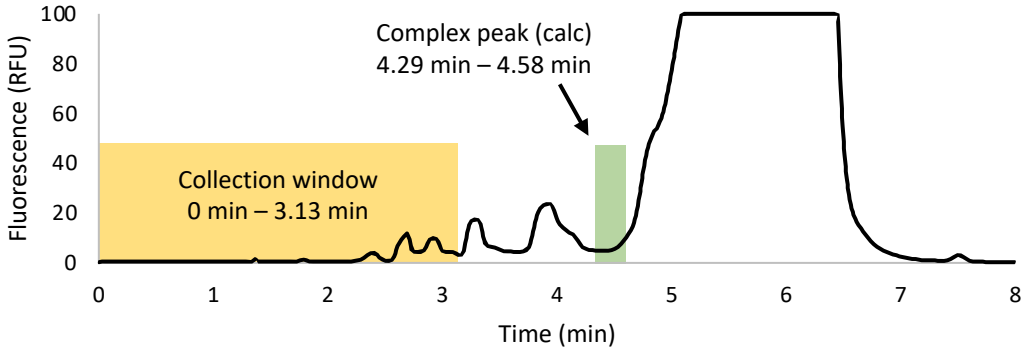

Figure 4.7: Leptin SELEX round 1 collection window and calculated complex peak time. The collection window used (C3 in Figure 4.4) ends at 3.13 minutes, over one minute before the earliest expected complex peak time based on calculations. This is a clear indication that DNA-leptin complexes were not collected during the round 1 selection as expected, likely the cause of the unsuccessful selection.

complex peak location regardless of daily changes in the EOF to avoid these issues in the future. However, if the collection window is moved later, the issue of collecting the unwanted early library peaks becomes more problematic. This can be solved by purification of the library before selection, such as by HPLC from the vendor or in-house pre-SELEX CE collection and amplification. Both introduce their own bias into the starting library, but cleaning up the peak and allowing much higher efficiency partitioning will likely outweigh this bias significantly. Another change that would help, with or without library cleanup, would be to increase the leptin concentration used in the first round of selection. The library unsurprisingly displays weaker affinity for leptin than for larger proteins like LDLR, so increasing the leptin concentration for the first partitioning would lead to collection of a much larger number of DNA complexes, hopefully overwhelming any unwanted DNA from the early peaks.

4.5 Conclusions

To fill the need for near-real time measurement of leptin secretion in cultured cells, an aptamer-based microfluidic system was proposed combining cell perfusion, on-line aptamer incubation, and quantification by μFFE-LIF. However, a well characterized high affinity aptamer against mouse leptin is required before a prototype can be effectively tested. Due to the similarity between mouse leptin and human leptin sequences, two aptamer sequences against human leptin from the literature (Lep2 and Lep3) were ordered to test affinity against mouse leptin in preparation for use of 3T3-L1 cells in the proposed device, a common system for the study of obesity. Three techniques were used to quantify the affinity: FP, CE, and ITC. FP yielded no fit data whatsoever, though this is not surprising given the frequency of false negative results in studying aptamers due to propeller motion and large probe size. CE and ITC both yielded results with high RSDs, but they suggested that our measured affinity for mouse leptin was significantly poorer than the affinity for human leptin that the authors demonstrated.

To begin CE-SELEX for new aptamers targeting mouse leptin, the sample buffer was adjusted only slightly from the Ringer's-based buffer planned for cell perfusion. Out of necessity, the NaCl concentration was reduced about 4-fold, and the physiological buffer

tris was added to improve pH stability during running. Surprisingly, the DNA peak exhibited very poor time reproducibility from day to day and significant peak size variation even from one run to the next. Attempts were made to correct the peak size uncertainty with small molecule dyes, but the variation was not observed in either dye to the same extent, suggesting a DNA-dependent phenomenon.

The library DNA peak exhibited a number of early features preceding the main peak by several minutes, making determination of the collection window problematic. In the first round, three different collection windows were used in case insufficient DNA was collected early on, but the earliest collection window (C3) gave rise to successful amplification and was used for future rounds. After four rounds, no affinity was observed by CE or FP for the library, round 2, or round 4. Additionally, a possible complex peak was observed in the library affinity assay but not in the others, a confusing fact. It was feared that the unsuccessful selection was due to accidental exclusion of the complex DNA during selection. A simple model was developed for calculation of the component mobilities and prediction of the complex peak location, which examined multiple different sample sets. According the model, the complex band was significantly later than the collection window used, which accounts for the poor selection. Future selection using updated collection window timing and a purified library is expected to result in successful selection, although additional techniques may be required to more accurately quantify affinity.

Chapter 5: Optimization of a differentiated cardiomyocyte system for evaluating the physiological effects of SPIDRs

5.1 Motivation

Heart muscle cells, or cardiomyocytes, engage in precisely timed transport of calcium ions within and around the cell to produce a healthy heart beat. Disorders in cardiomyocyte calcium management are frequently associated with cardiomyopathy and other cardiovascular diseases. The calcium pump sarco(endo)plasmic reticulum calcium ATPase (SERCA) and its control protein phospholamban (PLN) are largely responsible for regulating removal of calcium from the cytoplasm and initiating relaxation of the heart, making both proteins prime drug targets. It has been shown in recombinant systems that random sequence ssDNA, RNA, and some non-natural DNA analogues (XNAs) bind to one or both targets to increase apparent calcium affinity of SERCA. This interaction, which is dependent on oligonucleotide length and backbone, provides an excellent potential pharmacological mechanism for modulating heart relaxation. In order to investigate how this oligonucleotide interaction on a protein level translates to measurable changes in heart physiology, a more complex cardiac model system is needed. The work here aims to optimize a cardiomyocyte system differentiated from human induced pluripotent stem cells (iPSCs) as a suitable biological model to observe the physiological effects (and pharmacological potential) of oligos on the SERCA/PLN system.

5.2 Introduction

5.2.1 Cardiovascular disease and its impact

The human heart beats over 100,000 times per day, pumping 2,000 gallons of blood to every part of the body without a break.[226] Even though it is absolutely vital to our survival, we often take it for granted, as it generally carries out its complex and coordinated cellular ballet without our notice. Unfortunately, diseases of the heart and blood vessels, collectively called cardiovascular disease (CVD), are very prevalent and very serious, responsible for over 650,000 American deaths per year.[227] On top of this, healthcare costs of CVD are over $200 billion per year in the U.S.,[228] much of which is spent on alleviating the most pressing symptoms rather than on treating the biochemical source of the disease.

At a cellular level, the heart beat is driven by changing levels of cytoplasmic calcium ion, which is responsible for both triggering the beat (excitation) and the

contraction itself. A major part of that cycling is SERCA and its regulatory protein PLN, which together are largely responsible for controlling evacuation of calcium ions from the cytoplasm, causing muscle relaxation. Disorders in cardiac calcium cycling due to SERCA and PLN expression and activity are frequently associated with abnormal heart rhythm (arrhythmia) and weak heart beats (cardiomyopathy), both of which can lead to heart failure if left unchecked.[229, 230] Apparent causality can also be reversed, as it has been shown that reduced blood supply to the heart due to infarction (blockage) can lead to decreased SERCA expression in as little as four weeks.[231] Because of this common link between SERCA and heart health, it is believed that elevating SERCA activity could be used as a method to mitigate failing heart function even in cases where SERCA is not the underlying cause.

5.2.2 SERCA, PLN, and calcium cycling in cardiomyocytes

The finely tuned beating of individual cardiomyocytes (CMs) is achieved through spatial and temporal manipulation of calcium ions (Ca^{2+}) within the CM cytoplasm to control both signaling and contraction. The majority of intracellular calcium is stored in a tubular structure called the sarcoplasmic reticulum (SR). The cytoplasmic Ca^{2+} concentration rests at approximately 100 nM,[232] considerably lower than both the extracellular and SR concentrations. When triggered by an action potential, the cell membrane depolarizes and indirectly activates ryanodine receptors on the SR membrane. This allows a dramatic influx of calcium from the SR into the cytoplasm known as a calcium spark.[233] Cytoplasmic calcium binds to troponin and causes a structural rearrangement, which allows actin and myosin fibers to interact, leading to muscle contraction.

In order for the fibers to relax, the calcium concentration in the cytoplasm must decrease to resting levels.[232] This is achieved primarily by SERCA, a P-type ATPase in the SR membrane that transports calcium from the cytoplasm back into the SR lumen. Though some calcium is also expelled from the cell, at least 70% of calcium transfer out of the cytoplasm is performed by SERCA, giving SERCA the leading role in triggering relaxation of the heart muscle.[234]

SERCA activity is controlled in part by phospholamban (PLN), a 52-residue protein in the SR membrane. While PLN can be found as a lone monomer or a homopentamer, it is typically found in an equilibrium of states interacting with SERCA; this equilibrium tends toward states which lower SERCA's apparent calcium affinity, and therefore its activity.[235] In healthy hearts, phosphorylation at Ser16 by protein kinase A shifts PLN's equilibrium toward a non-inhibitory state, restoring SERCA activity and allowing control over calcium reuptake.[236]

5.2.3 SPIDRs and interactions with cardiac proteins

It has been observed previously that random sequences of RNA, ssDNA, and some XNAs interact strongly with PLN ($K_d \leq 10$ nM) and, more importantly, relieve PLN's inhibition of SERCA activity.[237] For a random sequence pool, this level of affinity towards a target other than a dedicated DNA- or RNA-binding protein is unprecedented. While these oligos undoubtedly share some similarity with aptamers, aptamers are defined by their specific sequence and structure, a specificity which is absent in this interaction. To differentiate from aptamers, an oligonucleotide which engages in high-affinity sequence-independent binding has been labeled a small protein-interacting DNA or RNA (SPIDR). Even more interesting is that the extent of relief of SERCA inhibition is dependent upon both SPIDR backbone (e.g. RNA versus XNA) and oligonucleotide length. This makes a strong case for investigating SPIDRs as a therapeutic agent to enhance heart contractility, as having systematic parameters besides concentration to fine tune drug interactions would increase drug applicability and decrease the likelihood of side effects. SPIDRs have shown significant affinity for PLN and a corresponding increase in SERCA calcium affinity, but these effects have primarily been observed in reconstituted vesicle systems using purified protein (Figure 5.1).[237] In order to tell whether the increased affinity of SERCA in the presence of SPIDRs leads to the predicted increase in muscle contractility, similar experiments must be carried out in an appropriate cardiac model system.

5.2.4 Impedance measurement of differentiated CMs as a suitable cardiac model

In any type of biological work, picking the appropriate model system can have a huge impact on the research practicalities as well as the conclusions that can be drawn. On one hand, a simple system with a small number of constituents and variables (such as the

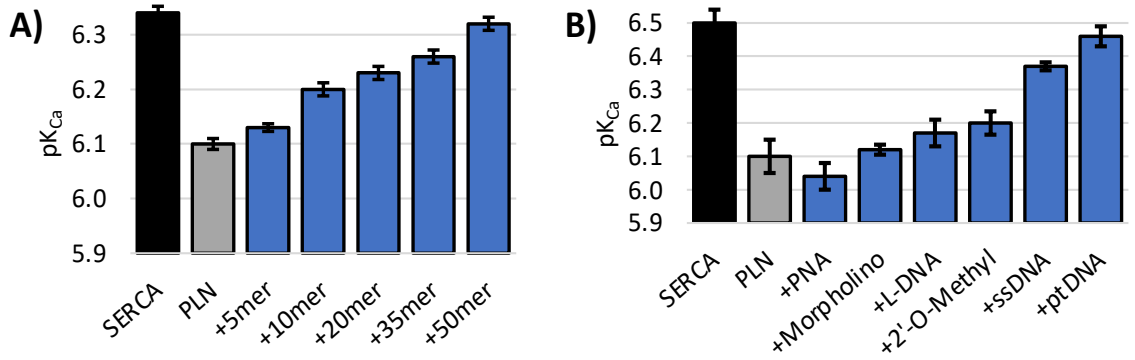

Figure 5.1: Effects of SPIDRs on PLN's inhibition of SERCA activity in reconstituted vesicle system. For each condition, normalized SERCA activity was measured using a coupled enzyme assay at increasing calcium concentrations to generate an activity curve (not shown) and estimate pKCa (pCa^{2+} at activity half maximum). As expected, SERCA alone showed significantly higher calcium affinity (pKCa) than upon the addition of PLN in both experiments. **(A)** The addition of increasing lengths of random sequence RNA to the SERCA+PLN system restores SERCA's calcium affinity, with the addition of 50mer RNA removing all inhibitory effect of PLN (no significant difference). **(B)** The addition of different types of random sequence oligonucleotide 20mers – peptide nucleic acid (PNA), morpholino nucleic acid, enantiomeric L-DNA, 2'-O-methyl DNA, ssDNA, and phosphorothioate DNA (ptDNA) – increased SERCA calcium affinity to different extents, with phosphorothioate DNA yielding the greatest effect. XNA structures are shown in the Appendix (Figure A.7). Adapted from Soller *et al*.[237]

reconstituted lipid system) will be cheaper, more reproducible, and easier to learn and manipulate. However, simple systems lack many components and much of the underlying complexity present in the original system, which may render the model unrepresentative and the results moot. Ultimately we settled on in-house differentiation of human iPSCs for a number of reasons. First, iPSCs can be propagated essentially indefinitely, providing the large supply of CMs to test various SPIDRs, concentrations, and time courses. Use of animal models or primary cardiomyocytes (which do not proliferate) would be extremely limiting to the number of independent experiments that could be performed. Second, the cardiac systems of small animals (i.e. mice) are not the most representative of humans', whether in simple matters like resting heart rate or complex issues like presentation of genetic disorders.[238] Third, primary cardiomyocytes are very difficult to obtain in the quantities needed for these experiments (particularly cells with a specific disease phenotype for future work), and measuring their base beat rate is difficult since they do not beat spontaneously like iPSC-derived CMs. Fourth, the differentiation of iPSCs to CMs is well established in the literature by a number of different strategies,[239-241] suggesting that the process will be easily optimizable for our uses without utilizing commercial CMs.

Once the CM model has been established, the effects of different SPIDRs can be assayed by exposing CMs to the oligos using a transfection agent, such as Lipofectamine. SPIDRs are expected to increase SERCA activity and decrease the time required for the relaxation process, which is hypothesized to lead to an increased beat rate and amplitude while decreasing fall time. (Fall time measures the rate of relaxation and is the amount of time required for the amplitude to return from 90% to 10% after a beat.) One emerging strategy to track mechanical beating with high accuracy is a cellular impedance platform, which uses gold-plated electrodes built into the well to measure changing impedance across the cells in response to a very small alternating current.[242-244] When relatively low frequency voltage is applied, current travels predominantly along the cell membranes (paracellular), and the impedance signal tracks changes in cell and junction morphology that occur during contraction.[244]

The main goal of my work was to lay the foundation for the project trajectory above by demonstrating reproducible CM generation and the suitability of our cells for impedance experiments. Herein, a procedure for culturing iPSCs for differentiation is developed, with a focus on optimizing cell passaging maximal cell coverage at the start of differentiation. The process of differentiation to CMs is optimized, including metabolic selection for improving CM purity. Finally, preliminary impedance measurements are shown, along with observations about replating cells and suggestions for future improvement.

5.3 Methods

The optimization of iPSC growth and differentiation to CMs makes up the majority of the work in this chapter and involved numerous conditions tested across dozens of variables. For this reason, enumerating individual experimental conditions in this section is unfeasible. The methods below represent only the optimized protocol selected based on experimental results and practical considerations. Details on adjustments to this protocol and the conditions tested are specified in the results (section 5.4) with respect to their impact on the growth and differentiation process.

5.3.1 Materials

Cells. Cells from the iPSC line BXS0116 were obtained from American Type Culture Collection (ATCC, Manassas, VA). Cells from iPSC line SCVI-15 were obtained from the Stanford University Cardiovascular Institute (SCVI) Biobank (Stanford, CA).

Chemicals. Dimethylsulfoxide (DMSO) was obtained from ATCC (Manassas, VA). Growth factor reduced Matrigel basement membrane extract (BME) was obtained from Corning (Corning, NY). Essential 8 media (E8), DMEM:F12 media, 1× phosphate-buffered saline minus Ca^{2+} and Mg^{2+} (PBS), Roswell Park Memorial Institute (RPMI) 1640 media, RPMI 1640 media minus glucose, 50× B-27 supplement, and 50× B-27 supplement minus insulin were obtained from Gibco (Waltham, MA). WNT inhibitor Wnt-C59 was obtained from Santa Cruz Biotechnology (Dallas, TX). Rho-associated kinase (ROCK) inhibitor Y27632 and glycogen synthase kinase-3 (GSK3) inhibitor Chir99021 were obtained from Selleckchem (Houston, TX). EDTA solution was obtained from Invitrogen (Waltham, MA). mTeSR1 media was obtained from Stemcell technologies (Vancouver, Canada). Cultrex stem cell qualified Pathclear reduced growth factor BME was obtained from Trevigen (Gaithersburg, MD). Bambanker was obtained from Wako Chemicals (Richmond, VA).

All chemicals besides inhibitors (Y27632, Chir99021, Wnt-C59) were sterile upon receipt. Inhibitors were dissolved in DMSO to at least 1000× working concentration, passed through a 0.2 μm filter, and stored in sterilized containers. Stock Matrigel and Cultrex BME (12-18 mg/mL) were aliquoted upon arrival and stored at -80˚C. Stock and aliquots were thawed at 4˚C overnight before use. To avoid premature gelling, BME was kept on ice during use, plastic tubes and pipet tips were refrigerated at least 15 minutes prior to contact with BME, and all handling of BME was done as quickly as reasonably possible.

5.3.2 Cell plate preparation

Matrigel was diluted 1:200 in ice cold DMEM:F12 and mixed by inversion. The mixture was added to each well – 2 mL/well for a 6 well plate (6WP), 1 mL/well for a 24WP, or 200 μL/well for a 96WP or 96-well sensor plate – and the plate was incubated at 37˚C for at least one hour but no more than three days prior to use.

5.3.3 iPSC growth and passaging

iPSCs frozen in liquid nitrogen vapor were thawed rapidly in a 37˚C water bath, mixed with 2 mL of mTeSR1 media, and centrifuged at 200×g for 5 minutes. The supernatant was aspirated and the cells were dispersed in 2 mL of mTeSR1 media with 10 μM Y27632 in one well of a 6WP. Cells were changed to a 1:1 mixture of mTeSR1 and E8 after 24 hours, and to pure E8 after another 24 hours and every 1-2 days.

iPSCs were passaged at 65-80% confluency, approximately every 4 days. Cells were rinsed with PBS then incubated in 1 mL PBS with 0.5 mM EDTA at 37˚ for 6 minutes until cells were translucent white to the naked eye, then PBS:EDTA was gently removed. One mL of passage media, E8 with 10 μM Y27632, was pipetted directly onto the cells to dislodge them and triturated (pipetted up and down) 4-5 times to break up large clumps. Suspended cells were diluted in passage media to achieve a split ratio of approximatey 1:7 and mixed gently. Media was removed from the coated plate (prepared above) and cell suspension was added to the new plate, 2 mL/well for 6WPs (for continued iPSC growth) or 1 mL/well for 24WPs (for differentiation to CMs). After ~24 hrs, media containing Y27632 was removed, cells were rinsed with PBS, and fresh E8 without Y27632 was added. Fresh media was supplied every 1-2 days, and within 24 hours prior to passaging where possible.

5.3.4 Differentiation to CMs

Base media were prepared and used for up to 8 weeks: 1× B-27 minus insulin in RPMI 1640 (“M1”), 1× B-27 in RPMI 1640 minus glucose (“M2”), and 1× B-27 in RPMI 1640 (“M3”).

iPSCs were grown in a 24WP for 4-5 days until most of the cells were highly compacted (see section 5.4.2) and cells were 90-95% confluent, defined as day 0 (D0). Cells were rinsed with PBS, then 1 mL of ice cold M1 with 8 μM Chir99021 and 1:200 BME was added to each well. After 24 hours (D1), cells were rinsed with PBS and 1 mL of M1 was added to each well. On D3, cells were rinsed and 1 mL of M1 with 2 μM Wnt-C59 was added to each well. Cell media was replaced with M1 with 2 μM Wnt-C59 every 2 days and cells were checked for evidence of spontaneous beating.

Once beating was observed over at least 50% of the well surface, and the amount of beating cells in each well had stopped increasing (typically D10–D14), cells were rinsed twice with PBS and 1.3 mL of M2 were added to each well. After three days, cells were rinsed with PBS and 1 mL of M3 was added to each well. For wells that still contained ≥25% non-beating cells, the M2 incubation process was repeated. Cells were maintained in 1 mL of M3, replaced every 1-2 days.

5.3.5 Replating of CMs

A well containing beating CMs was rinsed with PBS and incubated with 1 mL of Accutase for 2-3 minutes at 37˚C until dead cells stuck in the Matrigel (see section 5.4.3) were loosened. The plate was swirled to suspend these cells and the liquid was aspirated. The well was incubated with 1 mL of fresh Accutase at 37˚C for 5-10 additional minutes until previously beating cells had been loosened. Cells were gently triturated with a P1000 then added to a 15-mL centrifuge tube with 5 mL of M3. The tube was centrifuged at 200×g for 5 minutes, the supernatant was aspirated, and 200 µL of M3 was added per new well of a 96WP or sensor plate. Cells were gently triturated to break up the pellet and any large colonies remaining in suspension. Matrigel solution was removed from the new plate and 200 µL of suspension was added to each well.

Newly replated cells were allowed to incubate undisturbed for 24 hours. M3 media was changed 24 hours after replating and every 1-2 days after. For each media change, half the media from a well (100 µL) was removed and replaced with fresh media, then the process was repeated. Added media was allowed to gently drip down the side of each well to avoid disturbing the cells. The impedance of replated cells was measured every 3-4 days. Cells with no beating after 21 days were considered to have failed the replating process.

5.3.6 Microscopy and imaging

Cells were viewed on a Labomed TCM-400 inverted tissue culture microscope with phase contrast through a 4×, 10×, or 20× objective. Images were obtained with a Moticam-2 2.0 MP camera and Motic Images Plus 3.0. Brightness and contrast were adjusted in some images for ease of viewing.

5.3.7 Impedance measurement

Impedance measurements were made on the Nanion CardioExcyte 96 system. The system used an Ibidi gas mixer and humidifying column set to 37˚C, 5% CO_2, and 90% relative humidity. Once the correct conditions were reached, cells were allowed to incubate in the test chamber for 10 minutes prior to measurement. A 10kHz AC current provided 1000 measurements per second for a 7-second sweep every 3 minutes. No pacing stimulation was used in order to obtain informative beat rate data.

5.4 Results and Discussion

A number of sources served as good starting points for both iPSC growth and CM differentiation, including literature protocols,[241, 245] protocols from ATCC[246] and the SCVI Biobank,[247, 248] and preliminary procedures used previously in the group.[249] Optimization was largely broken into three parts. First, the iPSC culturing procedure was optimized to obtain a healthy monolayer across as much of the well as possible for efficient CM differentiation. Second, CM differentiation and metabolic selection were optimized primarily to maximize the number of beating CMs obtained, and secondarily to reduce the complexity and subjectivity of the differentiation procedure for future researchers in the group. Third, the process of replating CMs into the specialized 96-well electrode sensor plates was optimized with the primary goal that adhered cells resuming coordinated beating, and the secondary goal of maximizing impedance signal intensity and reproducibility. Preliminary impedance measurements are also shown.

5.4.1 Stem cell growth

iPSC thawing. A number of sources suggest normal growth of iPSCs in E8 media but thawing of cells from cryostorage into mTeSR1 media. Thawing cells is a rare occurrence and uses little of the thawing media, which would lead to wasting most of the mTeSR1 due to its six month expiration. Given the expense and (at times) poor availability of mTeSR1, I took the opportunity to evaluate the importance of mTeSR1 immediately after thawing to see if the procedure could be streamlined by removing it. Stanford iPSCs at passage 6 were thawed as indicated in section 5.3.3 except for differences in the media: cells were plated into E8, fresh mTeSR1, or mTeSR1 significantly past its listed expiration

date (each time with 10 μM Y27632). At 24 hours, each mTeSR1 condition was changed to a 1:1 mixture of mTeSR1 and E8 while the E8 condition was changed to new E8. Following the media change, the mTeSR1 conditions showed good coverage of healthy looking cells while the E8 condition showed poor attachment efficiency. Several more days of growth confirmed a lack of adhered cells for the E8 attachment condition. Interestingly, the cells thawed in expired media were indistinguishable from those in fresh media, even after several passages. To date, cells have been thawed in mTeSR1 kept at 4˚C up to 18 months past its expiration date and still displayed excellent morphology. This is important to know as obtaining new mTeSR1 is no longer a barrier to periodic iPSC thawing.

Optimizations to enhance the monolayer. Once cells were thawed and growing, one of the primary factors that seemed to affect differentiation efficiency was the establishment of a consistent, compacted monolayer of iPSCs, which in turn stemmed from homogenous distribution of seed colonies across the well during passaging. However, iPSCs are quite fastidious and do not tend to grow well from a single isolated cell. Therefore, the amount of homogenization during passaging was very particular: insufficiently homogenized cells led to adherence of large clumps of cells that caused uneven growth, while overly homogenized cells resulted in many single cells that didn't tend to grow well. Overall, 3-4 full mixes with a 1000 μL pipet seemed to deliver optimal homogenization, but multiple other factors were discovered that impacted good monolayer formation.

Initially, the cell passaging schedule used in the group called for splitting cells once fully or nearly confluent based on other sources and past experience. However, experimentation with earlier splitting demonstrated that highly confluent cells develop some stronger intercellular interactions that require more pipetting to break up. As a result, cells split at 60-80% confluence ("early" split) yielded a more even distribution of appropriately sized seed colonies across the new well that those split at 80-95% confluence ("late" split) and had a lower incidence of cell clumps (Figure 5.2), which disrupt the monolayer and may begin unwanted differentiation. Split ratios ranging from 1:3 to 1:10 are frequently quoted for iPSCs, though our iPSCs seemed to grow quite well, meaning that splitting less than about 1:5 resulted in cells ready to be split again almost immediately.

Contrary to some literature, we found that splitting 1:8 or harsher did not create wells seeded too sparsely to grow. However, because of the length of time until confluence in these situations, it was found that the well frequently became highly confluent in the center before there was much cell coverage on the sides, a problem for timing differentiation appropriately. A split ratio of about 1:7 was found to be ideal for creating even coverage in seeded wells, adjusting slightly higher or lower depending on confluence in the well being split.

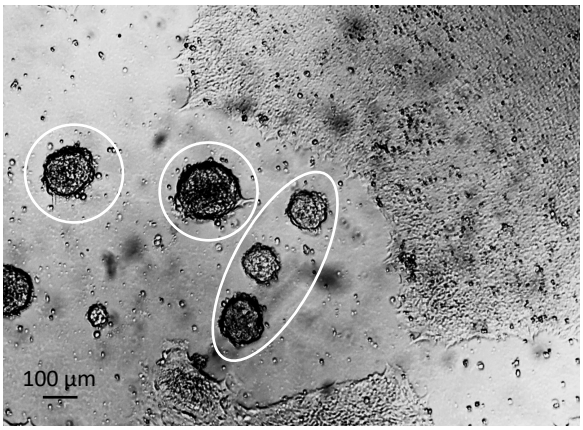

Figure 5.2: iPSC clumps (4×). iPSCs sometimes form small multilayer clumps consisting of dozens or hundreds of cells. These structures (circled) do not propagate outward as well as clean iPSC monolayers (top right and bottom) and may begin unwanted differentiation.

The recency of the BME application was also found to be a factor. Plates to which Matrigel had been applied five days or more before seeding seemed to grow unevenly and also developed more stacked cells. This was believed to be due to uneven deterioration or "flow" of the BME over time which led to differences in adherence and/or rate of growth based on location. Therefore, coating wells with BME individually and within 24 hours of plating was found to be far superior to large batch coating.

In comparing the each cell line, iPSCs from ATCC were found to be more spindly and spread outward earlier than the rounder cells and colonies of Stanford iPSCs (Figure 5.3). The cause is unknown, as the cell lines are largely similar in their source cell type and reprogramming method, but this resulted in the ATCC cells more quickly spreading over the entire well surface in a web-like network, whereas the Stanford cells had a tendency to grow outward only after forming a dense colony at the center. Consequently, ATCC cells formed the homogenous monolayer ideal for differentiation whereas Stanford cells often became overcrowded at the center of the well before the edges were sufficiently confluent. Initial attempts were made to differentiate both cell lines, but the Stanford cells were phased out over time as the ATCC cells showed better differentiation results.

The findings regarding iPSC growth and passaging are summarize in Table 5.1.

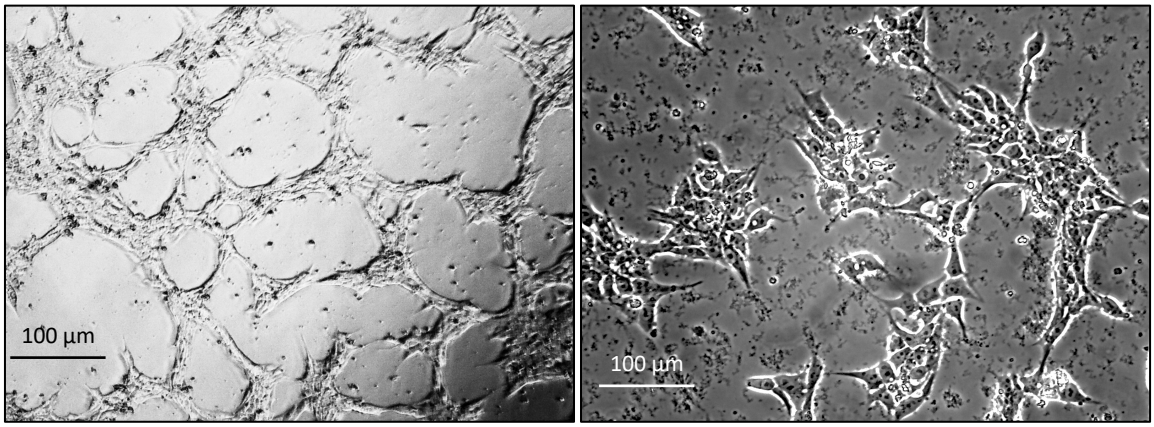

Figure 5.3: ATCC versus Stanford iPSC growth 24 hours after seeding (10×). **(Left)** ATCC iPSCs and colonies are more spindly, quickly spreading outward to form a web-like network. **(Right)** Stanford iPSC colonies are rounder and propagate in place for longer, not branching out until the central colony is denser.

Thawing media	E8	mTeSR1 (fresh)	mTeSR1 (old)	
	×	+	+	
Trituration (times pipetted)	1 - 2	3 - 5	6 +	
	–	+	×	
Confluence at passaging	60 – 80%		80 – 95%	
	+		–	
Split ratio	1:3	1:5	1:7	1:10
	–	+	+	–
iPSC line	Stanford		ATCC	
	–		+	

Table 5.1: Summary of the effects of thawing and splitting conditions on iPSC monolayer growth. For each variable investigated, the conditions tested are shown along with the effect on iPSC growth, where "+" indicates that cells established a homogenous monolayer, "–" indicates that cells grew unevenly or in multiple layers, and "×" indicates that cells died or adopted concerning morphologies. The shaded conditions indicate those chosen for future work.

5.4.2 CM differentiation

Successfully differentiated CMs begin to contract spontaneously approximately 7-12 days after the start of differentiation. Contraction typically occurs in isolated pockets at first, with small movements that can be difficult to see even at 4× objective magnification. Over the next several days, the number of beating cells gradually increases, and the size and frequency of the contractions generally grow as well. Luckily, this obvious phenotypic display makes positive identification of CM colonies very straightforward and circumvents the need for antibody labeling or morphology tracking. Still, iPSCs must go

through a week of carefully timed steps before any beating can be seen, and issues at any point can lead to weak or non-existent beating with no obvious clue as to the specific cause. The differentiation procedure and metabolic CM selection were optimized in order to generate the largest number and highest purity of beating cells for impedance assays. Throughout this section, references to "failed" or "unsuccessful" differentiation indicate that cells did not display any significant beating after 14 days or that noticeable cell detachment was observed prior to 14 days that did not grow back.

Timing the start of differentiation. Many sources suggest beginning CM differentiation when iPSCs have reached 85-100% confluence but also admit that the timing should be optimized for each cell line. A complicating factor is that the well may be highly (or overly) confluent in some areas, usually the center, and relatively sparce in others. This makes quantitative estimates of confluence an unrepresentative or incomplete description of the cells' status. Optimizations have already been shown to try to obtain consistent confluence across the well, but it is impossible to completely eliminate radial differences in confluence. Initially, experimental conditions were quantified by approximate confluence near the edges of the well (since the center was already fully confluent). The ends of the range displayed problematic signs: differentiation of wells not fully confluent at the center (est. 70-85% confluent at the edges) led to significant cell detachment, while wells that were confluent wall-to-wall developed some multilayer structures before differentiation and never successfully differentiated. However, there seemed to be no significant correlation with differentiation success over quite a wide range of confluence in the center of the range – conditions that appeared to be identical gave rise to completely different results from one time to the next. A number of different conditions did give rise to beating cells one time or another, but none more than half of the attempts.

Rather than focusing on confluence, the cells' morphology was tracked in an attempt to obtain more reproducible differentiation. Work by Wakui *et al*.[250] and by Healy and Ruban[251] provided good reference images and descriptions of iPSCs at different stages of growth. Highlighted in this and other work is the importance of compaction, the process by which stem cells increase the level of physical and chemical interaction with one another in preparation for differentiation. iPSCs need to be sufficiently compacted in order to

efficiently relay the signals for directed differentiation, which explains why the insufficiently confluent cells did not differentiate well. On the other hand, once iPSC have become fully confluent and have remained compacted for more than a day or so, there is a drastically increased likelihood that the cells will begin to form multilayer structures and/or differentiate randomly. This premature differentiation toward a different cell type could explain why waiting for full confluence did not result in beating cells either. With this knowledge in hand, iPSC were grown until the main monolayer had a high degree of compaction, indicated by distinct nucleoli and minimal visible separation between cells (Figure 5.4), to begin differentiation. Due to variation in growth and seeding, the ideal level of iPSC compaction did not correspond to the same level of cell confluence each time, which is likely why trying to time differentiation by confluence alone was not reliable.

Beginning differentiation once the center was well compacted led to more reliable differentiation, with some level of beating achieved 70-80% of the time. While a large number of cells still lifted off early in differentiation (more details later), judging

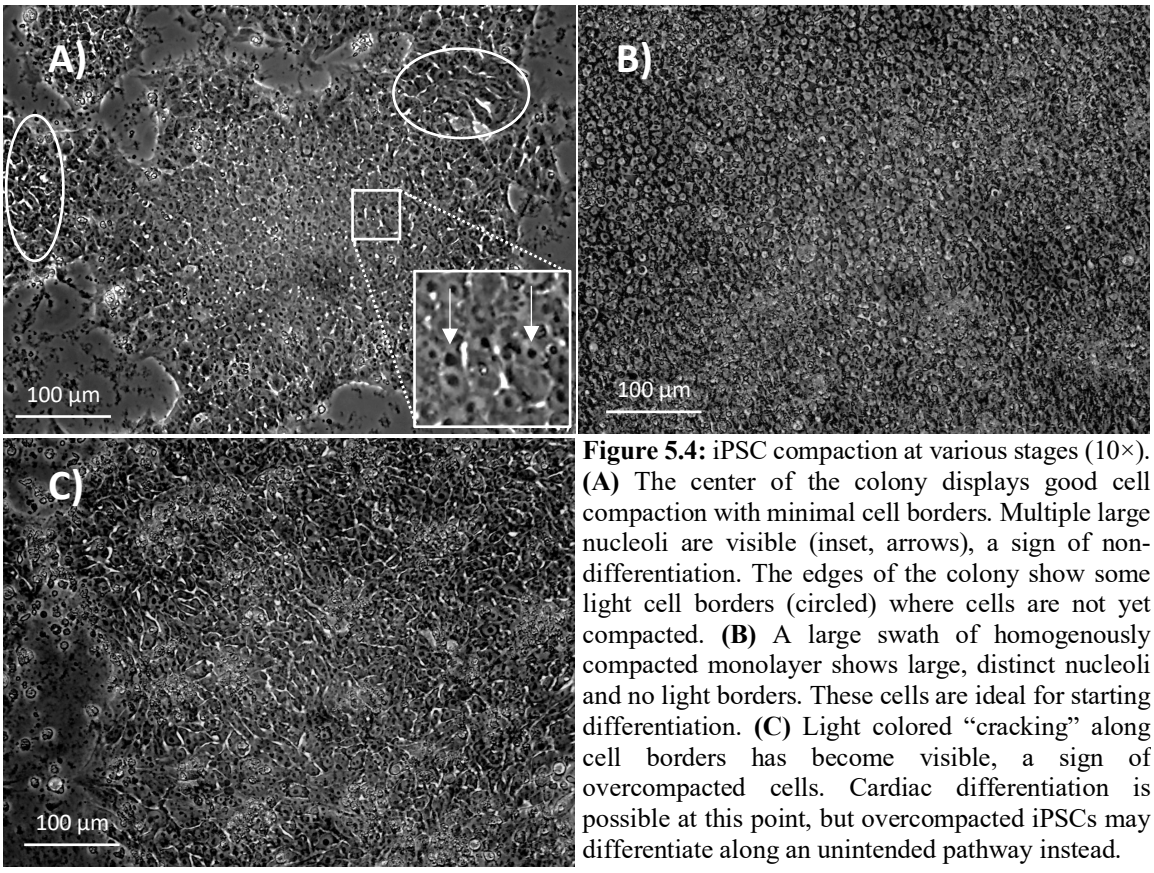

Figure 5.4: iPSC compaction at various stages (10×). **(A)** The center of the colony displays good cell compaction with minimal cell borders. Multiple large nucleoli are visible (inset, arrows), a sign of non-differentiation. The edges of the colony show some light cell borders (circled) where cells are not yet compacted. **(B)** A large swath of homogenously compacted monolayer shows large, distinct nucleoli and no light borders. These cells are ideal for starting differentiation. **(C)** Light colored "cracking" along cell borders has become visible, a sign of overcompacted cells. Cardiac differentiation is possible at this point, but overcompacted iPSCs may differentiate along an unintended pathway instead.

differentiation timing by compaction and morphology was significantly more reliable than by confluence alone. If colonies became overcompacted (Figure 5.4C), attempts were still made to differentiate the cells, but these wells generally never exhibited a large number of beating cells.

Media supplement and inhibitor schedule. Initial attempts to differentiate iPSCs to CMs used the procedure laid out by Burridge *et al*.[245] using chemically defined media in a 6WP. The advantages of a chemically defined media include better reproducibility compared to animal-derived components and improved cost efficiency and optimizability compared to commercial supplements. RPMI 1640 media supplemented with recombinant human albumin and L-ascorbic acid 2-phosphate (deemed CDM3) was used as the base media throughout. Canonical WNT signaling was activated at the start of differentiation (D0-D2) with Chir99021 and later subdued with Wnt-C59 (D2-D4). Significant changes in cell morphology occurred within the first 24-48 hours, including a multilayered architecture of varying thickness and density, the appearance of sections free of any cells, and cracking of the cell boundaries similar to Figure 5.4C. However, even in cases where most of the cells were retained and appeared healthy, fewer than 50% of attempted differentiations yielded any beating cells, and beating was typically limited to a few small colonies covering less than 5% of the well. Changes to concentrations of Chir99021 and Wnt-C59 were investigated (50%-150% of original concentrations), which impacted morphological changes somewhat but did not improve the proportion of beating cells.

In place of albumin and ascorbic acid phosphate, differentiation was attempted using the commercial supplement B-27 and substituting RPMI 1640 minus insulin, both of which feature in the work of Lian *et al*.[241] This work and others also apply a different time course, using a WNT activator D0-D1, no WNT modulation D1-D3, and a WNT inhibitor from D3 until significant beating was observed. The B-27 supplemented media was tried in both time courses (Figure 5.5), and in both seemed to initiate a more aggressive change in morphology. Significant portions of the well (usually around the edge) were bare when viewing on D1 or D2 after differentiation (Figure 5.6), which resulted in significantly fewer adhered cells moving forward. Again, only about 50% of attempts gave rise to beating

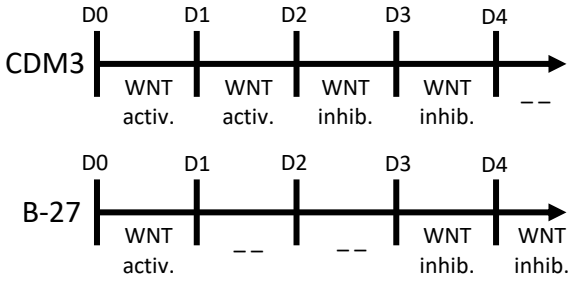

Figure 5.5: Different timelines for WNT activation and inhibition during CM differentiation. Notably, the CDM3 method (Burridge *et al.*)[245] applies two days of WNT activation while the B-27 method (Lian *et al.*)[241] has only one day of activation and a two day gap. Additionally, the B-27 method continues to apply a WNT inhibitor until substantial beating is observed, whereas the CDM3 method ceases WNT inhibition after D4.

cells, but many successful attempts saw significant beating across a much larger portion of the well (20-50%). There was no obvious difference between using the CDM3 timeline and the timeline from Lian *et al.*, but the latter was implemented moving forward because it had been developed in conjunction with the media system being used. With the new timeline attempts were made to decrease the concentration of Chir99021 from 8 μM to 6 μM or 4 μM. Doing so reduced the number of cells lost during differentiation but at the cost of less frequent and less extensive beating cells.

BME optimization. During these experiments and moving forward, differentiation was performed in 24WPs rather than 6WPs to allow a larger number of conditions and/or wells per condition to be tested and to facilitate easier quantification of cell adhesion and beating. In an attempt to decrease cell detachment without negatively affecting differentiation, the BME coating procedure was revisited. Some cells were grown on Cultrex BME with the same protein concentration and compared alongside cells grown on Matrigel as before, but no difference was observed. Additionally, cells were grown on

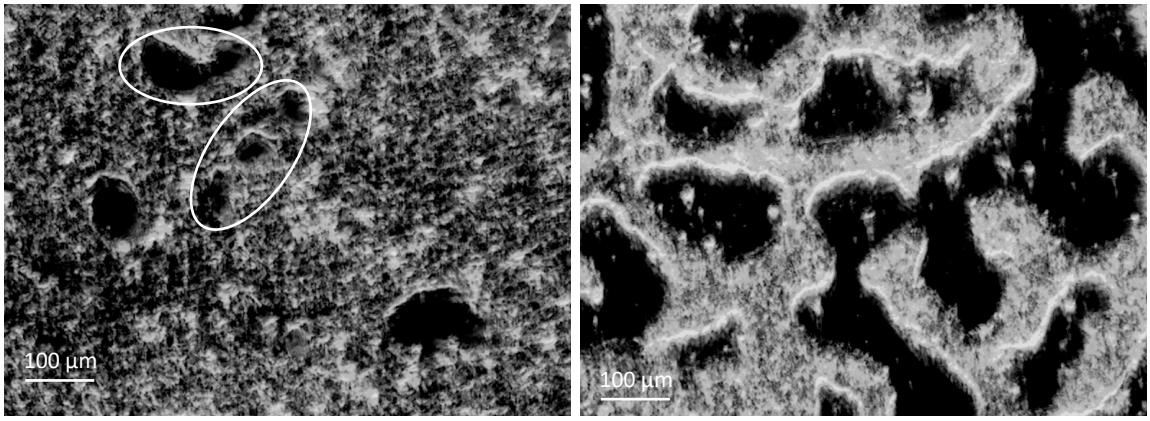

Figure 5.6: Cell detachment during CM differentiation (4×). 24 hours after starting B-27 differentiation, noticeable gaps in the monolayer appeared. **(Left)** The center of the well often retained most of the cells with only a few gaps appearing (small gaps circled), likely due to cell rearrangement. **(Right)** Farther from the center of the well, cells were often absent from 50% or more of the surface due to significant cell detachment.

plates coated with Matrigel at various concentrations up to 225 μg/mL, and the percent of surface area with beating cells and the proportion of beating cells were each estimated by eye. There were minimal visible differences during iPSC growth, but beating was achieved in much higher rates within the sweet spot of 90-180 μg/mL (Figure 5.7). Coating used 90 μg/mL Matrigel moving forward.

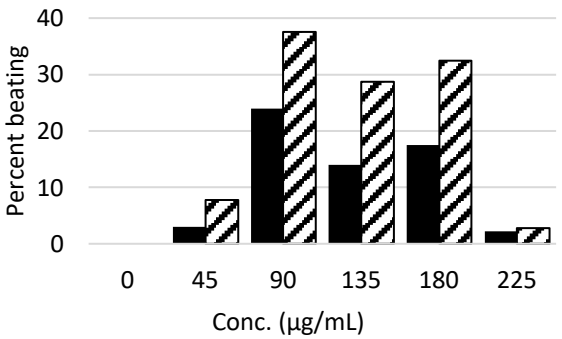

Figure 5.7: Effect of bottom Matrigel thickness on CM beating. CMs differentiated on a plate coated in 90 μg/mL Matrigel displayed the greatest surface area with beating cells (solid) and the greatest percent of cells beating (hatched). No iPSCs adhered to uncoated wells, leading to no CM coverage.

Another condition tested was the matrix "sandwich" method introduced by Zhang *et al*.,[252] whereby a new layer of BME is laid down on top of the cells at, or just before, the start of differentiation. While the authors' primary intention with this process was to enhance CM differentiation by better simulating the cellular environment of the developing embryo, it was also believed that this might help our cells remain affixed to the surface better during differentiation, resulting in more cardiomyocytes for replating. To test this, the D0 media with Chir99021 was prepared ice cold with a small amount of Matrigel (50 μg/mL) and the media was changed normally. The resulting plates were only about 50% full with cells by D2 but displayed beating across up to 80% of the cells by D12, a vast improvement over the previous method.

In an attempt to retain more cells, two test runs were performed adding the sandwich Matrigel in ice cold E8 to the cells 24 hours or 3 hours before switching the cells to differentiation media. The thought process was that this would provide extra stabilization to the cells before the destabilizing effect of the WNT activator was applied and prevent some cell loss. Interestingly, applying the sandwich layer 24 hours early, even in the absence of Chir99021, created a large number of gaps anyway that did not lead to improvement over simultaneous Matrigel and Chir99021 addition. Both of the conditions with early Matrigel addition led to a noticeable decrease in the number of beating cells by D14. This could be due to iPSCs under the influence of the Matrigel sandwich alone differentiating toward non-CM lines, reducing the number of iPSCs available for CM

differentiation. Another possibility is that Chir99021 added atop the already solidified Matrigel did not penetrate to the cells as well or did not affect the iPSCs in the same way in the presence of the new Matrigel layer. In light of these observations, the sandwich Matrigel and D0 differentiation media were applied simultaneously moving forward.

The findings regarding differentiation conditions are summarized in Table 5.2.

5.4.3 Cell replating and preliminary impedance results

The end goal of the differentiation process was to obtain spontaneously beating CMs that could undergo impedance measurements to monitor contraction in response to SPIDR dosing. The CardioExcyte system makes impedance measurements using a custom disposable electrode-embedded 96-well sensor plate, meaning that beating CMs must be replated from a 24-well differentiation plate to the sensor plate before measurements can

D0 timing by edge confluence	70-85%	85-95%	>95%		
	×	–	–		
D0 timing by compaction	Partly compacted	Mostly compacted	All compacted (some cracking)		
	–	+	–		
Media supplementation	CDM3	B-27			
	–	+			
[Chir99021]	4 µM	8 µM	12 µM		
	–	+	×		
[Wnt-C59]	1 µM	2 µM	3 µM		
	–	+	+		
Differentiation timeline	CDM3 (2-day WNT activ.)	B-27 (1-day WNT activ.)			
	+	+			
BME type	Matrigel	Cultrex			
	+	+			
Applied BME conc. (µg/mL)	45	90	135	180	225
	–	+	+	+	–
BME sandwich	None	Simultaneous	3 hrs before	24 hrs before	
	–	+	–	–	

Table 5.2: Summary of the effects of multiple variables on CM differentiation. For each variable investigated, the conditions tested are shown along with the effect on iPSC growth, where "+" indicates that beating cells were seen in large numbers or with high frequency, "–" indicates that cell beating was observed occasionally, and "×" indicates that cells adopted concerning morphologies or were never seen beating. The shaded conditions indicate those chosen for future work.

take place. Additionally, measurements are most precise when the CMs are high purity, covering a large portion of the surface area, and beating synchronously.

Metabolic selection. In order to improve CM purity, beating cells were subjected to a metabolic selection media without glucose. In this media, undifferentiated iPSCs are starved without their normal sugar source, but CMs are able to survive adequately by metabolizing the galactose present in B-27. Cells were generally grown in the selection media for 72 hours, returned to a glucose containing media for one day, then subjected to another 72 hours in the selection media. For many wells, there was a significant increase in the amount of beating observed, both in surface area and in magnitude of contraction, following metabolic selection. While it is possible that a large proportion of cell continued to differentiate in these cases (galactose is known to improve CM maturation[253]), the more likely explanation is that the presence of undifferentiated iPSCs amongst the CMs reduced CM mechanical and paracrine interactions, lessening or preventing beating.

Two problems were encountered during the selection. First, it was not uncommon for up to half of the cells to detach from the surface during metabolic selection, even those known to have contained beating sections previously. It was hypothesized that this was due to CMs being unable to continue growing in the absence of live neighbors, or due to dead iPSCs pulling attached CMs off the surface. In either of these cases, this occurrence would seem less likely in colonies with a high CM:iPSC ratio. This was confirmed by the observation that wells with a significant amount of beating prior to selection were more likely to have single cells or small colonies floating after selection. On the other hand, wells with fewer beating cells initially often had large sheets of cells floating following selection. The second issue was that many of the dead cells became trapped within the Matrigel. Though not easily distinguishable in still images, these cells were clearly isolated from other cells in the colony and were neither fixed to the surface nor completely free as though floating. Attempts were made to remove some of these cells during the replating process by performing two sequential rounds of cell detachment – a short incubation with accutase to detach and remove these weakly attached dead cells, and a longer incubation required to detach the larger beating colonies and transfer them to the sensor plates.

Replating. Many procedures for replating of cardiomyocytes are designed for commercial CM systems and recommend a specific seeding density to obtain the appropriate culture. However, counting by hemacytometer requires that the suspension contain predominantly single cells. This makes sense for commercial CMs, which are easily mixed into single cell suspension, but CMs which have been differentiated using a Matrigel sandwich method are not easily separated. While dissociating cells from the surface using Accutase did not require significant pipetting, extensive not-so-gentle trituration with a P1000 was required even after extended incubations with high concentrations of Accutase or Accumax in order to break up large colonies. Multiple attempts to obtain a single-cell suspension for hemacytometer counting resulted in significant cellular debris and dead cells even as 100-cell clumps remained intact. Variation in Accutase concentration and incubation time did not noticeably ameliorate the process.

Instead, the process of cell counting was skipped in favor of replating based on the estimated confluence of beating cells. For example, with some experimentation, it was found that one well of a 24WP with 50% coverage of beating cells was appropriate for seeding 3-5 wells of a 96WP, depending on the desired apparent density. Unfortunately, the opacity and dimensions of the sensor plates prevented viewing the well contents through either an upright or inverted microscope, so cells were reseeded into a sensor plate and a standard 96WP under identical conditions in the hopes of obtaining impedance data and visual information for the same conditions.

Adjusted variables included Matrigel coating concentration of the sensor plate (1:400–1:100 dilution), dissociation enzyme used (Accutase or Accumax), incubation time before trituration (5-15 minutes), extent of trituration, and relative density seeded. Overall, replating success was found to be largely random and independent of most of the conditions investigated. Very few wells (<5%) gave rise to an impedance pattern visible above baseline noise within the 21 days checked, and each differed from other successes by multiple variables. Numerous possible causes were hypothesized that could yield no measurable impedance profile including: insufficient cells, due to poor adherence, improper seeding density, or cell death following replating; CMs that lived but did not resume beating, due to low density, low purity, or excessive separation or trauma during

replating; or CMs that resumed beating randomly rather than synchronously. In clear 96WPs, sparse reseeding was less likely to ever resume beating, while denser reseeding had an increased likelihood of non-synchronous beating. Due to the inconsistency of wells replated under identical conditions, it was difficult to draw any link between impedance data and cell growth in clear 96WPs. More data, or a more quantitative procedure, will be required to reliably determine the ideal reseeding density.

Preliminary impedance measurements. Preliminary data[249] from a previous group member using commercial cardiomyocytes demonstrated that dosing with ptDNA gave rise to a 17% increase in beat rate and 13% decrease in fall time according to impedance measurements. This is consistent with increased SERCA calcium affinity in the presence of oligos, which is hypothesized to increase the rate of calcium reuptake into the SR. Before oligo dosing experiments could be performed with our differentiated CMs, the level of baseline consistency had to be established. Ideally, CMs would have a consistent beat rate and fall time over tens of minutes (for data averaging), over several days (for longitudinal experiments), and between wells (for parallel assays).

Only one well (Figure 5.8) gave quantifiable patterns on multiple days. The beat rate over 48 minutes (17 measurements) was found to be 60±2 min^{-1} with no apparent systematic change over the period. While the uncertainty was about double that observed in the commercial CMs, the sub-4% RSD was still substantially lower than the 17% change in beat rate observed previously, confirming that these changes would be visible over the

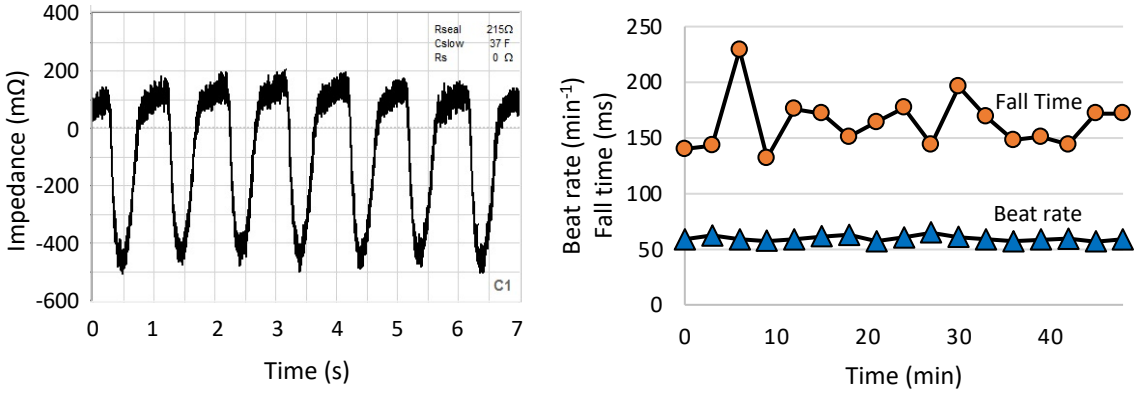

Figure 5.8: Sample impedance measurement data for differentiated cardiomyocytes. **(Left)** A representative impedance trace shows the consistent beat rate and amplitude during the sweep. **(Right)** The average beat rate and fall time for each sweep were plotted over time. The beat rate displayed good consistency (±3.7% RSD) but the variation in the fall time was evident (±15% RSD) likely due to the low impedance amplitude.

baseline noise in our differentiated CM system. A single sweep 48 hours later showed a beat rate of 59, suggesting long term consistency in beat rate, but more data is needed confirm this. Unfortunately, the fall time varied much more from one sweep to the next, yielding a RSD of 15%. This RSD is higher than the change in fall time observed in the commercial CM system, meaning that measuring a more consistent fall time is necessary before changes in fall time between conditions become detectable. The high RSD in the fall time likely stems from low absolute impedance changes. In order to obtain a stronger impedance fluctuation, future experiments will aim to use a greater seeding density.

The beat rate uncertainty for one well over time (±2 min^{-1}) was found to be much smaller than the differences between wells, which varied roughly from 40-90 min^{-1} even among the small number of wells with measurable impedance profiles. While the exact uncertainty could not be calculated, it seems unlikely that comparison between wells will be more reliable than long term comparison of one well over time.

5.5 Conclusions

Numerous variables were optimized in order to obtain a reliable procedure for the thawing, growth, and passaging of iPSCs. Cells grew to sufficient confluence for passaging in roughly four days, leading to a reliable supply of iPSCs with which to attempt differentiation. Timing the start of differentiation based on colony morphology and level of compaction was found to be more reliable than based on confluence alone, which is not noted in many literature protocols. Relatively pure beating CMs were obtained with better than 50% frequency through appropriately timed Matrigel application, WNT activation by Chir99021, WNT inhibition with Wnt-C59, and metabolic selection in the absence of glucose.

Replating beating CMs onto a CardioExcyte sensor plate for impedance measurement proved unreliable due to difficulties obtaining a monodisperse cell suspension for counting and predictable reseeding. Future work will focus on a wider variety of cell detachment strategies in order to obtain a procedure that is reproducible enough for more fine-tuned optimization. Preliminary impedance measurements showed that replated CMs that did resume synchronous beating could be detected well enough to

generate a signal quantifiable above baseline noise. Measurement of beat rate showed a high degree of consistency over one hour (±2 min^{-1}), and possibly over several days, that would allow quantification of beat rate by longitudinal SPIDR dosing assays. The high degree of uncertainty observed in the measurement of fall time would likely obscure small changes due to SPIDR application, but it is expected that improved replating strategies and CM purity will lead to a significantly decreased RSD in measured fall time.

Chapter 6: Summary and future directions

6.1 Summary

In summary, this dissertation centered on highlighting and improving microfluidic methods of aptamer selection, particularly CE-SELEX, in addition to expanding the scope of protein targets and biological applications for oligonucleotide affinity reagents.

Chapter 2 reviewed the wide variety of microfluidic techniques for selection and characterization of aptamers, focusing on the tremendous enhancement of efficiency and automatability offered by all microfluidic techniques. Specifically, selection techniques based on electrophoresis (CE and μFFE), magnetic and non-magnetic microbeads, and sol-gel encapsulation were covered in depth, including recent developments and example aptamers selected. Several prototypes of increasingly comprehensive integrated microfluidic SELEX systems, incorporating elements of negative selection, amplification, and/or purification into the same system, were enumerated. Finally, the capabilities of DNA microarrays as both characterization technique and selection tool, which will only improve with increased scale and decreased cost, were discussed at length.

Chapter 3 developed a strategy for CE-SELEX against untruncated LDL receptor by stabilizing the transmembrane region in surfactant micelles during selection. To our knowledge, this type of selection against an intact membrane-bound protein has not been documented in the literature to date, and the mechanisms developed here are applicable to a wide variety of membrane protein targets. Selection at physiological temperatures and increased (but still sub-physiological) NaCl concentrations were tolerated, but even trace glycerol was found to be detrimental and removed prior to separation. Three to four rounds of selection resulted in approximately a five-fold increase in affinity of the DNA pool, and two of the six aptamer sequences synthesized for characterization displayed a K_d below 20 nM. Further tests are needed to confirm K_d values as well as to characterize binding and possible endocytosis in LDLR-expressing cells.

Chapter 4 explored anti-leptin aptamers for use in a proposed real-time microfluidic leptin quantification assay for cultured 3T3-L1 adipocyte-like cells based on fluorescent aptamer detection by μFFE-LIF. Two literature aptamers against human leptin (Lep2 and Lep3) were evaluated in their ability to bind mouse leptin, but both were found to have a $K_d > 1$ μM, significantly worse affinity than against human leptin. Next, CE-SELEX was

performed against mouse leptin in a Ringer's-based buffer (to simulate the proposed assay). The random library displayed multiple early features that made it difficult to establish a late collection window. Affinity measurements by FP and CE were somewhat inconclusive but suggested an unsuccessful selection with no measurable increase in affinity. A method of mathematically approximating the complex peak time was developed based on literature analyses of ssDNA diffusion, and the complex peak was found to be later than expected and outside the collection window used.

Chapter 5 looked at SPIDRs, sequence-independent aptamer-like oligonucleotide affinity reagents that have been found to bind to proteins controlling the calcium cycling process in heart cells. Previous work had established a functional effect of binding on calcium affinity, and this chapter aimed to optimize a differentiated cardiomyocyte system to evaluate the physiological effects of SPIDRs on contraction by cell impedance assays. The process of iPSC culture and passaging were optimized, and a method of timing the start of differentiation based on morphology and compaction was found to be superior to evaluating confluence alone. Beating cardiomyocytes were obtained with better than 50% frequency through optimization of Matrigel application and WNT pathway modulation, but replating CMs into sensor plates for impedance measurement was found to be unreliable, partly due to difficulty obtaining a monodisperse suspension, and optimization was impossible because of the highly random outcomes of replating. With a small number of successfully replated wells, a high degree of beat rate consistency was established over one hour and possibly over several days, but all fall time measurements and cross-well beat rate measurements were found to be too inconsistent for precise comparison without improved replating strategies.

6.2 Future directions

6.2.1 Improvement of electrophoretic SELEX

CE-SELEX is a highly flexible technique because changing the collection window timing allows the stringency to be adjusted with ease. Unfortunately, as demonstrated in Chapter 4, incorrect collection window timing can lead to unsuccessful selection, so careful thought is required in determining the collection window. One potential solution is better

purification of the DNA library to remove the disruptive early peaks that pressure an early collection window. Because the sequences and structures in the pool are so diverse, though, there is some worry that purification techniques might unintentionally cause systematic bias by removing certain DNA structures, sequences high or low in particular nucleotides, or the like. If any of these groups were more likely to exhibit binding, their removal from the library could dramatically reduce the efficiency of the selection. In order to determine whether this type of biasing occurs and has an impact on selection, a comparison of different pre-SELEX library purification methods (such as liquid chromatography, size exclusion, or CE) should be carried out in parallel against the same target to evaluate their impact on the speed of convergence, the prevalence of high affinity aptamers, or magnitude of aptamer affinity obtained. While a small bias against some types of sequences is inevitable during purification, it is likely that the removal of early DNA peaks would allow a much higher efficiency separation step, improving the method overall.

Alternatively or additionally, the precision of the calculational model developed in Chapter 4 could be improved dramatically through incorporation of more experimental data from specifically designed experiments. The version shown here included a number of approximations and assumptions, but an improved version would allow much more precise calculation of the complex peak location for optimal timing of the collection window and higher efficiency separation. Experiments would aim to evaluate the electrophoretic mobility of aptamer library designs common in SELEX as well as mobility changes resulting from complexation with different sized protein or adjustments to the chemical environment. This work would benefit the CE-SELEX community greatly since most physical chemistry literature in this area does not focus on short (<100 base) oligos, ssDNA, or oligonucleotide-protein complex behavior.

In the long term, 3D printed μFFE devices represent a major step forward as a potential cost-effective, highly accessible microfluidic SELEX platform. Such a device would be ideal for application-focus groups interested in selecting their own aptamers but lacking the experience of many method-focused SELEX groups. Significant headway has already been made in this lab toward 3D printed ABS μFFE devices that are considerably faster and cheaper to produce than the original etched glass versions.[218] While μFFE-

SELEX has been demonstrated before on glass devices,[108] new attempts using a 3D printed device are warranted to confirm sufficient resolution and performance as a low-cost disposable SELEX device.

6.2.2 Testing of aptamer and SPIDR biological applications

In Chapter 3, multiple aptamers were obtained that display significant affinity for micelle-solubilized recombinant LDLR. While this is a significant achievement for CE-SELEX, the aptamers themselves ultimately mean very little if they do not display affinity towards wild-type LDLR in a physiological system. Future experiments are planned to evaluate the binding, and hopefully internalization, of these LDLR aptamers in HepG2 cells, a human hepatocarcinoma line known to overexpress multiple metabolically-significant receptors including LDLR. Internalization could be confirmed visually using confocal fluorescence microscopy or functionally using an aptamer-siRNA hybrid to trigger a phenotypic change. More quantitative experiments would require the use of flow cytometry to evaluate binding or internalization over a large population of cells. Commercially available fluorescent LDL and previously selected LDLR aptamers[254] could serve as effective positive controls for these experiments.

For SPIDRs, now that the iPSC-derived CM system is more reliable, extensive investigation of their physiological effects can take place. Similarly to previous experiments with recombinant protein, the effects of different oligo lengths and different XNA backbones will be investigated, this time observing their impact on beat rate, beat amplitude, and fall time. Once this relationship has been established more confidently and quantitatively, experiments with increasing biological complexity, and with more of an eye to therapeutic potential, can take place. Eventually, it will be important to evaluate SPIDRs in an environment with external pacing cues, such as a small or medium animal, which has complexities of the tissue and organ level absent in culture. It would also be beneficial to evaluate specific PLN mutants linked to CVD, which are available as iPSCs from SCVI biobank or other similar sources.

Bibliography

1. Kohler, G.; Milstein, C., CONTINUOUS CULTURES OF FUSED CELLS SECRETING ANTIBODY OF PREDEFINED SPECIFICITY. *Nature* **1975,** *256* (5517), 495-497.
2. Baker, M., BLAME IT ON THE ANTIBODIES. *Nature* **2015,** *521* (7552), 274-276.
3. Berglund, L.; Bjoerling, E.; Oksvold, P.; Fagerberg, L.; Asplund, A.; Szigyarto, C. A. K.; Persson, A.; Ottosson, J.; Wernerus, H.; Nilsson, P.; Lundberg, E.; Sivertsson, A.; Navani, S.; Wester, K.; Kampf, C.; Hober, S.; Ponten, F.; Uhlen, M., A Genecentric Human Protein Atlas for Expression Profiles Based on Antibodies. *Molecular & Cellular Proteomics* **2008,** *7* (10), 2019-2027.
4. Bradbury, A.; Pluckthun, A., Standardize antibodies used in research. *Nature* **2015,** *518* (7537), 27-29.
5. Begley, C. G.; Ellis, L. M., Raise standards for preclinical cancer research. *Nature* **2012,** *483* (7391), 531-533.
6. Crick, F., CENTRAL DOGMA OF MOLECULAR BIOLOGY. *Nature (London)* **1970,** *227* (5258), 561-563.
7. Stark, B. C.; Kole, R.; Bowman, E. J.; Altman, S., RIBONUCLEASE-P - ENZYME WITH AN ESSENTIAL RNA COMPONENT. *Proceedings of the National Academy of Sciences of the United States of America* **1978,** *75* (8), 3717-3721.
8. Ellington, A. D.; Szostak, J. W., INVITRO SELECTION OF RNA MOLECULES THAT BIND SPECIFIC LIGANDS. *Nature* **1990,** *346* (6287), 818-822.
9. Bock, L. C.; Griffin, L. C.; Latham, J. A.; Vermaas, E. H.; Toole, J. J., SELECTION OF SINGLE-STRANDED-DNA MOLECULES THAT BIND AND INHIBIT HUMAN THROMBIN. *Nature* **1992,** *355* (6360), 564-566.
10. Mattice, C. M. C.; DeRosa, M. C., Status and Prospects of Aptamers as Drug Components. *Biodrugs* **2015,** *29* (3), 151-165.
11. Tuerk, C.; Gold, L., SYSTEMATIC EVOLUTION OF LIGANDS BY EXPONENTIAL ENRICHMENT - RNA LIGANDS TO BACTERIOPHAGE-T4 DNA-POLYMERASE. *Science* **1990,** *249* (4968), 505-510.
12. Qu, H.; Csordas, A. T.; Wang, J. P.; Oh, S. S.; Eisenstein, M. S.; Soh, H. T., Rapid and Label-Free Strategy to Isolate Aptamers for Metal Ions. *ACS Nano* **2016,** *10* (8), 7558-7565.
13. Rajendran, M.; Ellington, A. D., Selection of fluorescent aptamer beacons that light up in the presence of zinc. *Analytical and Bioanalytical Chemistry* **2008,** *390* (4), 1067-1075.
14. Cho, Y. S.; Lee, E. J.; Lee, G. H.; Hah, S. S., Aptamer selection for fishing of palladium ion using graphene oxide-adsorbed nanoparticles. *Bioorganic & Medicinal Chemistry Letters* **2015,** *25* (23), 5536-5539.
15. Yang, J.; Bowser, M. T., Capillary Electrophoresis-SELEX Selection of Catalytic DNA Aptamers for a Small-Molecule Porphyrin Target. *Analytical Chemistry* **2013,** *85* (3), 1525-1530.
16. Mann, D.; Reinemann, C.; Stoltenburg, R.; Strehlitz, B., In vitro selection of DNA aptamers binding ethanolamine. *Biochemical and Biophysical Research Communications* **2005,** *338* (4), 1928-1934.
17. Ma, X. Y.; Wang, W. F.; Chen, X. J.; Xia, Y.; Duan, N.; Wu, S. J.; Wang, Z. P., Selection, characterization and application of aptamers targeted to Aflatoxin B2. *Food Control* **2015,** *47*, 545-551.

18. Chen, X. J.; Huang, Y. K.; Duan, N.; Wu, S. J.; Ma, X. Y.; Xia, Y.; Zhu, C. Q.; Jiang, Y.; Wang, Z. P., Selection and identification of ssDNA aptamers recognizing zearalenone. *Analytical and Bioanalytical Chemistry* **2013,** *405* (20), 6573-6581.
19. Stoltenburg, R.; Nikolaus, N.; Strehlitz, B., Capture-SELEX: Selection of DNA Aptamers for Aminoglycoside Antibiotics. *Journal of Analytical Methods in Chemistry* **2012**, 14.
20. Khvorova, A.; Kwak, Y. G.; Tamkun, M.; Majerfeld, I.; Yarus, M., RNAs that bind and change the permeability of phospholipid membranes. *Proceedings of the National Academy of Sciences of the United States of America* **1999,** *96* (19), 10649-10654.
21. Vlassov, A.; Khvorova, A.; Yarus, M., Binding and disruption of phospholipid bilayers by supramolecular RNA complexes. *Proceedings of the National Academy of Sciences of the United States of America* **2001,** *98* (14), 7706-7711.
22. Tasset, D. M.; Kubik, M. F.; Steiner, W., Oligonucleotide inhibitors of human thrombin that bind distinct epitopes. *Journal of Molecular Biology* **1997,** *272* (5), 688-698.
23. Nonaka, Y.; Sode, K.; Ikebukuro, K., Screening and Improvement of an Anti-VEGF DNA Aptamer. *Molecules* **2010,** *15* (1), 215-225.
24. Lupold, S. E.; Hicke, B. J.; Lin, Y.; Coffey, D. S., Identification and characterization of nuclease-stabilized RNA molecules that bind human prostate cancer cells via the prostate-specific membrane antigen. *Cancer Research* **2002,** *62* (14), 4029-4033.
25. Shigdar, S.; Lin, J.; Yu, Y.; Pastuovic, M.; Wei, M.; Duan, W., RNA aptamer against a cancer stem cell marker epithelial cell adhesion molecule. *Cancer Science* **2011,** *102* (5), 991-998.
26. Toscano-Garibay, J. D.; Benitez-Hess, M. L.; Alvarez-Salas, L. M., Targeting of the HPV-16 E7 Protein by RNA Aptamers. In *Cervical Cancer: Methods and Protocols*, Keppler, D.; Lin, A. W., Eds. Humana Press Inc: Totowa, 2015; Vol. 1249, pp 221-239.
27. Kwon, H. M.; Lee, K. H.; Han, B. W.; Han, M. R.; Kim, D. H.; Kim, D. E., An RNA Aptamer That Specifically Binds to the Glycosylated Hemagglutinin of Avian Influenza Virus and Suppresses Viral Infection in Cells. *Plos One* **2014,** *9* (5), 9.
28. Cho, S. J.; Woo, H. M.; Kim, K. S.; Oh, J. W.; Jeong, Y. J., Novel system for detecting SARS coronavirus nucleocapsid protein using an ssDNA aptamer. *Journal of Bioscience and Bioengineering* **2011,** *112* (6), 535-540.
29. Chen, H. L.; Hsiao, W. H.; Lee, H. C.; Wu, S. C.; Cheng, J. W., Selection and Characterization of DNA Aptamers Targeting All Four Serotypes of Dengue Viruses. *Plos One* **2015,** *10* (6).
30. Beier, R.; Pahlke, C.; Quenzel, P.; Henseleit, A.; Boschke, E.; Cuniberti, G.; Labudde, D., Selection of a DNA aptamer against norovirus capsid protein VP1. *Fems Microbiology Letters* **2014,** *351* (2), 162-169.
31. Dwivedi, H. P.; Smiley, R. D.; Jaykus, L. A., Selection and characterization of DNA aptamers with binding selectivity to Campylobacter jejuni using whole-cell SELEX. *Applied Microbiology and Biotechnology* **2010,** *87* (6), 2323-2334.
32. Lu, M.; Zhou, L.; Zheng, X. H.; Quan, Y.; Wang, X. L.; Zhou, X. N.; Ren, J., A novel molecular marker of breast cancer stem cells identified by cell-SELEX method. *Cancer Biomarkers* **2015,** *15* (2), 163-170.
33. Maimaitiyiming, Y.; Yang, C.; Wang, Y.; Hussain, L.; Naranmandura, H., Selection and characterization of novel DNA aptamer against colorectal carcinoma Caco-2 cells. *Biotechnology and Applied Biochemistry* **2019,** *66* (3), 412-418.

34. Li, W. M.; Zhou, L. L.; Zheng, M.; Fang, J., Selection of Metastatic Breast Cancer Cell-Specific Aptamers for the Capture of CTCs with a Metastatic Phenotype by Cell-SELEX. *Molecular Therapy-Nucleic Acids* **2018,** *12*, 707-717.
35. Zhao, Q.; Li, X. F.; Shao, Y. H.; Le, X. C., Aptamer-based affinity chromatographic assays for thrombin. *Analytical Chemistry* **2008,** *80* (19), 7586-7593.
36. Javaherian, S.; Musheev, M. U.; Kanoatov, M.; Berezovski, M. V.; Krylov, S. N., Selection of aptamers for a protein target in cell lysate and their application to protein purification. *Nucleic Acids Research* **2009,** *37* (8), e62 1-10.
37. Beloborodov, S. S.; Bao, J. Y.; Krylova, S. M.; Shala-Lawrence, A.; Johnson, P. E.; Krylov, S. N., Aptamer facilitated purification of functional proteins. *Journal of Chromatography B-Analytical Technologies in the Biomedical and Life Sciences* **2018,** *1073*, 201-206.
38. Ruta, J.; Ravelet, C.; Desire, J.; Decout, J.-L.; Peyrin, E., Covalently bonded DNA aptamer chiral stationary phase for the chromatographic resolution of adenosine. *Analytical and Bioanalytical Chemistry* **2008,** *390* (4), 1051-1057.
39. Michaud, M.; Jourdan, E.; Villet, A.; Ravel, A.; Grosset, C.; Peyrin, E., A DNA aptamer as a new target-specific chiral selector for HPLC. *Journal of the American Chemical Society* **2003,** *125* (28), 8672-8679.
40. Toh, S. Y.; Citartan, M.; Gopinath, S. C. B.; Tang, T. H., Aptamers as a replacement for antibodies in enzyme-linked immunosorbent assay. *Biosensors & Bioelectronics* **2015,** *64*, 392-403.
41. Drolet, D. W.; MoonMcDermott, L.; Romig, T. S., An enzyme-linked oligonucleotide assay. *Nature Biotechnology* **1996,** *14* (8), 1021-1025.
42. Nie, J.; Deng, Y.; Deng, Q. P.; Zhang, D. W.; Zhou, Y. L.; Zhang, X. X., A self-assemble aptamer fragment/target complex based high-throughput colorimetric aptasensor using enzyme linked aptamer assay. *Talanta* **2013,** *106*, 309-314.
43. Penner, G. Commercialization of an aptamer-based diagnostic test *IVD Technology* [Online], 2012, p. 31-37. https://neoventures.ca/wp-content/uploads/2018/05/Penner2012IVDTech31commercializationaptamer-baseddiagkits.pdf.
44. Bruno, J. G.; Phillips, T.; Montez, T.; Garcia, A.; Sivils, J. C.; Mayo, M. W.; Greis, A.; Metrix, L., Development of a Fluorescent Enzyme-Linked DNA Aptamer-Magnetic Bead Sandwich Assay and Portable Fluorometer for Sensitive and Rapid Listeria Detection. *Journal of Fluorescence* **2015,** *25* (1), 173-183.
45. Jung, Y. J.; Oh, I. J.; Kim, Y.; Jung, J. H.; Seok, M.; Lee, W.; Park, C. K.; Lim, J. H.; Kim, Y. C.; Kim, W. S.; Choi, C. M., Clinical Validation of a Protein Biomarker Panel for Non-Small Cell Lung Cancer. *Journal of Korean Medical Science* **2018,** *33* (53).
46. AptoDetect™-Lung. http://aptsci.com/en/diagnosis/aptodetect-lung/.
47. amsbio Aptamers: cell isolation, protein precipitation, flow cytometry. https://resources.amsbio.com/Handbook/Aptamer-Cell-and-Protein-Isolation.pdf.
48. EpiMark ® Hot Start T*aq* DNA Polymerase. https://www.neb.com/products/m0490-epimark-hot-start-taq-dna-polymerase#Product%20Information.
49. Hong, H.; Goel, S.; Zhang, Y.; Cai, W., Molecular Imaging with Nucleic Acid Aptamers. *Current Medicinal Chemistry* **2011,** *18* (27), 4195-4205.
50. Dougherty, C. A.; Cai, W. B.; Hong, H., Applications of Aptamers in Targeted Imaging: State of the Art. *Current Topics in Medicinal Chemistry* **2015,** *15* (12), 1138-1152.

51. McNamara, J. O.; Andrechek, E. R.; Wang, Y.; D Viles, K.; Rempel, R. E.; Gilboa, E.; Sullenger, B. A.; Giangrande, P. H., Cell type-specific delivery of siRNAs with aptamer-siRNA chimeras. *Nature Biotechnology* **2006,** *24* (8), 1005-1015.
52. Lee, J. H.; Yigit, M. V.; Mazumdar, D.; Lu, Y., Molecular diagnostic and drug delivery agents based on aptamer-nanomaterial conjugates. *Advanced Drug Delivery Reviews* **2010,** *62* (6), 592-605.
53. Drug Approval Package. https://www.accessdata.fda.gov/drugsatfda_docs/nda/2004/21-756_Macugen.cfm.
54. Ruckman, J.; Green, L. S.; Beeson, J.; Waugh, S.; Gillette, W. L.; Henninger, D. D.; Claesson-Welsh, L.; Janjic, N., 2 '-fluoropyrimidine RNA-based aptamers to the 165-amino acid form of vascular endothelial growth factor (VEGF(165)) - Inhibition of receptor binding and VEGF-induced vascular permeability through interactions requiring the exon 7-encoded domain. *Journal of Biological Chemistry* **1998,** *273* (32), 20556-20567.
55. Biesecker, G.; Dihel, L.; Enney, K.; Bendele, R. A., Derivation of RNA aptamer inhibitors of human complement C5. *Immunopharmacology* **1999,** *42* (1-3), 219-230.
56. ZIMURA in Combination With LUCENTIS in Patients With Neovascular Age Related Macular Degeneration (NVAMD). https://clinicaltrials.gov/ct2/show/NCT03362190.
57. Phase II Study of AS1411 Combined With Cytarabine to Treat Acute Myeloid Leukemia https://clinicaltrials.gov/ct2/show/NCT00512083.
58. Olaptesed (NOX-A12) Alone and in Combination With Pembrolizumab in Colorectal and Pancreatic Cancer (Keynote-559) https://clinicaltrials.gov/ct2/show/NCT03168139.
59. Roccaro, A. M.; Sacco, A.; Purschke, W. G.; Moschetta, M.; Buchner, K.; Maasch, C.; Zboralski, D.; Zollner, S.; Vonhoff, S.; Mishima, Y.; Maiso, P.; Reagan, M. R.; Lonardi, S.; Ungari, M.; Facchetti, F.; Eulberg, D.; Kruschinski, A.; Vater, A.; Rossi, G.; Klussmann, S.; Ghobrial, I. M., SDF-1 Inhibition Targets the Bone Marrow Niche for Cancer Therapy. *Cell Reports* **2014,** *9* (1), 118-128.
60. NOX-E36 in Patients With Type 2 Diabetes Mellitus and Albuminuria https://www.clinicaltrials.gov/ct2/show/NCT01547897.
61. Menne, J.; Eulberg, D.; Beyer, D.; Baumann, M.; Saudek, F.; Valkusz, Z.; Wiecek, A.; Haller, H.; Emapticap Study, G., C-C motif-ligand 2 inhibition with emapticap pegol (NOX-E36) in type 2 diabetic patients with albuminuria. *Nephrology Dialysis Transplantation* **2017,** *32* (2), 307-315.
62. Boyce, M.; Warrington, S.; Cortezi, B.; Zollner, S.; Vauleon, S.; Swinkels, D. W.; Summo, L.; Schwoebel, F.; Riecke, K., Safety, pharmacokinetics and pharmacodynamics of the anti-hepcidin Spiegelmer lexaptepid pegol in healthy subjects. *British Journal of Pharmacology* **2016,** *173* (10), 1580-1588.
63. Efficacy of NOX-H94 on Anemia of Chronic Disease in Patients With Cancer https://clinicaltrials.gov/ct2/show/NCT01691040.
64. ARC1779 Injection in Patients With Von Willebrand Factor-Related Platelet Function Disorders https://clinicaltrials.gov/ct2/show/NCT00632242.
65. Spiel, A. O.; Mayr, F. B.; Ladani, N.; Wagner, P. G.; Schaub, R. G.; Gilbert, J. C.; Jilma, B., The aptamer ARC1779 is a potent and specific inhibitor of von willebrand factor mediated ex vivo platelet function in acute myocardial infarction. *Platelets* **2009,** *20* (5), 334-340.

66. A Study To Determine the Efficacy and Safety of REG1 Compared to Bivalirudin in Patients Undergoing PCI (Regulate) https://clinicaltrials.gov/ct2/show/NCT01848106.
67. Feasibility and Safety Study Comparing REG1 Anticoagulation System With Unfractionated Heparin in Elective PCI (REVERSAL-PCI) https://clinicaltrials.gov/ct2/show/NCT00715455.
68. Rusconi, C. P.; Scardino, E.; Layzer, J.; Pitoc, G. A.; Ortel, T. L.; Monroe, D.; Sullenger, B. A., RNA aptamers as reversible antagonists of coagulation factor IXa. *Nature* **2002,** *419* (6902), 90-94.
69. A Phase 3 Safety and Efficacy Study of Fovista® (E10030) Intravitreous Administration in Combination With Lucentis® Compared to Lucentis® Monotherapy. https://clinicaltrials.gov/ct2/show/NCT01944839.
70. Floege, J.; Ostendorf, T.; Janssen, U.; Burg, M.; Radeke, H. H.; Vargeese, C.; Gill, S. C.; Green, L. S.; Janjic, N., Novel approach to specific growth factor inhibition in vivo - Antagonism of platelet-derived growth factor in glomerulonephritis by aptamers. *American Journal of Pathology* **1999,** *154* (1), 169-179.
71. First-in-Human and Proof-of-Mechanism Study of ARC19499 Administered to Hemophilia Patients https://clinicaltrials.gov/ct2/show/NCT01191372.
72. Gissel, M.; Orfeo, T.; Foley, J. H.; Butenas, S., Effect of BAX499 aptamer on tissue factor pathway inhibitor function and thrombin generation in models of hemophilia. *Thrombosis Research* **2012,** *130* (6), 948-955.
73. Study of NU172 as Anticoagulation in Patients Undergoing Off-pump CABG Surgery (SNAP-CABG-OFF) https://clinicaltrials.gov/ct2/show/NCT00808964.
74. Mascini, M., *Aptamers in Bioanalysis*. John Wiley & Sons, Inc.: Hoboken, NJ, 2009.
75. SantaLucia, J.; Hicks, D., The thermodynamics of DNA structural motifs. *Annual Review of Biophysics and Biomolecular Structure* **2004,** *33*, 415-440.
76. Nutiu, R.; Li, Y. F., Structure-switching signaling aptamers. *Journal of the American Chemical Society* **2003,** *125* (16), 4771-4778.
77. Li, D.; Song, S.; Fan, C., Target-Responsive Structural Switching for Nucleic Acid-Based Sensors. *Accounts of Chemical Research* **2010,** *43* (5), 631-641.
78. Szeto, K.; Latulippe, D. R.; Ozer, A.; Pagano, J. M.; White, B. S.; Shalloway, D.; Lis, J. T.; Craighead, H. G., RAPID-SELEX for RNA Aptamers. *Plos One* **2013,** *8* (12).
79. Fologea, D.; Ledden, B.; McNabb, D. S.; Li, J. L., Electrical characterization of protein molecules by a solid-state nanopore. *Applied Physics Letters* **2007,** *91* (5).
80. Hall, K. B.; Kranz, J. K., Nitrocellulose filter binding for determination of dissociation constants. In *RNA-protein interaction protocols*, Haynes, S. R., Ed. Humana Press: Totawa, NJ, 1999.
81. Jing, M.; Bowser, M. T., Methods for measuring aptamer-protein equilibria: A review. *Analytica Chimica Acta* **2011,** *686* (1-2), 9-18.
82. Web of Science analysis of search results for *Aptamer** published prior to 1 January, 2021.
83. Limi, T.; Lee, S. Y.; Yang, J.; Hwang, S. Y.; Ahn, Y., Microfluidic Biochips for Simple Impedimetric Detection of Thrombin Based on Label-free DNA Aptamers. *Biochip Journal* **2017,** *11* (2), 109-115.
84. Moon, J. M.; Kim, D. M.; Kim, M. H.; Han, J. Y.; Jung, D. K.; Shim, Y. B., A disposable amperometric dual-sensor for the detection of hemoglobin and glycated hemoglobin in a finger prick blood sample. *Biosensors & Bioelectronics* **2017,** *91*, 128-135.

85. Jin, S. R.; Ye, Z. Z.; Wang, Y. X.; Ying, Y. B., A Novel Impedimetric Microfluidic Analysis System for Transgenic Protein Cry1Ab Detection. *Scientific Reports* **2017,** *7*, 8.
86. Matharu, Z.; Patel, D.; Gao, Y. D.; Hague, A.; Zhou, Q.; Revzin, A., Detecting Transforming Growth Factor-beta Release from Liver Cells Using an Aptasensor Integrated with Microfluidics. *Analytical Chemistry* **2014,** *86* (17), 8865-8872.
87. Fu, H. Y.; Yang, J. H.; Guo, L.; Nie, J. F.; Yin, Q. B.; Zhang, L.; Zhang, Y., Using the Rubik's Cube to directly produce paper analytical devices for quantitative point-of-care aptamer-based assays. *Biosensors & Bioelectronics* **2017,** *96*, 194-200.
88. Jiang, P.; He, M. Y.; Shen, L.; Shi, A. N.; Liu, Z. H., A paper-supported aptasensor for total IgE based on luminescence resonance energy transfer from upconversion nanoparticles to carbon nanoparticles. *Sensors and Actuators B-Chemical* **2017,** *239*, 319-324.
89. Sathish, S.; Ricoult, S. G.; Toda-Peters, K.; Shen, A. Q., Microcontact printing with aminosilanes: creating biomolecule micro- and nanoarrays for multiplexed microfluidic bioassays. *Analyst* **2017,** *142* (10), 1772-1781.
90. Bruno, J. G.; Carrillo, M. P.; Phillips, T.; King, B., Development of DNA aptamers for cytochemical detection of acetylcholine. *In Vitro Cellular & Developmental Biology-Animal* **2008,** *44* (3-4), 63-72.
91. Kowalska, E.; Bartnicki, F.; Pels, K.; Strzalka, W., The impact of immobilized metal affinity chromatography (IMAC) resins on DNA aptamer selection. *Analytical and Bioanalytical Chemistry* **2014,** *406* (22), 5495-5499.
92. Latulippe, D. R.; Szeto, K.; Ozer, A.; Duarte, F. M.; Kelly, C. V.; Pagano, J. M.; White, B. S.; Shalloway, D.; Lis, J. T.; Craighead, H. G., Multiplexed Microcolumn-Based Process for Efficient Selection of RNA Aptamers. *Analytical Chemistry* **2013,** *85* (6), 3417-3424.
93. Kim, C. H.; Lee, L. P.; Min, J. R.; Lim, M. W.; Jeong, S. H., An indirect competitive assay-based aptasensor for detection of oxytetracycline in milk. *Biosensors & Bioelectronics* **2014,** *51*, 426-430.
94. Mudili, V.; Makam, S. S.; Sundararaj, N.; Siddaiah, C.; Gupta, V. K.; Rao, P. V. L., A novel IgY-Aptamer hybrid system for cost-effective detection of SEB and its evaluation on food and clinical samples. *Scientific Reports* **2015,** *5*, 12.
95. Yang, D. K.; Chen, L. C.; Lee, M. Y.; Hsu, C. H.; Chen, C. S., Selection of aptamers for fluorescent detection of alpha-methylacyl-CoA racemase by single-bead SELEX. *Biosensors & Bioelectronics* **2014,** *62*, 106-112.
96. Grozio, A.; Gonzalez, V. M.; Millo, E.; Sturla, L.; Vigliarolo, T.; Bagnasco, L.; Guida, L.; D'Arrigo, C.; De Flora, A.; Salis, A.; Martin, E. M.; Bellotti, M.; Zocchi, E., Selection and Characterization of Single Stranded DNA Aptamers for the Hormone Abscisic Acid. *Nucleic Acid Therapeutics* **2013,** *23* (5), 322-331.
97. Levine, H. A.; Nilsen-Hamilton, M., A mathematical analysis of SELEX. *Computational Biology and Chemistry* **2007,** *31* (1), 11-35.
98. Mendonsa, S. D.; Bowser, M. T., In vitro evolution of functional DNA using capillary electrophoresis. *Journal of the American Chemical Society* **2004,** *126* (1), 20-21.
99. Mosing, R. K.; Mendonsa, S. D.; Bowser, M. T., Capillary electrophoresis-SELEX selection of aptamers with affinity for HIV-1 reverse transcriptase. *Analytical Chemistry* **2005,** *77* (19), 6107-6112.
100. Jing, M.; Bowser, M. T., Tracking the Emergence of High Affinity Aptamers for rhVEGF(165) During Capillary Electrophoresis-Systematic Evolution of Ligands by

Exponential Enrichment Using High Throughput Sequencing. *Analytical Chemistry* **2013,** *85* (22), 10761-10770.
101. Dong, L. L.; Tan, Q. W.; Ye, W.; Liu, D. L.; Chen, H. F.; Hu, H. W.; Wen, D.; Liu, Y.; Cao, Y.; Kang, J. W.; Fan, J.; Guo, W.; Wu, W. Z., Screening and Identifying a Novel ssDNA Aptamer against Alpha-fetoprotein Using CE-SELEX. *Scientific Reports* **2015,** *5*, 10.
102. Eaton, R. M.; Shallcross, J. A.; Mael, L. E.; Mears, K. S.; Minkoff, L.; Scoville, D. J.; Whelan, R. J., Selection of DNA aptamers for ovarian cancer biomarker HE4 using CE-SELEX and high-throughput sequencing. *Analytical and Bioanalytical Chemistry* **2015,** *407* (23), 6965-6973.
103. Mendonsa, S. D.; Bowser, M. T., In vitro selection of aptamers with affinity for neuropeptide Y using capillary electrophoresis. *Journal of the American Chemical Society* **2005,** *127* (26), 9382-9383.
104. Berezovski, M.; Drabovich, A.; Krylova, S. M.; Musheev, M.; Okhonin, V.; Petrov, A.; Krylov, S. N., Nonequilibrium capillary electrophoresis of equilibrium mixtures: A universal tool for development of aptamers. *Journal of the American Chemical Society* **2005,** *127* (9), 3165-3171.
105. Berezovski, M.; Musheev, M.; Drabovich, A.; Krylov, S. N., Non-SELEX selection of aptamers. *Journal of the American Chemical Society* **2006,** *128* (5), 1410-1411.
106. Tok, J.; Lai, J.; Leung, T.; Li, S. F. Y., Selection of aptamers for signal transduction proteins by capillary electrophoresis. *Electrophoresis* **2010,** *31* (12), 2055-2062.
107. Ashley, J.; Ji, K. L.; Li, S. F. Y., Selection of cholesterol esterase aptamers using a dual-partitioning approach. *Electrophoresis* **2015,** *36* (20), 2616-2621.
108. Jing, M.; Bowser, M. T., Isolation of DNA aptamers using micro free flow electrophoresis. *Lab on a Chip* **2011,** *11* (21), 3703-3709.
109. Bruno, J. G., In vitro selection of DNA to chloroaromatics using magnetic microbead-based affinity separation and fluorescence detection. *Biochemical and Biophysical Research Communications* **1997,** *234* (1), 117-120.
110. Xi, Z. J.; Huang, R. R.; Li, Z. Y.; He, N. Y.; Wang, T.; Su, E. B.; Deng, Y., Selection of HBsAg-Specific DNA Aptamers Based on Carboxylated Magnetic Nanoparticles and Their Application in the Rapid and Simple Detection of Hepatitis B Virus Infection. *ACS Applied Materials & Interfaces* **2015,** *7* (21), 11215-11223.
111. Lou, X. H.; Qian, J. R.; Xiao, Y.; Viel, L.; Gerdon, A. E.; Lagally, E. T.; Atzberger, P.; Tarasow, T. M.; Heeger, A. J.; Soh, H. T., Micromagnetic selection of aptamers in microfluidic channels. *Proceedings of the National Academy of Sciences of the United States of America* **2009,** *106* (9), 2989-2994.
112. Qian, J. R.; Lou, X. H.; Zhang, Y. T.; Xiao, Y.; Soh, H. T., Generation of Highly Specific Aptamers via Micromagnetic Selection. *Analytical Chemistry* **2009,** *81* (13), 5490-5495.
113. Cho, M.; Xiao, Y.; Nie, J.; Stewart, R.; Csordas, A. T.; Oh, S. S.; Thomson, J. A.; Soh, H. T., Quantitative selection of DNA aptamers through microfluidic selection and high-throughput sequencing. *Proceedings of the National Academy of Sciences of the United States of America* **2010,** *107* (35), 15373-15378.
114. Csordas, A. T.; Jorgensen, A.; Wang, J. Y.; Gruber, E.; Gong, Q.; Bagley, E. R.; Nakamoto, M. A.; Eisenstein, M.; Soh, H. T., High-Throughput Discovery of Aptamers for Sandwich Assays. *Analytical Chemistry* **2016,** *88* (22), 10842-10847.

115. Oh, S. S.; Ahmad, K. M.; Cho, M.; Kim, S.; Xiao, Y.; Soh, H. T., Improving Aptamer Selection Efficiency through Volume Dilution, Magnetic Concentration, and Continuous Washing in Microfluidic Channels. *Analytical Chemistry* **2011,** *83* (17), 6883-6889.
116. Oh, S. S.; Plakos, K.; Lou, X. H.; Xiao, Y.; Soh, H. T., In vitro selection of structure-switching, self-reporting aptamers. *Proceedings of the National Academy of Sciences of the United States of America* **2010,** *107* (32), 14053-14058.
117. Hong, S. L.; Wan, Y. T.; Tang, M.; Pang, D. W.; Zhang, Z. L., Multifunctional Screening Platform for the Highly Efficient Discovery of Aptamers with High Affinity and Specificity. *Analytical Chemistry* **2017,** *89* (12), 6535-6542.
118. Wang, Q.; Liu, W.; Xing, Y. Q.; Yang, X. H.; Wang, K. M.; Jiang, R.; Wang, P.; Zhao, Q., Screening of DNA Aptamers against Myoglobin Using a Positive and Negative Selection Units Integrated Microfluidic Chip and Its Biosensing Application. *Analytical Chemistry* **2014,** *86* (13), 6572-6579.
119. Liu, X. H.; Li, H.; Jia, W. C.; Chen, Z.; Xu, D. K., Selection of aptamers based on a protein microarray integrated with a microfluidic chip. *Lab on a Chip* **2017,** *17* (1), 178-185.
120. Park, J. W.; Lee, S. J.; Ren, S.; Lee, S.; Kim, S.; Laurell, T., Acousto-microfluidics for screening of ssDNA aptamer. *Scientific Reports* **2016,** *6*, 9.
121. Avnir, D.; Coradin, T.; Lev, O.; Livage, J., Recent bio-applications of sol-gel materials. *Journal of Materials Chemistry* **2006,** *16* (11), 1013-1030.
122. Bhatia, R. B.; Brinker, C. J.; Gupta, A. K.; Singh, A. K., Aqueous sol-gel process for protein encapsulation. *Chemistry of Materials* **2000,** *12* (8), 2434-2441.
123. Nguyen, D. T.; Smit, M.; Dunn, B.; Zink, J. I., Stabilization of creatine kinase encapsulated in silicate sol-gel materials and unusual temperature effects on its activity. *Chemistry of Materials* **2002,** *14* (10), 4300-4306.
124. Jin, W.; Brennan, J. D., Properties and applications of proteins encapsulated within sol-gel derived materials. *Analytica Chimica Acta* **2002,** *461* (1), 1-36.
125. Park, S. M.; Ahn, J. Y.; Jo, M.; Lee, D. K.; Lis, J. T.; Craighead, H. G.; Kim, S., Selection and elution of aptamers using nanoporous sol-gel arrays with integrated microheaters. *Lab on a Chip* **2009,** *9* (9), 1206-1212.
126. Ahn, J. Y.; Jo, M.; Dua, P.; Lee, D. K.; Kim, S., A Sol-Gel-Based Microfluidics System Enhances the Efficiency of RNA Aptamer Selection. *Oligonucleotides* **2011,** *21* (2), 93-100.
127. Lee, S.; Kang, J.; Ren, S.; Laurell, T.; Kim, S.; Jeong, O. C., A cross-contamination-free SELEX platform for a multi-target selection strategy. *Biochip Journal* **2013,** *7* (1), 38-45.
128. Bae, H.; Ren, S.; Kang, J.; Kim, M.; Jiang, Y.; Jin, M. M.; Min, I. M.; Kim, S., Sol-Gel SELEX Circumventing Chemical Conjugation of Low Molecular Weight Metabolites Discovers Aptamers Selective to Xanthine. *Nucleic Acid Therapeutics* **2013,** *23* (6), 443-449.
129. Ahn, J. Y.; Lee, S.; Jo, M.; Kang, J.; Kim, E.; Jeong, O. C.; Laurell, T.; Kim, S., Sol-Gel Derived Nanoporous Compositions for Entrapping Small Molecules and Their Outlook toward Aptamer Screening. *Analytical Chemistry* **2012,** *84* (6), 2647-2653.
130. Hybarger, G.; Bynum, J.; Williams, R. F.; Valdes, J. J.; Chambers, J. P., A microfluidic SELEX prototype. *Analytical and Bioanalytical Chemistry* **2006,** *384* (1), 191-198.
131. Huang, C. J.; Lin, H. I.; Shiesh, S. C.; Lee, G. B., Integrated microfluidic system for rapid screening of CRP aptamers utilizing systematic evolution of ligands by exponential enrichment (SELEX). *Biosensors & Bioelectronics* **2010,** *25* (7), 1761-1766.

132. Huang, C. J.; Lin, H. I.; Shiesh, S. C.; Lee, G. B., An integrated microfluidic system for rapid screening of alpha-fetoprotein-specific aptamers. *Biosensors & Bioelectronics* **2012,** *35* (1), 50-55.
133. Lai, H. C.; Wang, C. H.; Liou, T. M.; Lee, G. B., Influenza A virus-specific aptamers screened by using an integrated microfluidic system. *Lab on a Chip* **2014,** *14* (12), 2002-2013.
134. Hung, L. Y.; Wang, C. H.; Hsu, K. F.; Chou, C. Y.; Lee, G. B., An on-chip Cell-SELEX process for automatic selection of high-affinity aptamers specific to different histologically classified ovarian cancer cells. *Lab on a Chip* **2014,** *14* (20), 4017-4028.
135. Weng, C. H.; Hsieh, I. S.; Hung, L. Y.; Lin, H. I.; Shiesh, S. C.; Chen, Y. L.; Lee, G. B., An automatic microfluidic system for rapid screening of cancer stem-like cell-specific aptamers. *Microfluidics and Nanofluidics* **2013,** *14* (3-4), 753-765.
136. Kim, J.; Olsen, T. R.; Zhu, J.; Hilton, J. P.; Yang, K. A.; Pei, R.; Stojanovic, M. N.; Lin, Q., Integrated Microfluidic Isolation of Aptamers Using Electrophoretic Oligonucleotide Manipulation. *Scientific Reports* **2016,** *6*, 10.
137. Olsen, T.; Zhu, J.; Kim, J.; Pei, R. J.; Stojanovic, M. N.; Lin, Q., An Integrated Microfluidic SELEX Approach Using Combined Electrokinetic and Hydrodynamic Manipulation. *Slas Technology* **2017,** *22* (1), 63-72.
138. Berezhnoy, A.; Stewart, C. A.; McNamara, J. O.; Thiel, W.; Giangrande, P.; Trinchieri, G.; Gilboa, E., Isolation and Optimization of Murine IL-10 Receptor Blocking Oligonucleotide Aptamers Using High-throughput Sequencing. *Molecular Therapy* **2012,** *20* (6), 1242-1250.
139. Song, Y. L.; Shi, Y. Z.; Li, X. R.; Ma, Y. L.; Gao, M. X.; Liu, D.; Mao, Y.; Zhu, Z.; Lin, H.; Yang, C. Y., Afi-Chip: An Equipment-Free, Low-Cost, and Universal Binding Ligand Affinity Evaluation Platform. *Analytical Chemistry* **2016,** *88* (16), 8294-8301.
140. Bumgarner, R., Overview of DNA microarrays: types, applications, and their future. In *Current Protocols in Molecular Biology*, 2013; Vol. 101, pp 1-11.
141. Wang, L.; Li, P. C. H., Microfluidic DNA microarray analysis: A review. *Analytica Chimica Acta* **2011,** *687* (1), 12-27.
142. Katilius, E.; Flores, C.; Woodbury, N. W., Exploring the sequence space of a DNA aptamer using microarrays. *Nucleic Acids Research* **2007,** *35* (22), 7626-7635.
143. Fischer, N. O.; Tok, J. B. H.; Tarasow, T. M., Massively Parallel Interrogation of Aptamer Sequence, Structure and Function. *Plos One* **2008,** *3* (7), 9.
144. Tome, J. M.; Ozer, A.; Pagano, J. M.; Gheba, D.; Schroth, G. P.; Lis, J. T., Comprehensive analysis of RNA-protein interactions by high-throughput sequencing-RNA affinity profiling. *Nature Methods* **2014,** *11* (6), 683-+.
145. Kinghorn, A. B.; Dirkzwager, R. M.; Liang, S. L.; Cheung, Y. W.; Fraser, L. A.; Shiu, S. C. C.; Tang, M. S. L.; Tanner, J. A., Aptamer Affinity Maturation by Resampling and Microarray Selection. *Analytical Chemistry* **2016,** *88* (14), 6981-6985.
146. Cho, M.; Oh, S. S.; Nie, J.; Stewart, R.; Eisenstein, M.; Chambers, J.; Marth, J. D.; Walker, F.; Thomson, J. A.; Soh, H. T., Quantitative selection and parallel characterization of aptamers. *Proceedings of the National Academy of Sciences of the United States of America* **2013,** *110* (46), 18460-18465.
147. Cho, M.; Oh, S. S.; Nie, J.; Stewart, R.; Radeke, M. J.; Eisenstein, M.; Coffey, P. J.; Thomson, J. A.; Soh, H. T., Array-based Discovery of Aptamer Pairs. *Analytical Chemistry* **2015,** *87* (1), 821-828.

148. Uhlen, M.; Fagerberg, L.; Hallstrom, B. M.; Lindskog, C.; Oksvold, P.; Mardinoglu, A.; Sivertsson, A.; Kampf, C.; Sjostedt, E.; Asplund, A.; Olsson, I.; Edlund, K.; Lundberg, E.; Navani, S.; Szigyarto, C. A.; Odeberg, J.; Djureinovic, D.; Takanen, J. O.; Hober, S.; Alm, T.; Edqvist, P. H.; Berling, H.; Tegel, H.; Mulder, J.; Rockberg, J.; Nilsson, P.; Schwenk, J. M.; Hamsten, M.; von Feilitzen, K.; Forsberg, M.; Persson, L.; Johansson, F.; Zwahlen, M.; von Heijne, G.; Nielsen, J.; Ponten, F., Tissue-based map of the human proteome. *Science* **2015,** *347* (6220).
149. Overington, J. P.; Al-Lazikani, B.; Hopkins, A. L., Opinion - How many drug targets are there? *Nature Reviews Drug Discovery* **2006,** *5* (12), 993-996.
150. Chen, C. H. B.; Chernis, G. A.; Hoang, V. Q.; Landgraf, R., Inhibition of heregulin signaling by an aptamer that preferentially binds to the oligomeric form of human epidermal growth factor receptor-3. *Proceedings of the National Academy of Sciences of the United States of America* **2003,** *100* (16), 9226-9231.
151. Rentmeister, A.; Bill, A.; Wahle, T.; Walter, J.; Famulok, M., RNA aptamers selectively modulate protein recruitment to the cytoplasmic domain of beta-secretase BACE1 in vitro. *Rna-a Publication of the Rna Society* **2006,** *12* (9), 1650-1660.
152. Dhar, S.; Gu, F. X.; Langer, R.; Farokhzad, O. C.; Lippard, S. J., Targeted delivery of cisplatin to prostate cancer cells by aptamer functionalized Pt(IV) prodrug-PLGA-PEG nanoparticles. *Proceedings of the National Academy of Sciences of the United States of America* **2008,** *105* (45), 17356-17361.
153. Rask-Andersen, M.; Almen, M. S.; Schioth, H. B., Trends in the exploitation of novel drug targets. *Nature Reviews Drug Discovery* **2011,** *10* (8), 579-590.
154. Petrovskaya, L. E.; Shulga, A. A.; Bocharova, O. V.; Ermolyuk, Y. S.; Kryukova, E. A.; Chupin, V. V.; Blommers, M. J. J.; Arseniev, A. S.; Kirpichnikov, M. P., Expression of G-Protein Coupled Receptors in Escherichia coli for Structural Studies. *Biochemistry-Moscow* **2010,** *75* (7), 881-891.
155. Shangguan, D.; Li, Y.; Tang, Z.; Cao, Z. C.; Chen, H. W.; Mallikaratchy, P.; Sefah, K.; Yang, C. J.; Tan, W., Aptamers evolved from live cells as effective molecular probes for cancer study. *Proceedings of the National Academy of Sciences of the United States of America* **2006,** *103* (32), 11838-11843.
156. Chen, H. W.; Medley, C. D.; Sefah, K.; Shangguan, D.; Tang, Z. W.; Meng, L.; Smith, J. E.; Tan, W. H., Molecular recognition of small-cell lung cancer cells using aptamers. *Chemmedchem* **2008,** *3* (6), 991-1001.
157. Sefah, K.; Meng, L.; Lopez-Colon, D.; Jimenez, E.; Liu, C.; Tan, W. H., DNA Aptamers as Molecular Probes for Colorectal Cancer Study. *Plos One* **2010,** *5* (12).
158. Domingues, C. C.; Ciana, A.; Buttafava, A.; Casadei, B. R.; Balduini, C.; de Paula, E.; Minetti, G., Effect of Cholesterol Depletion and Temperature on the Isolation of Detergent-Resistant Membranes from Human Erythrocytes. *Journal of Membrane Biology* **2010,** *234* (3), 195-205.
159. Kremser, L.; Petsch, M.; Blaas, D.; Kenndler, E., Capillary electrophoresis of affinity complexes between subviral 80S particles of human rhinovirus and monoclonal antibody 2G2. *Electrophoresis* **2006,** *27* (13), 2630-2637.
160. Brown, M. S.; Anderson, R. G. W.; Basu, S. K.; Goldstein, J. L., RECYCLING OF CELL-SURFACE RECEPTORS - OBSERVATIONS FROM THE LDL RECEPTOR SYSTEM. *Cold Spring Harbor Symposia on Quantitative Biology* **1981,** *46*, 713-721.

161. Patel, D. J.; Suri, A. K.; Jiang, F.; Jiang, L. C.; Fan, P.; Kumar, R. A.; Nonin, S., Structure, recognition and adaptive binding in RNA aptamer complexes. *Journal of Molecular Biology* **1997,** *272* (5), 645-664.
162. Hetzke, T.; Vogel, M.; Gophane, D. B.; Weigand, J. E.; Suess, B.; Sigurdsson, S. T.; Prisner, T. F., Influence of Mg2+ on the conformational flexibility of a tetracycline aptamer. *Rna* **2019,** *25* (1), 158-167.
163. Nagatoishi, S.; Tanaka, Y.; Tsumoto, K., Circular dichroism spectra demonstrate formation of the thrombin-binding DNA aptamer G-quadruplex under stabilizing-cation-deficient conditions. *Biochemical and Biophysical Research Communications* **2007,** *352* (3), 812-817.
164. Delcourt, S. G.; Blake, R. D., STACKING ENERGIES IN DNA. *Journal of Biological Chemistry* **1991,** *266* (23), 15160-15169.
165. Schildkraut, C.; Lifson, S., DEPENDENCE OF MELTING TEMPERATURE OF DNA ON SALT CONCENTRATION. *Biopolymers* **1965,** *3* (2), 195-+.
166. Khandelwal, G.; Bhyravabhotla, J., A Phenomenological Model for Predicting Melting Temperatures of DNA Sequences. *Plos One* **2010,** *5* (8).
167. Eagle, H., BUFFER COMBINATIONS FOR MAMMALIAN CELL CULTURE. *Science (Washington D C)* **1971,** *174* (4008), 500-503.
168. Largy, E.; Mergny, J. L.; Gabelica, V., Role of Alkali Metal Ions in G-Quadruplex Nucleic Acid Structure and Stability. *Alkali Metal Ions: Their Role for Life* **2016,** *16*, 203-258.
169. Pena, F.; Jansens, A.; van Zadelhoff, G.; Braakman, I., Calcium as a Crucial Cofactor for Low Density Lipoprotein Receptor Folding in the Endoplasmic Reticulum. *Journal of Biological Chemistry* **2010,** *285* (12), 8656-8664.
170. Zheng, Z.; Hansford, D. J.; Conlisk, A. T., Effect of multivalent ions on electroosmotic flow in micro- and nanochannels. *Electrophoresis* **2003,** *24* (17), 3006-3017.
171. Mala, Z.; Krivankova, L.; Gebauer, P.; Bocek, P., Contemporary sample stacking in CE: A sophisticated tool based on simple principles. *Electrophoresis* **2007,** *28* (1-2), 243-253.
172. Osbourn, D. M.; Weiss, D. J.; Lunte, C. E., On-line preconcentration methods for capillary electrophoresis. *Electrophoresis* **2000,** *21* (14), 2768-2779.
173. Williams, E. P.; Mesidor, M.; Winters, K.; Dubbert, P. M.; Wyatt, S. B., Overweight and Obesity: Prevalence, Consequences, and Causes of a Growing Public Health Problem. *Current Obesity Reports* **2015,** *4* (3), 363-370.
174. Guh, D. P.; Zhang, W.; Bansback, N.; Amarsi, Z.; Birmingham, C. L.; Anis, A. H., The incidence of co-morbidities related to obesity and overweight: A systematic review and meta-analysis. *Bmc Public Health* **2009,** *9*.
175. CDC, Obesity: Halting the epidemic by making health easier. Prevention, C. f. D. C. a., Ed. 2009.
176. Obesity, Race/Ethnicity, and COVID-19. https://www.cdc.gov/obesity/data/obesity-and-covid-19.html.
177. Hartemink, N.; Boshuizen, H. C.; Nagelkerke, N. J. D.; Jacobs, M. A. M.; van Houwelingen, H. C., Combining risk estimates from observational studies with different exposure cutpoints: A meta-analysis on body mass index and diabetes type 2. *American Journal of Epidemiology* **2006,** *163* (11), 1042-1052.
178. Mhurchu, C. N.; Parag, V.; Woo, J.; Lam, T.; Woodward, M.; Asia Pacific Cohort Studies, C., Central obesity and risk of cardiovascular disease in the Asia Pacific Region. *Asia Pacific Journal of Clinical Nutrition* **2006,** *15* (3), 287-292.

179. Bergstrom, A.; Pisani, P.; Tenet, V.; Wolk, A.; Adami, H. O., Overweight as an avoidable cause of cancer in Europe. *International Journal of Cancer* **2001,** *91* (3), 421-430.
180. Obesity and Overweight. http://www.who.int/mediacentre/factsheets/fs311/en/.
181. Gonzalez-Muniesa, P.; Martinez-Gonzalez, M. A.; Hu, F. B.; Despres, J. P.; Matsuzawa, Y.; Loos, R. J. F.; Moreno, L. A.; Bray, G.; Martinez, J. A., Obesity. *Nature Reviews Disease Primers* **2017,** *3*.
182. Prevalence of Obesity and Severe Obesity Among Adults: United States, 2017–2018. https://www.cdc.gov/nchs/products/databriefs/db360.htm.
183. Craig M. Hales, M. D., Margaret D. Carroll, M.S.P.H., Cheryl D. Fryar, M.S.P.H., and Cynthia L. Ogden, Ph.D. *Prevalence of Obesity and Severe Obesity Among Adults: United States, 2017–2018*; Centers for Disease Control and Prevention: National Center for Health Statistics: 2020.
184. Sellayah, D.; Cagampang, F. R.; Cox, R. D., On the Evolutionary Origins of Obesity: A New Hypothesis. *Endocrinology* **2014,** *155* (5), 1573-1588.
185. Bhupathiraju, S. N.; Hu, F. B., Epidemiology of Obesity and Diabetes and Their Cardiovascular Complications. *Circulation Research* **2016,** *118* (11), 1723-1735.
186. Obesity: Symptoms and Causes https://www.mayoclinic.org/diseases-conditions/obesity/symptoms-causes/syc-20375742.
187. Zhang, Y. Y.; Proenca, R.; Maffei, M.; Barone, M.; Leopold, L.; Friedman, J. M., Positional cloning of the mouse obese gene and its human homolog. *Nature* **1994,** *372* (6505), 425-432.
188. Campfield, L. A.; Smith, F. J.; Guisez, Y.; Devos, R.; Burn, P., RECOMBINANT MOUSE OB PROTEIN - EVIDENCE FOR A PERIPHERAL SIGNAL LINKING ADIPOSITY AND CENTRAL NEURAL NETWORKS. *Science* **1995,** *269* (5223), 546-549.
189. Lonnqvist, F.; Arner, P.; Nordfors, L.; Schalling, M., OVEREXPRESSION OF THE OBESE (OB) GENE IN ADIPOSE-TISSUE OF HUMAN OBESE SUBJECTS. *Nature Medicine* **1995,** *1* (9), 950-953.
190. Blum, W. F.; Englaro, P.; Hanitsch, S.; Juul, A.; Hertel, N. T.; Muller, J.; Skakkebaek, N. E.; Heiman, M. L.; Birkett, M.; Attanasio, A. M.; Kiess, W.; Rascher, W., Plasma leptin levels in healthy children and adolescents: Dependence on body mass index, body fat mass, gender, pubertal stage, and testosterone. *Journal of Clinical Endocrinology & Metabolism* **1997,** *82* (9), 2904-2910.
191. Maffei, M.; Halaas, J.; Ravussin, E.; Pratley, R. E.; Lee, G. H.; Zhang, Y.; Fei, H.; Kim, S.; Lallone, R.; Ranganathan, S.; Kern, P. A.; Friedman, J. M., LEPTIN LEVELS IN HUMAN AND RODENT - MEASUREMENT OF PLASMA LEPTIN AND OB RNA IN OBESE AND WEIGHT-REDUCED SUBJECTS. *Nature Medicine* **1995,** *1* (11), 1155-1161.
192. Ahima, R. S.; Osei, S. Y., Leptin signaling. *Physiology & Behavior* **2004,** *81* (2), 223-241.
193. Considine, R. V.; Sinha, M. K.; Heiman, M. L.; Kriauciunas, A.; Stephens, T. W.; Nyce, M. R.; Ohannesian, J. P.; Marco, C. C.; McKee, L. J.; Bauer, T. L.; Caro, J. F., Serum immunoreactive leptin concentrations in normal-weight and obese humans. *New England Journal of Medicine* **1996,** *334* (5), 292-295.
194. Ahima, R. S.; Prabakaran, D.; Mantzoros, C.; Qu, D. Q.; Lowell, B.; MaratosFlier, E.; Flier, J. S., Role of leptin in the neuroendocrine response to fasting. *Nature* **1996,** *382* (6588), 250-252.
195. Boden, G.; Chen, X.; Mozzoli, M.; Ryan, I., Effect of fasting on serum leptin in normal human subjects. *Journal of Clinical Endocrinology & Metabolism* **1996,** *81* (9), 3419-3423.

196. Taheri, S.; Lin, L.; Austin, D.; Young, T.; Mignot, E., Short sleep duration is associated with reduced leptin, elevated ghrelin, and increased body mass index. *Plos Medicine* **2004,** *1* (3), 210-217.
197. Buxton, O. M.; Cain, S. W.; O'Connor, S. P.; Porter, J. H.; Duffy, J. F.; Wang, W.; Czeisler, C. A.; Shea, S. A., Adverse Metabolic Consequences in Humans of Prolonged Sleep Restriction Combined with Circadian Disruption. *Science Translational Medicine* **2012,** *4* (129).
198. Weigert, J.; Neumeier, M.; Wanninger, J.; Filarsky, M.; Bauer, S.; Wiest, R.; Farkas, S.; Scherer, M. N.; Schaffler, A.; Aslanidis, C.; Scholmerich, J.; Buechler, C., Systemic chemerin is related to inflammation rather than obesity in type 2 diabetes. *Clinical Endocrinology* **2010,** *72* (3), 342-348.
199. de Boer, T. N.; van Spil, W. E.; Huisman, A. M.; Polak, A. A.; Bijlsma, J. W. J.; Lafeber, F.; Mastbergen, S. C., Serum adipokines in osteoarthritis; comparison with controls and relationship with local parameters of synovial inflammation and cartilage damage. *Osteoarthritis and Cartilage* **2012,** *20* (8), 846-853.
200. Mirza, S.; Hossain, M.; Mathews, C.; Martinez, P.; Pino, P.; Gay, J. L.; Rentfro, A.; McCormick, J. B.; Fisher-Hoch, S. P., Type 2-diabetes is associated with elevated levels of TNF-alpha, IL-6 and adiponectin and low levels of leptin in a population of Mexican Americans: A cross-sectional study. *Cytokine* **2012,** *57* (1), 136-142.
201. Aye, I.; Lager, S.; Ramirez, V. I.; Gaccioli, F.; Dudley, D. J.; Jansson, T.; Powell, T. L., Increasing Maternal Body Mass Index Is Associated with Systemic Inflammation in the Mother and the Activation of Distinct Placental Inflammatory Pathways. *Biology of Reproduction* **2014,** *90* (6).
202. Kitao, N.; Fukui, D.; Shibata, H.; Saito, M.; Osborne, P. G.; Hashimoto, M., Seasonality and Fasting Effect in Raccoon Dog Nyctereutes procyonoides Serum Leptin Levels Determined by Canine Leptin-Specific Enzyme-Linked Immunosorbent Assay. *Journal of Experimental Zoology Part a-Ecological and Integrative Physiology* **2011,** *315A* (2), 84-89.
203. Koprucu, S.; Algul, S., Investigation of the leptin levels in the blood serum of Cyprinus carpio (Linnaeus, 1758) and Capoeta trutta (Heckel, 1843). *Journal of Animal Physiology and Animal Nutrition* **2015,** *99* (3), 430-435.
204. Marousez, L.; Hanssens, S.; Butruille, L.; Petit, C.; Pourpe, C.; Besengez, C.; Rakza, T.; Storme, L.; Deruelle, P.; Lesage, J.; Eberle, D., Breast milk apelin level increases with maternal obesity and high-fat feeding during lactation. *International Journal of Obesity*.
205. Lin, S.; Thomas, T. C.; Storlien, L. H.; Huang, X. F., Development of high fat diet-induced obesity and leptin resistance in C57BI/6J mice. *International Journal of Obesity* **2000,** *24* (5), 639-646.
206. Baranowska-Bik, A.; Baranowska, B.; Martynska, L.; Litwiniuk, A.; Kalisz, M.; Kochanowski, J.; Bik, W., Adipokine profile in patients with anorexia nervosa. *Endokrynologia Polska* **2017,** *68* (4), 422-429.
207. Xu, B.; Hu, Q. H.; Zhao, B.; Zhou, Z. K., Variation and significance of serum leptin, blood lipid level, adiponectin, NO and TNF-alpha for patients with non-traumatic ischemic necrosis of the femoral head. *Saudi Journal of Biological Sciences* **2017,** *24* (8), 1763-1766.
208. Selthofer-Relatic, K.; Radic, R.; Stupin, A.; Sisljagic, V.; Bosnjak, I.; Bulj, N.; Selthofer, R.; Brkljacic, D. D., Leptin/adiponectin ratio in overweight patients - gender differences. *Diabetes & Vascular Disease Research* **2018,** *15* (3), 260-262.

209. Pickens, C. A.; Sordillo, L. M.; Zhang, C.; Fenton, J. I., Obesity is positively associated with arachidonic acid-derived 5-and 11-hydroxyeicosatetraenoic acid (HETE). *Metabolism-Clinical and Experimental* **2017,** *70*, 177-191.
210. Kumar, A. A.; Satheesh, G.; Vijayakumar, G.; Chandran, M.; Prabhu, P. R.; Simon, L.; Kutty, V. R.; Kartha, C. C.; Jaleel, A., Plasma leptin level mirrors metabolome alterations in young adults. *Metabolomics* **2020,** *16* (8).
211. Fonslow, B. R.; Bowser, M. T., Free-flow electrophoresis on an anodic bonded glass microchip. *Analytical Chemistry* **2005,** *77* (17), 5706-5710.
212. Rudisch, B. M.; Pfeiffer, S. A.; Geissler, D.; Speckmeier, E.; Robitzki, A. A.; Zeitler, K.; Belder, D., Nonaqueous Micro Free-Flow Electrophoresis for Continuous Separation of Reaction Mixtures in Organic Media. *Analytical Chemistry* **2019,** *91* (10), 6689-6694.
213. Geiger, M.; Frost, N. W.; Bowser, M. T., Comprehensive Multidimensional Separations of Peptides Using Nano-Liquid Chromatography Coupled with Micro Free Flow Electrophoresis. *Analytical Chemistry* **2014,** *86* (10), 5136-5142.
214. Johnson, A. C.; Bowser, M. T., High-Speed, Comprehensive, Two Dimensional Separations of Peptides and Small Molecule Biological Amines Using Capillary Electrophoresis Coupled with Micro Free Flow Electrophoresis. *Analytical Chemistry* **2017,** *89* (3), 1665-1673.
215. Benz, C.; Boomhoff, M.; Appun, J.; Schneider, C.; Belder, D., Chip-Based Free-Flow Electrophoresis with Integrated Nanospray Mass-Spectrometry. *Angewandte Chemie-International Edition* **2015,** *54* (9), 2766-2770.
216. Pfeiffer, S. A.; Rudisch, B. M.; Glaeser, P.; Spanka, M.; Nitschke, F.; Robitzki, A. A.; Schneider, C.; Nagl, S.; Belder, D., Continuous purification of reaction products by micro free-flow electrophoresis enabled by large area deep-UV fluorescence imaging. *Analytical and Bioanalytical Chemistry* **2018,** *410* (3), 853-862.
217. Jezierski, S.; Klein, A. S.; Benz, C.; Schaefer, M.; Nagl, S.; Belder, D., Towards an integrated device that utilizes adherent cells in a micro-free-flow electrophoresis chip to achieve separation and biosensing. *Analytical and Bioanalytical Chemistry* **2013,** *405* (16), 5381-5386.
218. Anciaux, S. K.; Geiger, M.; Bowser, M. T., 3D Printed Micro Free-Flow Electrophoresis Device. *Analytical Chemistry* **2016,** *88* (15), 7675-7682.
219. Ashley, J.; Li, S. F. Y., Three-dimensional selection of leptin aptamers using capillary electrophoresis and implications for clone validation. *Analytical Biochemistry* **2013,** *434* (1), 146-152.
220. Abcam Anti-Leptin antibody (ab16227). https://www.abcam.com/leptin-antibody-ab16227.html.
221. Bateman, A.; Martin, M. J.; Orchard, S.; Magrane, M.; Agivetova, R.; Ahmad, S.; Alpi, E.; Bowler-Barnett, E. H.; Britto, R.; Bursteinas, B.; Bye-A-Jee, H.; Coetzee, R.; Cukura, A.; Da Silva, A.; Denny, P.; Dogan, T.; Ebenezer, T.; Fan, J.; Castro, L. G.; Garmiri, P.; Georghiou, G.; Gonzales, L.; Hatton-Ellis, E.; Hussein, A.; Ignatchenko, A.; Insana, G.; Ishtiaq, R.; Jokinen, P.; Joshi, V.; Jyothi, D.; Lock, A.; Lopez, R.; Luciani, A.; Luo, J.; Lussi, Y.; Mac-Dougall, A.; Madeira, F.; Mahmoudy, M.; Menchi, M.; Mishra, A.; Moulang, K.; Nightingale, A.; Oliveira, C. S.; Pundir, S.; Qi, G. Y.; Raj, S.; Rice, D.; Lopez, M. R.; Saidi, R.; Sampson, J.; Sawford, T.; Speretta, E.; Turner, E.; Tyagi, N.; Vasudev, P.; Volynkin, V.; Warner, K.; Watkins, X.; Zaru, R.; Zellner, H.; Bridge, A.; Poux, S.; Redaschi, N.; Aimo, L.; Argoud-Puy, G.; Auchincloss, A.; Axelsen, K.; Bansal, P.; Baratin, D.; Blatter,

M. C.; Bolleman, J.; Boutet, E.; Breuza, L.; Casals-Casas, C.; de Castro, E.; Echioukh, K. C.; Coudert, E.; Cuche, B.; Doche, M.; Dornevil, D.; Estreicher, A.; Famiglietti, M. L.; Feuermann, M.; Gasteiger, E.; Gehant, S.; Gerritsen, V.; Gos, A.; Gruaz-Gumowski, N.; Hinz, U.; Hulo, C.; Hyka-Nouspikel, N.; Jungo, F.; Keller, G.; Kerhornou, A.; Lara, V.; Le Mercier, P.; Lieberherr, D.; Lombardot, T.; Martin, X.; Masson, P.; Morgat, A.; Neto, T. B.; Paesano, S.; Pedruzzi, I.; Pilbout, S.; Pourcel, L.; Pozzato, M.; Pruess, M.; Rivoire, C.; Sigrist, C.; Sonesson, K.; Stutz, A.; Sundaram, S.; Tognolli, M.; Verbregue, L.; Wu, C. H.; Arighi, C. N.; Arminski, L.; Chen, C. M.; Chen, Y. X.; Garavelli, J. S.; Huang, H. Z.; Laiho, K.; McGarvey, P.; Natale, D. A.; Ross, K.; Vinayaka, C. R.; Wang, Q. H.; Wang, Y. Q.; Yeh, L. S.; Zhang, J.; UniProt, C., UniProt: the universal protein knowledgebase in 2021. *Nucleic Acids Research* **2021,** *49* (D1), D480-D489.

222. Josuran, R. Prot pi. https://www.protpi.ch/Calculator/ProteinTool.

223. Faller, T.; Engelhardt, H., How to achieve higher repeatability and reproducibility in capillary electrophoresis. *Journal of Chromatography A* **1999,** *853* (1-2), 83-94.

224. Ali, I.; Aboul-Enein, H. Y.; Gupta, V. K., Precision in capillary electrophoresis. *Analytical Letters* **2006,** *39* (11), 2345-2357.

225. Nowak, P. M.; Wozniakiewicz, M.; Gladysz, M.; Janus, M.; Koscielniak, P., Improving repeatability of capillary electrophoresis-a critical comparison of ten different capillary inner surfaces and three criteria of peak identification. *Analytical and Bioanalytical Chemistry* **2017,** *409* (18), 4383-4393.

226. About Arrhythmia. https://www.heart.org/en/health-topics/arrhythmia/about-arrhythmia#.WLRlaW8rKCg.

227. American Heart Association: Annual Report 2018-2019. https://www.heart.org/-/media/files/about-us/annual-report/american-heart-association-annual-report-for-2018-2019.pdf?la=en&hash=2BFC3195D998C960CFC7C186FFE0B1AC82513ECA.

228. Heart Disease Facts. https://www.cdc.gov/heartdisease/facts.htm.

229. Hasenfuss, G., Alterations of calcium-regulatory proteins in heart failure. *Cardiovascular Research* **1998,** *37* (2), 279-289.

230. Lompre, A. M.; Hajjar, R. J.; Harding, S. E.; Kranias, E. G.; Lohse, M. J.; Marks, A. R., Ca2+ Cycling and New Therapeutic Approaches for Heart Failure. *Circulation* **2010,** *121* (6), 822-830.

231. ZarainHerzberg, A.; Afzal, N.; Elimban, V.; Dhalla, N. S., Decreased expression of cardiac sarcoplasmic reticulum Ca2+-pump ATPase in congestive heart failure due to myocardial infarction. *Molecular and Cellular Biochemistry* **1996,** *164*, 285-290.

232. Bers, D. M., Calcium fluxes involved in control of cardiac myocyte contraction. *Circulation Research* **2000,** *87* (4), 275-281.

233. Cheng, H.; Lederer, W. J.; Cannell, M. B., CALCIUM SPARKS - ELEMENTARY EVENTS UNDERLYING EXCITATION-CONTRACTION COUPLING IN HEART-MUSCLE. *Science* **1993,** *262* (5134), 740-744.

234. Bers, D. M., Calcium cycling and signaling in cardiac myocytes. *Annual Review of Physiology* **2008,** *70*, 23-49.

235. Gustavsson, M.; Verardi, R.; Mullen, D. G.; Mote, K. R.; Traaseth, N. J.; Gopinath, T.; Veglia, G., Allosteric regulation of SERCA by phosphorylation-mediated conformational shift of phospholamban. *Proceedings of the National Academy of Sciences of the United States of America* **2013,** *110* (43), 17338-17343.

236. Simmerman, H. K. B.; Collins, J. H.; Theibert, J. L.; Wegener, A. D.; Jones, L. R., SEQUENCE-ANALYSIS OF PHOSPHOLAMBAN - IDENTIFICATION OF PHOSPHORYLATION SITES AND 2 MAJOR STRUCTURAL DOMAINS. *Journal of Biological Chemistry* **1986,** *261* (28), 3333-3341.
237. Soller, K. J.; Yang, J.; Veglia, G.; Bowser, M. T., Reversal of Phospholamban Inhibition of the Sarco(endo)plasmic Reticulum Ca2+-ATPase (SERCA) Using Short, Protein-interacting RNAs and Oligonucleotide Analogs. *Journal of Biological Chemistry* **2016,** *291* (41), 21510-21518.
238. Hamlin, R. L.; Altschuld, R. A., Extrapolation From Mouse to Man. *Circulation-Cardiovascular Imaging* **2011,** *4* (1), 2-4.
239. Bedada, F. B.; Wheelwright, M.; Metzger, J. M., Maturation status of sarcomere structure and function in human iPSC-derived cardiac myocytes. *Biochimica Et Biophysica Acta-Molecular Cell Research* **2016,** *1863* (7), 1829-1838.
240. Zhang, J. H.; Wilson, G. F.; Soerens, A. G.; Koonce, C. H.; Yu, J. Y.; Palecek, S. P.; Thomson, J. A.; Kamp, T. J., Functional Cardiomyocytes Derived From Human Induced Pluripotent Stem Cells. *Circulation Research* **2009,** *104* (4), E30-E41.
241. Lian, X. J.; Zhang, J. H.; Azarin, S. M.; Zhu, K. X.; Hazeltine, L. B.; Bao, X. P.; Hsiao, C.; Kamp, T. J.; Palecek, S. P., Directed cardiomyocyte differentiation from human pluripotent stem cells by modulating Wnt/beta-catenin signaling under fully defined conditions. *Nature Protocols* **2013,** *8* (1), 162-175.
242. Bot, C. T.; Juhasz, K.; Haeusermann, F.; Polonchuk, L.; Traebert, M.; Stoelzle-Feix, S., Cross - site comparison of excitation-contraction coupling using impedance and field potential recordings in hiPSC cardiomyocytes. *Journal of Pharmacological and Toxicological Methods* **2018,** *93*, 46-58.
243. Scott, C. W.; Zhang, X. Y.; Abi-Gerges, N.; Lamore, S. D.; Abassi, Y. A.; Peters, M. F., An Impedance-Based Cellular Assay Using Human iPSC-Derived Cardiomyocytes to Quantify Modulators of Cardiac Contractility. *Toxicological Sciences* **2014,** *142* (2), 331-338.
244. Peters, M. F.; Lamore, S. D.; Guo, L.; Scott, C. W.; Kolaja, K. L., Human Stem Cell-Derived Cardiomyocytes in Cellular Impedance Assays: Bringing Cardiotoxicity Screening to the Front Line. *Cardiovascular Toxicology* **2015,** *15* (2), 127-139.
245. Burridge, P. W.; Matsa, E.; Shukla, P.; Lin, Z. C.; Churko, J. M.; Ebert, A. D.; Lan, F.; Diecke, S.; Huber, B.; Mordwinkin, N. M.; Plews, J. R.; Abilez, O. J.; Cui, B.; Gold, J. D.; Wu, J. C., Chemically defined generation of human cardiomyocytes. *Nature Methods* **2014,** *11* (8), 855-860.
246. ATCC ATCC-BXS0116 Human [Non-Hispanic Caucasian Female] Induced Pluripotent Stem (IPS) Cells (ATCC ® ACS-1030 ™). https://www.atcc.org/products/all/ACS-1030.aspx#culturemethod.
247. SCVI Biobank Forms: SCVI SOP for iPSC thawing and culture. https://med.stanford.edu/scvibiobank/forms.html.
248. SCVI Biobank Forms: SCVI SOP for cardiomyocyte thawing and culture. https://med.stanford.edu/scvibiobank/forms.html.
249. Soller, K. J. Tuning the Equilibrium: A Biophysical Approach to Controlling Cardiac Muscle Contractility through SERCA and Phospholamban University of Minnesota–Twin Cities, Minneapolis, MN, 2017.

250. Wakui, T.; Matsumoto, T.; Matsubara, K.; Kawasaki, T.; Yamaguchi, H.; Akutsu, H., Method for evaluation of human induced pluripotent stem cell quality using image analysis based on the biological morphology of cells. *Journal of Medical Imaging* **2017,** *4* (4).
251. Healy, L.; Ruban, L., Atlas of Human Pluripotent Stem Cells in Culture. Springer Science+Business Media: New York, 2015.
252. Zhang, J. H.; Klos, M.; Wilson, G. F.; Herman, A. M.; Lian, X. J.; Raval, K. K.; Barron, M. R.; Hou, L. Q.; Soerens, A. G.; Yu, J. Y.; Palecek, S. P.; Lyons, G. E.; Thomson, J. A.; Herron, T. J.; Jalife, J.; Kamp, T. J., Extracellular Matrix Promotes Highly Efficient Cardiac Differentiation of Human Pluripotent Stem Cells The Matrix Sandwich Method. *Circulation Research* **2012,** *111* (9), 1125-1136.
253. Correia, C.; Koshkin, A.; Duarte, P.; Hu, D. J.; Teixeira, A.; Domian, I.; Serra, M.; Alves, P. M., Distinct carbon sources affect structural and functional maturation of cardiomyocytes derived from human pluripotent stem cells. *Scientific Reports* **2017,** *7*.
254. Wang, T.; Rahimizadeh, K.; Veedu, R. N., Development of a Novel DNA Oligonucleotide Targeting Low-Density Lipoprotein Receptor. *Molecular Therapy-Nucleic Acids* **2020,** *19*, 190-198.

Appendix

Aptamer	Count	Sequence (random region)
A1	740	CTCATACGTTTAACTTGATTCTGCTAATTTAAGACTCTGG
A3	448	TTGCATGGATTGAGTTTCATTACGTTATACATGGTCATTG
A4	359	ACATCATGGGTTATATGCACACAGGTTTAACATCGTGTAC
A5	124	ATCACTCTGCATGTCAAATAGAAACGACAAAGAATCGTGA
A9	68	ATTGAGATAGTTTGTGAAGACTGGTCTAGCAATCATGTAA
A10	62	AGGAGTACACAAGCATAAGTTAATCAGGGTTTCTGTCTCA
A11	61	AGTATTCAGAGTCCAAATAGAGCAATGGTTAAGACAATCA
A12	58	TGTTAAATATCGCTAGCTGAGTATTACTTGTAGGTCTTGA
A13	53	CCCATCACTAGTGTCACCATGCAAGCGTCTATCCATTGCC
A14	48	ATCACTATCGAAAGATTCTGATCGTAAGTAGTTTTGAACG
A17	39	TCTTCATCGTAAGATTCAACGTCGATTTGATAGAGCGTAT
A19	36	CGGATATGCATTCCTCATCTCCCCAATCCGTCCCAAGCCT
A25	25	GTTTGAGTCAAACTTGTATCGGATCGACAATATCCACGTG
A31	23	TTCATACGTTTAACTTGATTCTGCTAATTTAAGACTCTGG
A32	22	TCGTTTATATTGACGAAGTTGATCGACAGTATTTCAACAG
A33	22	TACCCTGTATGTAAGCCATAAACCTTGTGATAGTTATTTG
A35	20	TCTTGTTATCACTGTTCTATCCATTAGACTTATGAATGTA
A37	20	CTCATACGTTTAACTTGATTCTGCTAATTTAAGACTCTGA
A38	20	CTCATACGTTTAACCTGATTCTGCTAATTTAAGACTCTGG
A41	19	CTCATACGTTTAACTTGATTCCGCTAATTTAAGACTCTGG
A42	17	CTCATACGTTTAACTTGATTCTGCTAATCTAAGACTCTGG
A46	16	CCCACTCCTCACCTTGCACACCCAGCTTGGGCTTGCTGTC
A47	16	CTCATACGTCTAACTTGATTCTGCTAATTTAAGACTCTGG
A49	15	TCACGCAGATTGCTAATATTACCTACCACTGTTTACTACC
A50	15	CTCATACGTTTAACTTGACTCTGCTAATTTAAGACTCTGG
A55	13	AGATTGGTATGGTTGCACAAGAATAGCATCCATTGAAAGC
A58	13	CTCATACGTTTAACTCGATTCTGCTAATTTAAGACTCTGG
A61	13	CGGATATCCTGTTGGATGGGAATACTATGGTGAGTGGAGC
A62	12	CTCATACGTTTAACTTGATTCTGCTAATTTAAGACTCCGG
A63	12	CTCATACGTTTAACTTGATTCTGCTAACTTAAGACTCTGG
A65	12	CTCATACGTTTAACTTGATTCTGCTAATTTAGGACTCTGG
A68	11	GCATCATGGGTTATATGCACACAGGTTTAACATCGTGTAC
A70	11	AGGATGTTTATTCCGTTTGTTTAAATATGCCTCCAACACA
A71	11	TCATATCTCTTCGCTCACTATTCGCTTATTCCTACCTCTT
A73	11	CTCATACGTTTAACTTGATTCTGCTGATTTAAGACTCTGG
A75	11	CTCATACGTTTATCTTGATTCTGCTAATTTAAGACTCTGG
A76	11	TGCAGAGATCTAAGTCCTACATTTGTACTGTTCCGACTAT
A77	11	TTGCATGGATTGAGTTTCATTACGTTATACGTGGTCATTG
A79	10	TTGCATGGATTGAGTCTCATTACGTTATACATGGTCATTG
A80	10	CTCATACGTTTAACTTGATTCTGCTAGTTTAAGACTCTGG
A81	10	TCGCATGGATTGAGTTTCATTACGTTATACATGGTCATTG
A85	10	CTCATACGCTTAACTTGATTCTGCTAATTTAAGACTCTGG

Table A.1: Ranked list of LDLR aptamer sequences with read count ≥10. For each aptamer, the full sequence is: AGCAGCACAGAGGTCAGATG–[Random region]–TTCACGGTAGCACGCATAGG. Missing sequences (such as A2) were removed due to primer sequences within the random region. Additional sequences are listed in the supplementary materials.

Aptamer	Count	Sequence (random region)
A4	359	A C A T C A T G G G T T A T A T G C A C A C A G G T T T A A C A T C G T G T A C
A68	11	G C A T C A T G G G T T A T A T G C A C A C A G G T T T A A C A T C G T G T A C
A166	6	A C A T C A T G G G T T G T A T G C A C A C A G G T T T A A C A T C G T G T A C
A172	6	A C G T C A T G G G T T A T A T G C A C A C A G G T T T A A C A T C G T G T A C
A179	5	A C A T C A T G G G T T A T A T G C A C A C A G G T T T A A C A T C G C G T A C
A197	5	A C A T C A T G G G T T A T A T G C A C A C A G G T T T A A C A T C G T G C A C
A200	5	A C A T C A T G G G T T A T A T G C A C A C A G G T T T G A C A T C G T G T A C
A205	5	A C A T C A T G G G T T A T A T G C A C A C A G G T T T A A C A T C A T G T A C
A213	5	A C A T C A T G G G T T A T A T G C A C A C A G G T T T T A C A T C G T G T A C
A216	5	A C A T C A T G G G T T T T A T G C A C A C A G G T T T A A C A T C G T G T A C
A229	5	A C A T C A T G G G T T A T A T G C A C A C A G G T T T A G C A T C G T G T A C
A253	4	A C A T C A C G G G T T A T A T G C A C A C A G G T T T A A C A T C G T G T A C
A254	4	A C A T C A T G G G T A A T A T G C A C A C A G G T T T A A C A T C G T G T A C
A284	4	A C A T C G T G G G T T A T A T G C A C A C A G G T T T A A C A T C G T G T A C
A288	4	A C A T C A T G G G C T A T A T G C A C A C A G G T T T A A C A T C G T G T A C
A294	4	A C A T C T T G G G T T A T A T G C A C A C A G G T T T A A C A T C G T G T A C
A316	3	A C A T C A A G G G T T A T A T G C A C A C A G G T T T A A C A T C G T G T A C
A322	3	A C A T C A T G G G T T A T A C G C A C A C A G G T T T A A C A T C G T G T A C
A379	3	A C A T C A T G G G T T A T A T G C A C A C A G G T T T A A C A T C G A G T A C
A392	3	A C A T C A T G G G T T A T A T G C A C A C A G G T T T A T C A T C G T G T A C
A402	3	A C A T C A T G G G T T A T A T G C A C A C A A G T T T A A C A T C G T G T A C
A486	2	G C A T C G T G G G T T A T A T G C A C A C A G G T T T A A C A T C G T G T A C
A973	2	A C A T C A T G G G T T A T A A G C A C A C A G G T T T A A C A T C G T G T A C
A2026	2	C C A T C A C G G G T T A T A C G C A C A C A G G T T T A A C A T C G T G T A C
A2446	2	A C A T C A T G G G T T A T A T G C A T A C A G G T T T A A C A T C G T G T A C
A2779	2	A T A T C A T G G G T T A T A T G C A C A C A G G T T T A A C A T C G T G T A C
A2906	2	A C A T C A T G G G T A A T A T G C A C A C A G G T T T A A C A T C G T G T A C
A3184	2	A C A T C A C G G G T T A T A T G C A C A C A G A T T T A A C A T C G T G T A C
A4157	2	A C A T C A T G G G A T A T A T G C A C A C A G G T T T A A C A T C G T G T A C

Table A.2: Comparison of sequences in LDLR aptamer Cluster #1. The aptamer number, read count, and color-coded random region sequence of all 29 sequences in Cluster #1 are shown. There is 100% base match at more than half of the positions, and most sequences differ from the consensus sequence by only a single base. Additional clusters are shown in the supplementary materials.

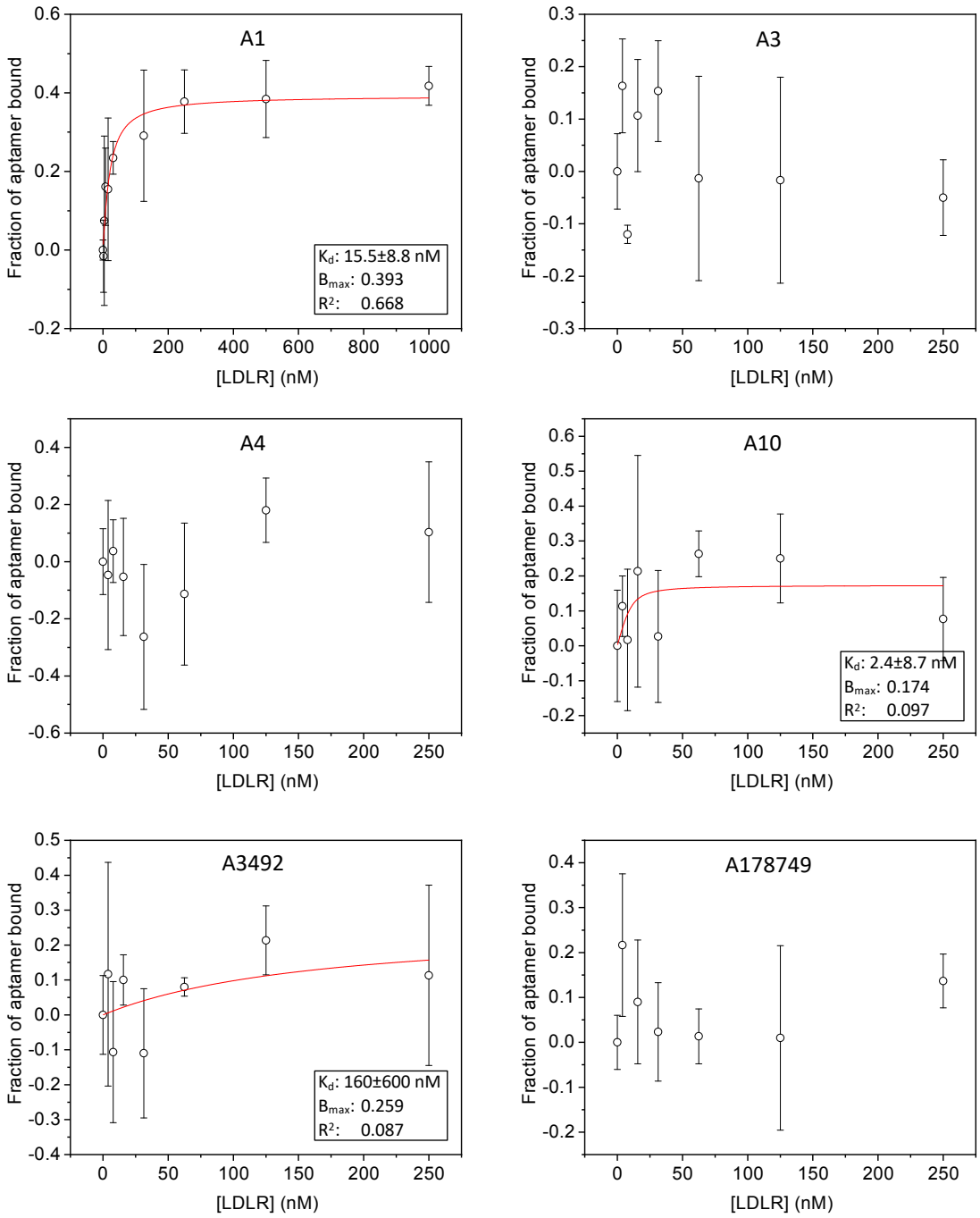

Figure A.1: FP fraction bound plots for LDLR aptamers. Y-values indicate uncorrected (non-normalized) fraction bound calculated from Equation 1.10. Error bars indicate standard deviation of all replicate measurements of each sample. The red line shows the hyperboloid fit obtained (if it converged), even if the results were questionable due to low absolute binding (B_{max}<0.3) or poor fit (R^2<0.5). The K_d is reported ± standard error calculated from the fit.

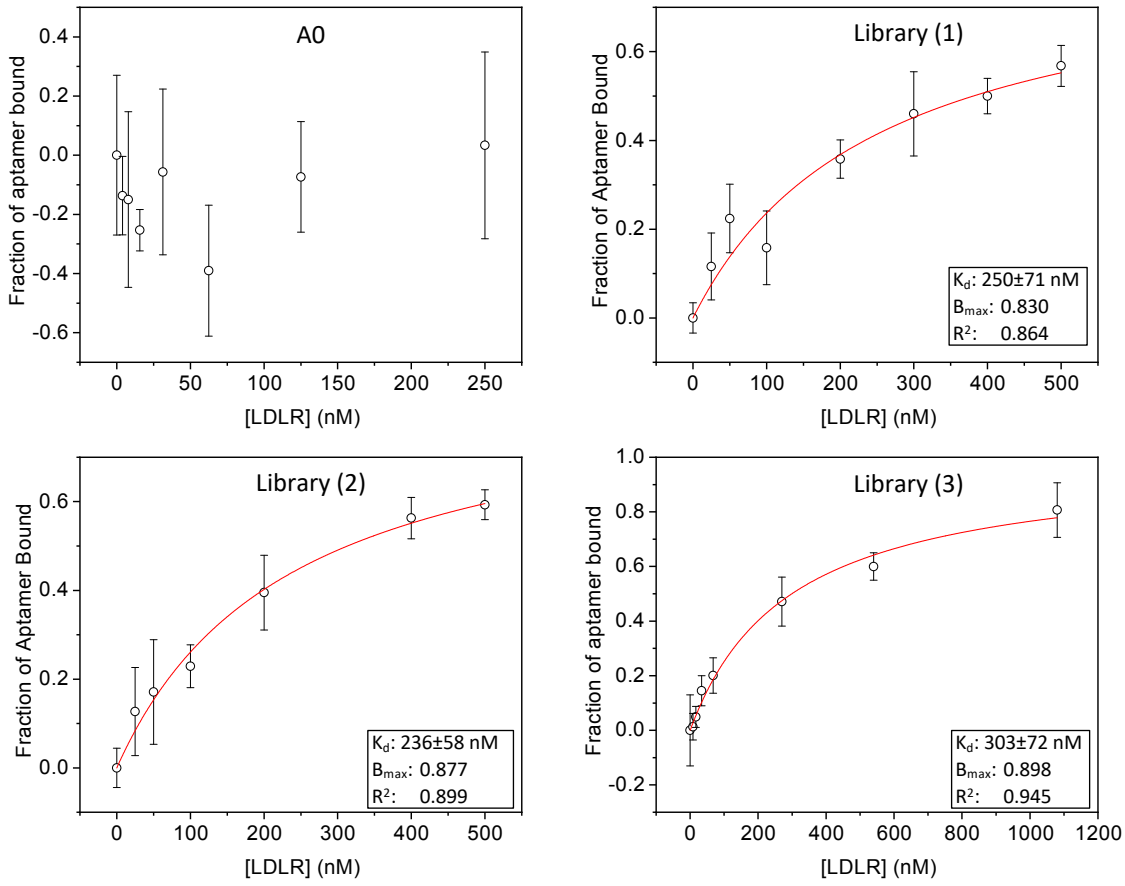

Figure A.2: FP fraction bound plots for LDLR negative control aptamer and starting library. Y-values indicate uncorrected (non-normalized) fraction bound calculated from Equation 1.10. Error bars indicate standard deviation of all replicate measurements of each sample. The red line shows the hyperboloid fit obtained (if it converged). Three separate assays of the library were performed and averaged to obtain the value in Table 3.3.The K_d is reported ± standard error calculated from the fit.

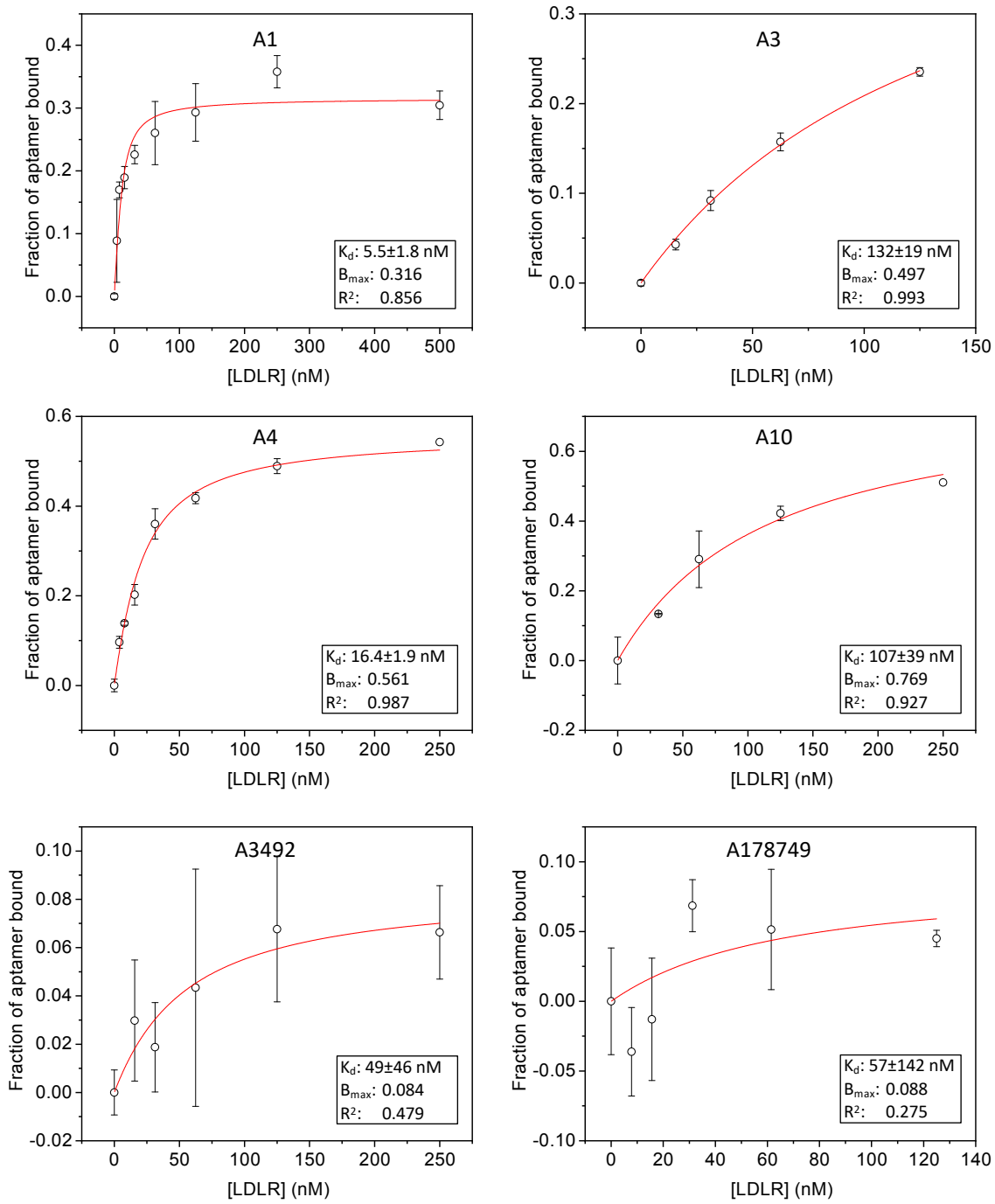

Figure A.3: CE fraction bound plots for LDLR aptamers. Y-values indicate uncorrected (non-normalized) fraction bound calculated from Equations 1.11 or 1.13. Error bars indicate standard deviation of all replicate measurements of each sample. The red line shows the hyperboloid fit obtained, even if the results were rejected due to low absolute binding (B_{max}<0.3) or poor fit (R^2<0.5) in Table 3.3. The K_d is reported ± standard error calculated from the fit. The A1 plot shows data for the ratiometric calculation (Equations 1.12 and 1.13) while all others show the subtractive calculation (Equation 1.11).

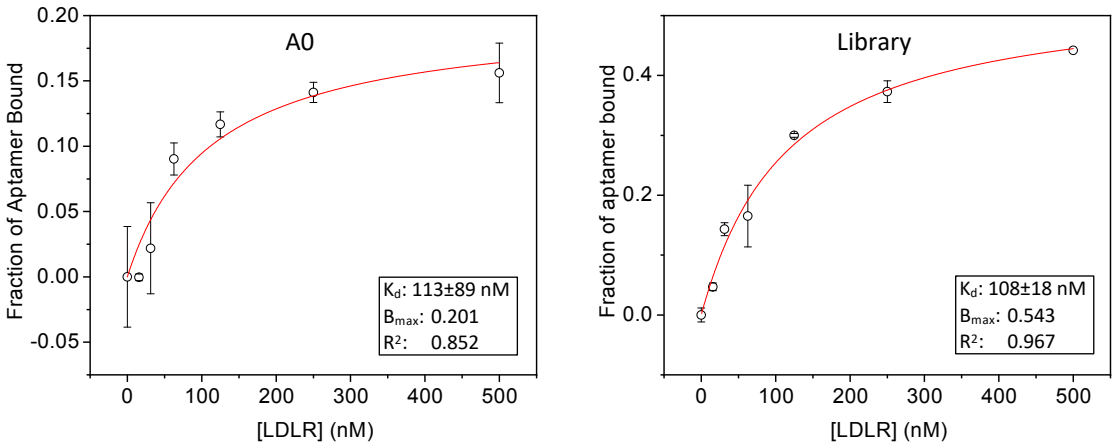

Figure A.4: CE fraction bound plots for LDLR negative control aptamer and starting library. Y-values indicate uncorrected (non-normalized) fraction bound calculated from Equation 1.11. Error bars indicate standard deviation of all replicate measurements of each sample. The red line shows the hyperboloid fit obtained, even if the results were rejected due to low absolute binding (B_{max}<0.3) or poor fit (R^2<0.5) in Table 3.3. The K_d is reported ± standard error calculated from the fit.

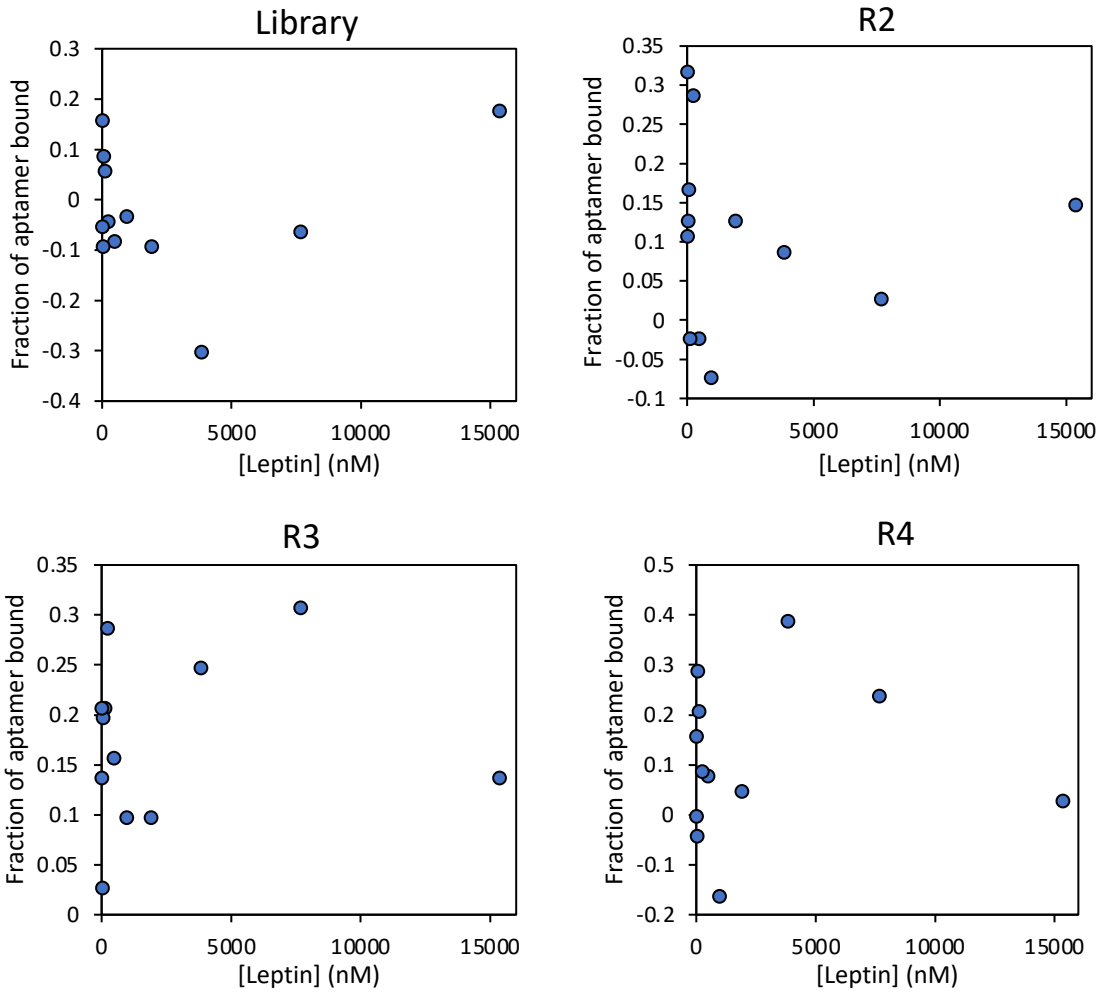

Figure A.5: DNA binding plots against leptin for multiple SELEX pools, collected by FP. Plots are shown for the starting library and for rounds 2 to 4 (R2-R4). Y-values indicate uncorrected (non-normalized) fraction bound calculated from Equation 1.10. Each plot is highly random with no clear trend, indicating no visible affinity of the aptamer pool for leptin. This supports the hypothesis that binding complexes were excluded during the first round, leading to unsuccessful selection. Measurements were repeated with different detector sensitivity (not shown) but showed no significant improvement.

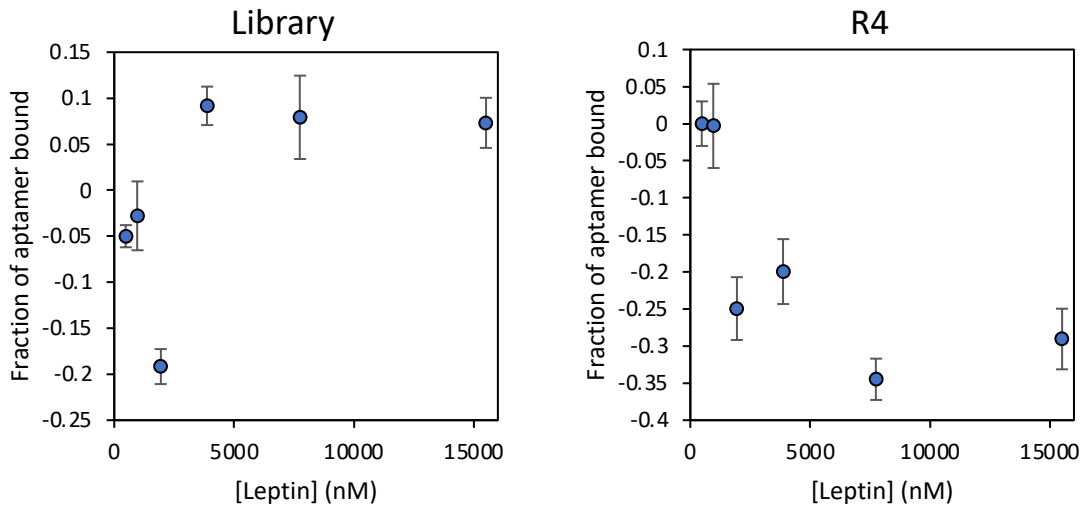

Figure A.6: DNA binding plots against leptin for multiple SELEX pools, collected by CE. Plots are shown for the starting library and for round 4 (R4). Y-values indicate the mean and standard deviation for triplicate measurements calculated by Equation 1.11 using free DNA peak height. No clear trend emerged for either plot, indicating no visible affinity of the aptamer pool for leptin. This supports the hypothesis that binding complexes were excluded during the first round, leading to unsuccessful selection.

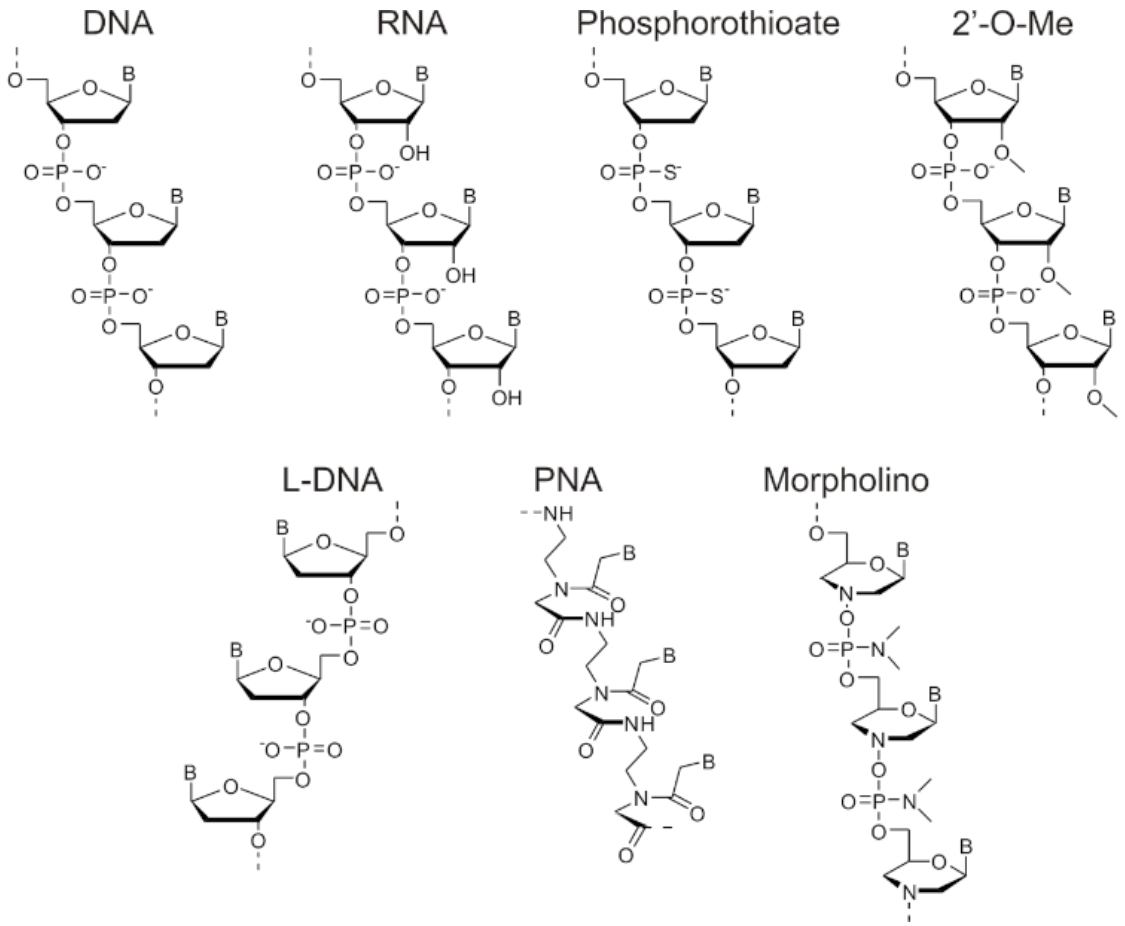

Figure A.7: Backbone structures of DNA, RNA, and XNAs. In each structure, B indicates the location of the nucleobase. From top to bottom, left to right, the nucleic acids are: deoxyribonucleic acid (DNA); ribonucleic acid (RNA); phosphorothioate (ptDNA); 2'-O-methyl RNA (2'-O-Me); enantiomeric DNA (L-DNA); peptide nucleic acid (PNA); and morpholino DNA. Adapted from Soller *et al.*[237]